

**Study on Multipath Propagation Modeling and
Characterization in Advanced MIMO Communication Systems**

Yi Wang

University of Electro-Communications
March 2013

Study on Multipath Propagation Modeling and Characterization in Advanced MIMO Communication Systems



Yi Wang

Department of Communication Engineering and Informatics

University of Electro-Communications

A thesis submitted for the degree of

DOCTOR OF PHILOSOPHY

MARCH 2013

**Study on Multipath Propagation Modeling and
Characterization in Advanced MIMO Communication Systems**

APPROVED BY SUPERVISORY COMMITTEE

Chairperson Professor *Yoshio Karasawa*

Member Professor *Takeshi Hashimoto*

Member Professor *Yasushi Yamao*

Member Professor *Takeo Fujii*

Member Professor *Toshiharu Kojima*

Copyright @ 2013 by Yi Wang

All Rights Reserved

MIMO 通信システムにおける、マルチパス伝搬 モデルと特性解析に関する研究

論文概要

無線通信の周波数有効利用の技術の一つとして、送受信の双方にアレーアンテナを用いる MIMO 通信技術があり、無線 LAN から、WiMAX, LTE など新世代の携帯電話システムへとその応用が広がっている。このため、学術分野での MIMO の研究は、多岐にわたり、ワイヤレス通信分野での研究が極めて盛んになっている。伝送特性は、通信路の特性、すなわちマルチパス伝搬チャネルの特性に支配されるため、マルチパス環境下での MIMO 伝送特性の解析や、伝搬路そのもののモデル化の研究も重要な位置づけにある。

本研究では、これまでの MIMO の研究の主な対象である屋内通信や移動体通信の電波伝搬研究をベースに、さらにアドバンストな通信である ITS の車車間通信に着目し、この環境での新たな伝搬モデルを提案している。一般的な MIMO 伝搬モデルに関する研究では、アレーアンテナの通信環境は直接波のない見通し外 (NLOS) 環境と見通し内 (LOS) 環境に分けられている。しかし道路上のような中、短距離通信の場合は、道路や交通状況によって、全てのアレーペアの通信環境は同じになっていないケースもある。例えば、ITS 車車間通信の場合、自動車の左右につけられた 2 つのアンテナは、見通しの悪い交差点で通信相手の自動車のアンテナに対して、一方が NLOS、一方が LOS といった MIMO のアレーアンテナパス間に LOS と NLOS が混在する環境になる。このような見通しの悪い交差点における出会い頭の衝突を防止する目的での通信特性評価に必要なチャネルモデルを提案し、さらにはそれを具体化した複合チャネルモデルの構築を行っている。障害物の位置やサイズによって伝搬モデルは五つのケースに分けられる。この混在する環境での通信特性を評価するための理論式を導出している。それぞれのケースに対応でき、更に伝搬損失距離特性の影響を考慮した特性解析式を提示している。このモデルでの計算値と、交差点を模擬した実測データと比較して、精度良い伝搬特性の推定が可能であることを明らかにし、モデルの有効性を実証している。

さらに、MIMO では、到来波が水平面ばかりでなく、3 次元的広がりを有して到来する通信環境もあり、このモデル化も重要になっている。例えば、屋内環境、または密度の高い高層ビルに囲まれる伝搬環境には、電波の 3 次元的広がりが特徴である。この場合は、3 次元の到来方向の性質は空間相関で規定されるが、それを一般的に表現

するモデルがまだ完成していなかった。本論文の後半では、この問題に取り組み、汎用的な理論モデルの構築により、その一般式を得ることができた。従来の研究で、3次元に到来する電波環境を $\cos^n(\cdot)$ で表すとき、 $n=0, 2, \infty$ のみが解析的に解かれているだけであったが、得られた理論式は n の任意の値について適用でき、従来モデルを包含する新しいモデルの完成となった。また、得られた理論式は、積分演算のない超幾何関数で表れているため、計算に極めて簡易である特徴を持っている。実際に金属で取り囲まれているような特殊な環境である電波反射箱での信号空間相関の実測データとも、良い一致が得られている。3次元に到来する電波環境を $\cos^n(\cdot)$ で表すという提案で得られたモデルとソリューションは、汎用性と有効性を持ち、今後マルチパスリッチ環境での MIMO 端末の空間相関特性を解析することに応用できる。

Abstract

With a great amount of research and experiments, Multiple Input Multiple Output (MIMO) technology has been proved to be a powerful tool for improving system capacity and link performance. When applying MIMO in advanced communication systems in various wireless situations including indoor and outdoor environments, selecting an adequate system model is crucial. Study on multipath propagation modeling have a significant importance for the research of MIMO transmission. For the estimation of system performance, effective characterization is highly desired. Even with powerful modern mathematical tools which can handle many complicated scenarios, search for the generalized models with low computational complexity and high practicality that can represent a wide range of situations is worth the effort.

The dissertation contributes to MIMO study from two aspects. Firstly, in the physical layer level we propose a propagation model that involves the mixture of None-Line-of-Sight (NLOS) and Line-of-Sight (LOS) environments. Classical MIMO propagation models are based on either a NLOS environment or a LOS environment. However when the situation is more complicated and multiple antennas in a MIMO system suffer from different fading environments, those models are not applicable any more. Our first proposal focuses on this issue and analyze all possible propagation cases in detail. Then we derive a function for the evaluation of Signal-to-Noise Ratio (SNR) performance in such kind of propagation, and the derived function are proved to be applicable for different cases if given the number of LOS or NLOS sub-channels.

Secondly, at the terminal side where spatial correlation has a significant impact on transmission performance due to the implementation of multi-antennas or array antennas, an approximation approach considering three-dimensional angular power spectrum enables evaluation and characterization of spatial correlation performance of MIMO terminals in multipath-rich environment. The method is

to use the n -th power of cosine function to model the Angular Power Spectrum (APS), which is a combination of antenna effects and propagation properties of the physical environment. As a result, the method for evaluating spatial correlation performance can be simplified as the closed-form expressions in both horizontal and vertical directions.

The proposals for propagation modeling and spatial correlation evaluation are verified to be effective and valid by simulation results. The newly-developed solutions that are derived for modeling and characterization in terms of Hypergeometric functions are utilized to complete some computer calculations. For channel modeling in the mixed NLOS and LOS environment, fairly good agreements of results from our newly-developed functions with the result of a field experiment of Intelligent Transportation Systems Inter Vehicle Communication (ITS-IVC) indicate the practicality of the proposed method. For the characterization of spatial correlation of MIMO terminals, simulations as well as measurements in reverberation chamber show that the proposed approach of APS modeling has a good approximation result to the theoretical values.

Although the proposed models are only good under some conditions and limitations such as Independent and Identically Distributed (IID) channels, the research scope of modeling and characterization for MIMO systems is highly improved and complemented with our proposals. For multipath propagation, the proposals of channel modeling in the mixed NLOS and LOS sub-channels and spatial correlation in the three-dimensional APS of n -th power of cosine function are novel. Based on the proposed models, the derived attractive functions are proven to be able to involve some results of previous study.

Contents

List of Figures	xix
List of Symbols	xiii
1 Introduction	1
1.1 An Overview of MIMO: History, Present and Future	1
1.2 Research on MIMO Technology: Modeling, Evaluating and Testing	2
1.3 Context of the Works	3
1.4 Main Contributions	4
1.5 Outline of the Dissertation	5
2 Multipath in Wireless Communications & Diversity Techniques in MIMO Systems	7
2.1 Multipath Effects	7
2.1.1 Fading in Wireless Propagation	8
2.1.2 Channel Classification Based on Direct-wave Component .	12
2.1.3 The Treatment of Multipath Phenomenon	14
2.2 Diversity Techniques in MIMO Systems	14
2.2.1 Classification of Diversity Schemes	14
2.2.2 Diversity Reception	16
2.2.3 Space-Time Transmit Diversity	17
2.3 Spatial Multiplexing in MIMO Systems	19
3 Propagation Modeling in the Mixture of NLOS & LOS Environ- ment for Outdoor MIMO System	21
3.1 Propagation Channel Modeling	22

CONTENTS

3.1.1	Channel Characteristics of NLOS & LOS path	22
3.1.2	General Model within a mixed NLOS & LOS Environment	23
3.1.3	SNR Analysis under MRC-like Effect	26
3.2	Evaluation of SNR Performance	27
3.2.1	Derivation of Functions for SNR Performance Evaluation .	27
3.2.2	Cases of 2×2 MIMO System	29
3.3	Application of the Model to ITS-IVC	30
3.3.1	Proposal of MIMO-ITS Model in A Right-turn Scenario . .	33
3.3.2	A Field Experiment	33
3.3.3	Analysis & Calculations	36
3.3.4	Evaluation of MIMO Merit	39
4	Spatial Correlation Modeling & Characterization with Three-dimensional APS of $\cos^n \theta$ for Indoor MIMO Terminal	43
4.1	Spatial Correlation Modeling	44
4.1.1	Previous 2D Spatial Correlation Models	44
4.1.2	3D Spatial Correlation Modeling	46
4.1.3	Spatial Correlation Approximation	48
4.2	Characterization of Spatial Correlation Performance	48
4.2.1	In the Case of APS with $\cos^n \theta$	48
4.2.2	Derivation of Functions for Spatial Correlation Characterization	49
4.2.3	Calculations of Existing Formulas by the New Expressions	52
4.3	An Example of Two-element MIMO Terminal	53
4.3.1	Matching of Angular Power Spectrum	53
4.3.2	Numerical Results	53
4.3.3	Measurements in a Reverberation Chamber	55
5	Conclusions & Future Work	61
5.1	Conclusions	61
5.2	Future Work	62
	Appendix	65
	Derivation of $\rho_{\mathbf{a},\mathbf{z}}(\Delta\mathbf{z})$	65

References	67
------------	----

CONTENTS

List of Figures

1.1	Structure and main contributions of the dissertation.	5
2.1	Direct and scattering waves in a multipath environment.	8
2.2	Signal power fluctuation vs range in wireless channels.	9
2.3	The Doppler power spectrum represents the average power of channel output as a function of Doppler frequency ν	10
2.4	The Delay power profile represents the average power of channel output as a function of delay τ	11
2.5	The Angular power spectrum is the average power as a function of angle θ	13
2.6	The 2×1 Alamouti's Space-time block coding transmission scheme.	17
3.1	The PDFs when $\sigma = 1$ and $x_0 = \sqrt{2}$	24
3.2	MIMO propagation channel in a mixture of NLOS and LOS environment with an obstacle inside.	25
3.3	Transmission cases based on the proposed model according to the number of LOS paths in 2×2 MIMO configuration.	30
3.4	The CDFs of output SNR of simulative and theoretical values for 5 cases of 2×2 MIMO propagation model, with $K = 9$ dB and $\gamma_D = 10$	31
3.5	A scenario of dangerous situations in traffic systems.	32
3.6	Applying MIMO to a right-turn collision scenario.	33
3.7	A field experiment for using MIMO in ITS-IVC in a shadowing environment.	34
3.8	The schematic plan view of the field experiment.	35

LIST OF FIGURES

3.9	Received signal power with respect to distance from intersection.	37
3.10	Moving average values of received level.	38
3.11	The CDFs of received power in MRC of the theoretical values and experimental values.	40
3.12	Evaluations of received power through distance from intersection of 10 to 50 m in the right-turn situation of ITS-IVC for SISO worst transmission, SISO best transmission, SIMO transmission using Tx#1 as transmitter, SIMO transmission using Tx#2 as transmitter and proposed MIMO transmission.	42
4.1	Widely used two-dimensional multipath propagation models.	45
4.2	An incident wave α with moving vector $\Delta\mathbf{r}$	47
4.3	A dipole array of two elements with vertical interval distance $d=\lambda$ and moving vector $\Delta\mathbf{r}$ with angular of $\{\phi_r, \theta_r\}$	54
4.4	The reception patterns in the case of $n = 0, 2, 8$ and the case of $n = 23$ which corresponds to the half-power beamwidth of the dipole array given in Fig. 4.3.	55
4.5	Spatial correlation calculations along x axis for the cases in which $n = 0, 2, 8$ and ∞ with aid of Eq. (4.26).	56
4.6	Spatial correlation calculations along z axis for the cases in which $n = 0, 2, 8$ and ∞ with aid of Eq. (4.27).	57
4.7	Spatial correlation calculations of theoretical value and approximated value for the case in which $n = 23$ and $\phi_r = 30^\circ, \theta_r = 45^\circ, 60^\circ$ and 90° , respectively.	58
4.8	Outside view of the chamber.	59
4.9	Performance comparison of spatial correlation of x and z axis in a reverberation chamber with the approximation values of $n = 2.75$ applying Eqs. (4.26) and (4.27).	60

Chapter 1

Introduction

1.1 An Overview of MIMO: History, Present and Future

With decades of research and experiments, the Multiple Input Multiple Output (MIMO) technology has been proposed to be one of the key technologies in the next-generation wireless communication systems for its significant improvement of link throughput and propagation reliability, and still attracts the attention of engineers and mathematicians because of its promising application to other fields such as Intelligent Transport Systems (ITS). MIMO technology includes smart antenna, which is also known as adaptive array antennas or multiple antennas with smart signal processing algorithms. Actually, the very first concepts in this field can be recalled back to the 1970s in the works of A.R. Kaye and D.A. George (1970) [1], Branderburg and Wyner (1974) [2] and W. van Etten (1975, 1976) [3, 4]. In 1980s, researchers in Bell Laboratories published several papers on beamforming related applications. And further with new approaches to the multi-antenna configuration respectively in the works of [5] and [6], which considered that multiple transmit antennas are co-located at one transmitter, MIMO theory has been driven to be a worldwide research theme with high expectations.

The first laboratory prototype implementing MIMO technique mainly by spatial multiplexing was demonstrated by Bell Labs in 1998, and the first commercial system was developed by Iospan Wireless Inc. in 2001 which used MIMO with or-

1. INTRODUCTION

thogonal frequency-division multiple access technology (MIMO-OFDMA). Today, for all upcoming 4G systems like WiMAX (Worldwide Interoperability for Microwave Access) and LTE (Long Term Evolution), MIMO technology is assumed as a standard technology to satisfy the needs of higher data rate and cell capacity.

1.2 Research on MIMO Technology: Modeling, Evaluating and Testing

MIMO propagation modeling, especially channel modeling is essential to the research of MIMO because of the usage of multiple antennas in MIMO systems. MIMO channel modeling is roughly categorized into two ways: a physical/geometry-based method and an analytical/correlation-based method. The physical channel modeling method focuses on the geometrical situation of transmission. Therefore, when applying the approach of physical channel modeling to an MIMO system, the distribution of scatters, including shadowing and obstacles, characterizes fading environments like Rayleigh or Nakagami-Rice fading. On the other hand, studies of MIMO channel modeling by an analytical method pays more attention to the angle of arrival (AOA) and angular power spectrum (APS) of waves in a multipath environment. For antenna designs and simulations, the analytical modeling method is preferred, as from this we can obtain the essential characteristics of a variety of channels without being too complicated. Even in the up-to-date research on MIMO technology such as cooperative MIMO and network MIMO, the study on channel modeling is still important and often will involve both of the two ways such as the proposed models in [7-10].

Given a framework that is expected to be able to describe the system propagation, investigations under different conditions are requested for the evaluation and characterization of system performance. Error probability, signal-to-noise ratio (SNR) and capacity are mostly used as the indices of a system performance. The error probability is a measure of the rate at which errors occur. The SNR is defined as the ratio of desired signal power to the noise power, and the capacity is a measure of the maximum data rate that can be supported by a channel with a given SNR and an arbitrarily small error probability. It provides an upper bound

(instead of the actual performance) of a communication system, and is a function of SNR, the number of transceiver array elements, the bandwidth and the channel characteristics. Between the error probability and capacity, the former is a more pragmatic indicator. It has several flavors including bit error rate (BER) and symbol error rate (SER). BER is most commonly used to indicate the reliability of a communication system.

For the MIMO system simulation, a channel emulator can be utilized to simulate how a terminal performs at the cell edge or inside the cell, add noise and describe what the channel looks like at a given speed. For example, to fully qualify the performance of a transmitter or receiver, a vector signal generator (VSG), a vector signal analyzer (VSA) and a channel emulator can be used to simulate a variety of different conditions.

Recently, the concept of MIMO-OTA (over the air) attracts attention and efforts because of its capability of building MIMO environments and testing MIMO systems from field to lab. When the results obtained by the MIMO-OTA measurement is very close to the field test results, the MIMO-OTA measurement would be a cost-effective solution for checking a MIMO wireless terminal. Moreover, the propagation environment emulated by the MIMO-OTA system are usually easy to re-produce. Thus the MIMO-OTA system can precisely compare the performance of different antenna configurations or terminals under exactly the same propagation environment. Recent reports and progress can be seen in [11-16].

1.3 Context of the Works

As the interest of applications of MIMO technology to industry areas increases, and the needs of characterization methods of an MIMO system are brought to our attention. In the conventional MIMO channel modeling that is physically motivated, multi-channel environment is often divided into a none-line-of-sight (NLOS) and a line-of-sight (LOS) situation. For example in the urban area where a base station is probably blocked from mobile users by numbers of buildings or trees, the signals of each array antenna are only propagated by scattering waves. Indoor MIMO environments are considered as a LOS situation since the received signals of each element contain a component of direct waves. Generally those

1. INTRODUCTION

models works well and can describe the channel statistics in most scenarios, as shown in the results of works [17-21]. But when it comes to more complicated cases such as the propagation in ITS, the existences of components of direct waves are properly different among sub-channels due to the traffic situations and road conditions.

As for the analytical MIMO modeling, spatial correlation functions that are applicable in three dimensional multipath environments are highly desired for multipath-rich scenarios. Many previous studies and reports like [22-24] have claimed that there is an elevation spread for several environments, and the multipath richness in those environments leads to a significant error due to azimuth-only assumption.

In a word, study of MIMO channel modeling and characterization are worth the effort for both researchers and engineers.

1.4 Main Contributions

The main contributions of this dissertation consist of several newly developed methods and solutions to the modeling and evaluation of MIMO systems in two ways.

Firstly, a general method for evaluating SNR performance of output signals in an outdoor MIMO maximal-ratio-combining (MRC) system is presented. As for the concerns we described in a situation that NLOS and LOS channels coexist and the numbers of NLOS and LOS channels are case-based, this proposal under adequate diversity techniques can not only involve conventional MIMO channel modeling but also handle the dramatic change case by case. The proposal and derived functions are verified to be effective and applicable by computer simulations and a field experiment [25].

Secondly, a general method for evaluating performances of the spatial correlation that is a main concern in analytical MIMO modeling is presented. The proposed method considering a three-dimensional APS expressed by the n th-power of a cosine function, gives closed-form expressions. The achieved solutions allow to consider radiation patterns in existing propagation scenarios, and the validity

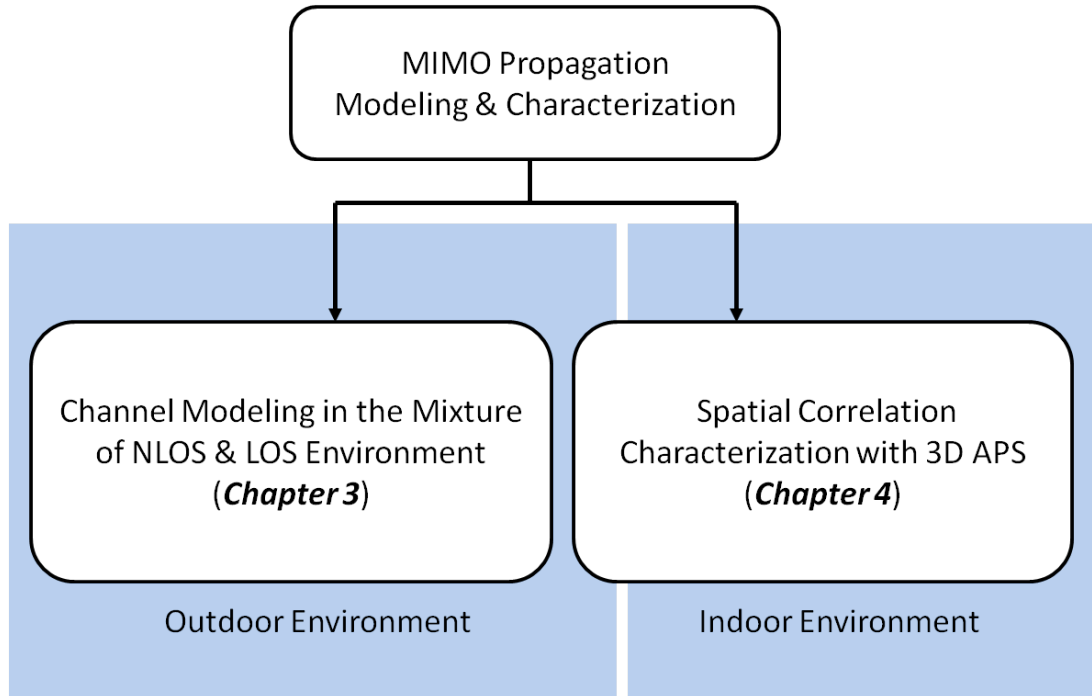


Figure 1.1: Structure and main contributions of the dissertation.

of the proposed method is verified by numerical results along with measurements in a reverberation chamber [26].

1.5 Outline of the Dissertation

The dissertation consists of five chapters, of which the authors main contributions are respectively presented in Chapter 3 and 4.

Chapter 2- In this chapter, we review the background of MIMO research in principles and techniques: the role of multipath and diversity theory. The behavior of wireless channel which is the essential of wireless communication is demonstrated. The associated multipath effects and the concepts of those are explained. In addition, as an effective approach against fading in multipath, diversity techniques including transmit diversity and combining techniques are introduced, of which Alamoutis space-time block coding (STBC) and MRC are the most widely cited techniques in diversity theory.

1. INTRODUCTION

Chapter 3- Channel modeling of MIMO system in a mixed LOS and NLOS environment is demonstrated, which forms the first contribution of the dissertation. The modeling is based on the physical/geometrical approach because single stream is characterized as either a NLOS or a LOS path according to the component of direct waves, and the achieved function can be generalized to estimate the MIMO channels in conventional NLOS and LOS environments. The kind of scenario can be found reasonable in some situations such as inter-vehicle communication (ITS-IVC). A field experiment conducted by Toyota Central R&D Labs in a related research is also introduced, and the data of that are used to verify the effectiveness of the proposed method.

Chapter 4- General functions for three-dimensional APS in the case of $\cos^n \theta$ which form the second contribution of the dissertation are demonstrated in this chapter. Unlike outdoor MIMO channels which sometimes can be assumed to be i.i.d, indoor and areas among high-rising buildings in a small area result in a multipath richness, which is always associated with strong spatial correlation. Without taking too much care of the physical properties of multipath environment like the distribution of scattering, an applicable method in an analytical way for characterizing spatial correlation performance is developed. The author focuses on the analysis of APS which is a combination of antenna effects and propagation properties of physical environment, and the supposed method can correspond to a variety of radiation patterns very conveniently with the help of generalized Hypergeometric functions. An array example is given for validation and the comparison result is fairly good.

Chapter 5- In this chapter we summary our dissertation with solid conclusions and in the meanwhile we highlight some interesting and promising directions for future research.

Chapter 2

Multipath in Wireless Communications & Diversity Techniques in MIMO Systems

In this chapter, we review the background of the MIMO research from the effect of multipath, which is the essential issue when conducting the wireless communication. We will also introduce the techniques which are used to treat the multipath effects, called diversity techniques. The knowledge of these is important for understanding history and trends of the MIMO research and is helpful to explain the contributions of our research to the MIMO technology.

2.1 Multipath Effects

When a signal propagating through the wireless channel arrives at the destination, it experiences a number of different paths due to scatters, ground reflection and diffraction as shown in Fig. [2.1](#). The propagation environment is collectively referred to as multipath. Multipath results in the fundamental issue in wireless communication: drop-off of the signal power. Hereafter, we introduce the multipath effects in terms of fading and propagation models of wireless channels so as to help understand the models which will be shown in the subsequent chapters in this dissertation.

2. MULTIPATH IN WIRELESS COMMUNICATIONS & DIVERSITY TECHNIQUES IN MIMO SYSTEMS

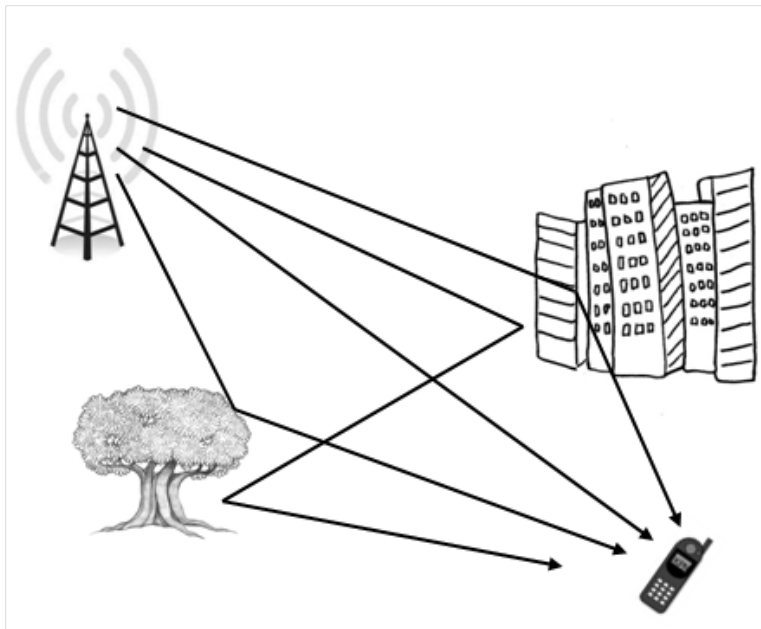


Figure 2.1: Direct and scattering waves in a multipath environment.

2.1.1 Fading in Wireless Propagation

Generally, the signal power drops off due to three reasons: mean path loss, macroscopic fading and microscopic fading.

Path loss- The path loss is the reduction in power attenuation of a radio wave when it propagates through space. It is range dependent and is influenced by many physical situations such as refraction, diffraction, reflection and absorption. In ideal free space propagation, the loss model of inverse square law is most used and the received signal power is given by

$$P_r = P_t \left(\frac{\lambda_c}{4\pi d} \right)^2 G_t G_r \quad (2.1)$$

where P_t , P_r are the transmitted and received power respectively, λ_c is the wave length, G_t , G_r are the power gains of transmit and receive antennas respectively and d is the range separation. Equation (2.1) is also known as Friis equation. In real environments such as macro-cellular and micro-cellular system, the path loss exponent varies from 2.5 to 4 in empirically based models such as the Okumura Hata, COST-231 and Erceg model [27-29].

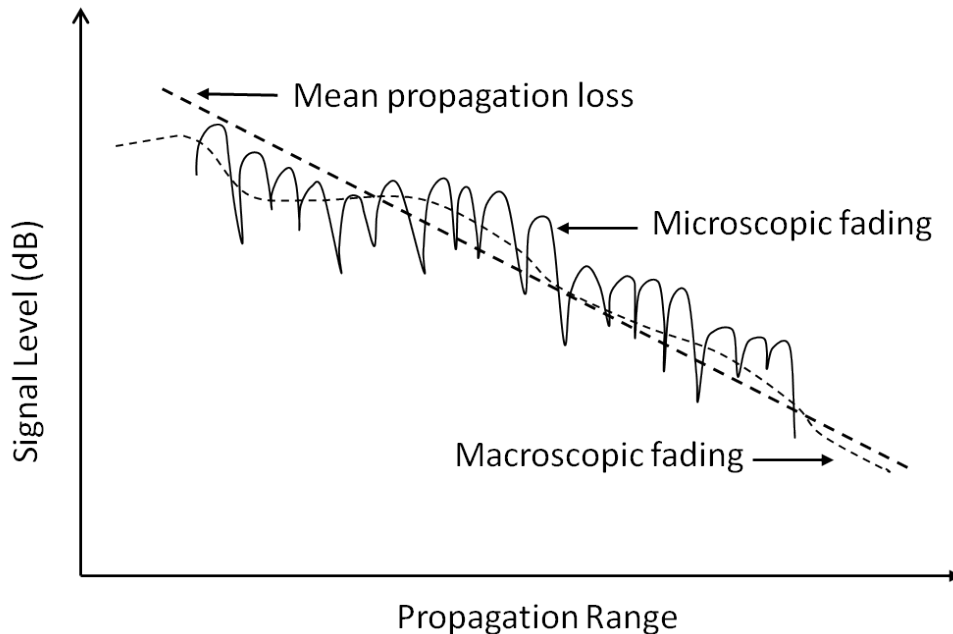


Figure 2.2: Signal power fluctuation vs range in wireless channels.

Macroscopic fading- This fading is also known as long-term fading or shadowing, and is an effect results from a blocking effect by buildings and natural features. Signals through the macroscopic fading will experience a long-term fluctuation with a statistical performance of a log-normal distribution. The probability density function (PDF) of the received power is then given by

$$f(x) = \frac{1}{\sqrt{2\pi}\sigma} e^{-\frac{(x-\mu)^2}{2\sigma^2}} \quad (2.2)$$

where x is a variable representing the long-term signal power in dB level, and μ , σ are the mean and standard deviations of x respectively.

Microscopic fading- Microscopic fading results from the constructive and destructive combination of a signal propagated through a multipath environment and is also known as short-term fading. It is caused by the scatterers between the link ends. Assuming that wireless signals are transmitted and reflected by a large number of independent scatterers, the effect of microscopic fading on wireless signals will lead to a Rayleigh density function for the envelope of the received

2. MULTIPATH IN WIRELESS COMMUNICATIONS & DIVERSITY TECHNIQUES IN MIMO SYSTEMS

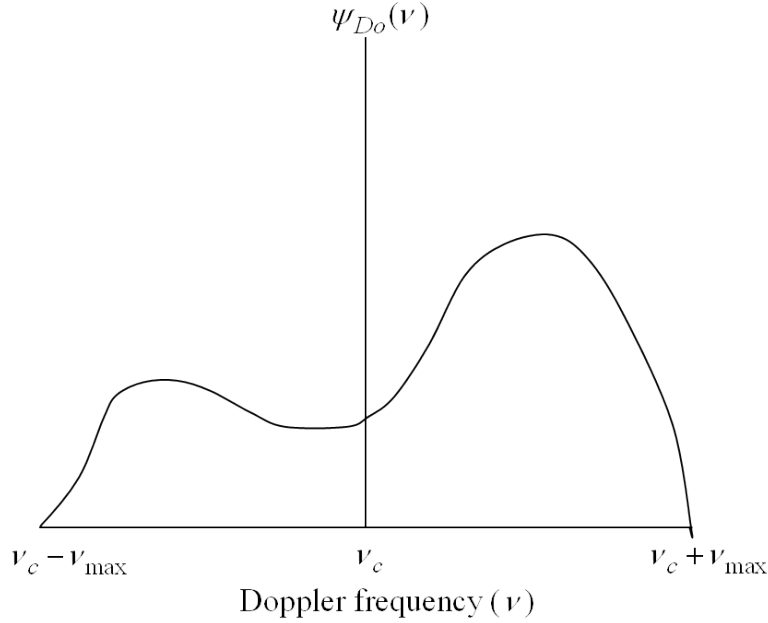


Figure 2.3: The Doppler power spectrum represents the average power of channel output as a function of Doppler frequency ν .

signal, given by

$$f(x) = \frac{2x}{\Omega} e^{-\frac{x^2}{\Omega}} \quad (2.3)$$

where Ω is the average received power with $\Omega = 2\sigma^2$.

Figure 2.2 shows the combined effects of path loss, macroscopic and microscopic fading on the received power in a wireless channel. Besides, there are also fading effects caused in wireless propagation by another dimension, called spread, which are represented as: Doppler spread, Delay spread and Angular spread respectively.

Doppler spread- The Doppler spread is resulted from time-varying fading which is due to the motion of scatterer or transceiver. Thus, a pure tone spreads over a finite spectral band. The Doppler power spectrum $\psi_{Do}(\nu)$, which is a function of the Doppler frequency ν describing the Fourier transform of the time autocorrelation of the channel response to a continuous wave tone, gives the average power of the channel output as shown in Fig. 2.3. Then the root mean square (RMS) bandwidth of $\psi_{Do}(\nu)$ is called the RMS Doppler spread, ν_{RMS} ,

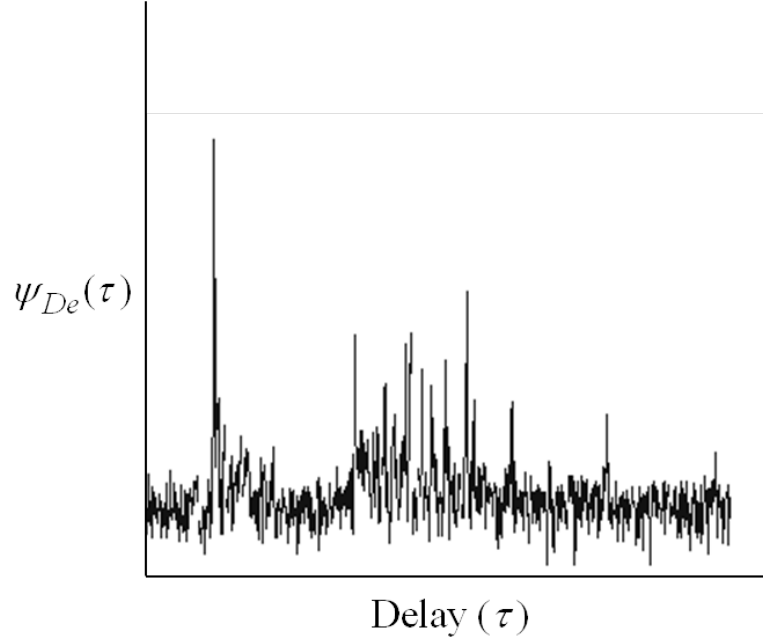


Figure 2.4: The Delay power profile represents the average power of channel output as a function of delay τ .

given by

$$\nu_{RMS} = \sqrt{\frac{\int_{\mathcal{F}} (\nu - \bar{\nu})^2 \psi_{Do}(\nu) d\nu}{\int_{\mathcal{F}} \psi_{Do}(\nu) d\nu}} \quad (2.4)$$

where \mathcal{F} represents the interval $\nu_c - \nu_{max} \leq \nu \leq \nu_c + \nu_{max}$ and $\bar{\nu}$ is the average frequency of the Doppler spectrum given by

$$\bar{\nu} = \frac{\int_{\mathcal{F}} \nu \psi_{Do}(\nu) d\nu}{\int_{\mathcal{F}} \psi_{Do}(\nu) d\nu} \quad (2.5)$$

For the case that scatterers uniformly exist around a terminal, the Doppler power spectrum has the classical U-shaped form, as approximated by the Jakes model [30].

Delay spread- The Delay spread is due to the delayed and scaled versions of the transmitted signal at the receiver in multipath propagation. It causes frequency-selective fading and is the span of path delays. The RMS delay spread

2. MULTIPATH IN WIRELESS COMMUNICATIONS & DIVERSITY TECHNIQUES IN MIMO SYSTEMS

of a channel, τ_{RMS} , is defined as

$$\tau_{RMS} = \sqrt{\frac{\int_0^{\tau_{max}} (\tau - \bar{\tau})^2 \psi_{De}(\tau) d\tau}{\int_0^{\tau_{max}} \psi_{De}(\tau) d\tau}} \quad (2.6)$$

where $\psi_{De}(\tau)$ is the multipath intensity profile or spectrum, τ_{max} is the maximum path delay and $\bar{\tau}$ is the average delay spread given by

$$\bar{\tau} = \frac{\int_0^{\tau_{max}} \tau \psi_{De}(\tau) d\tau}{\int_0^{\tau_{max}} \psi_{De}(\tau) d\tau}. \quad (2.7)$$

The spectrum which is the average power of channel output as a function of delay τ can be seen in Fig [2.4](#)

Angular spread- The Angular spread results in the space-selective fading, referring to the spread in AOAs of the multipath components at the receiver antenna array (AA) or that from the transmitter AA. Similarly, the angular spectrum $\psi_A(\theta)$, is the average power as a function of AOA θ as shown in Fig [2.5](#). The RMS angular spread θ_{RMS} is defined as

$$\theta_{RMS} = \sqrt{\frac{\int_{-\pi}^{\pi} (\theta - \bar{\theta})^2 \psi_A(\theta) d\theta}{\int_{-\pi}^{\pi} \psi_A(\theta) d\theta}} \quad (2.8)$$

where $\bar{\theta}$ is the mean AOA given by

$$\bar{\theta} = \frac{\int_{-\pi}^{\pi} \theta \psi_A(\theta) d\theta}{\int_{-\pi}^{\pi} \psi_A(\theta) d\theta}. \quad (2.9)$$

2.1.2 Channel Classification Based on Direct-wave Component

In the channel modeling, a single wireless channel can often be geometrically divided into a NLOS path and a LOS path.

NLOS- This is a condition where the signal encounters significant physical interference along the link path and only altered signals reach the receiving antenna. These altered signals have the tendency to interfere with each other, which often destructively results in serious multipath fading. The NLOS propagation will

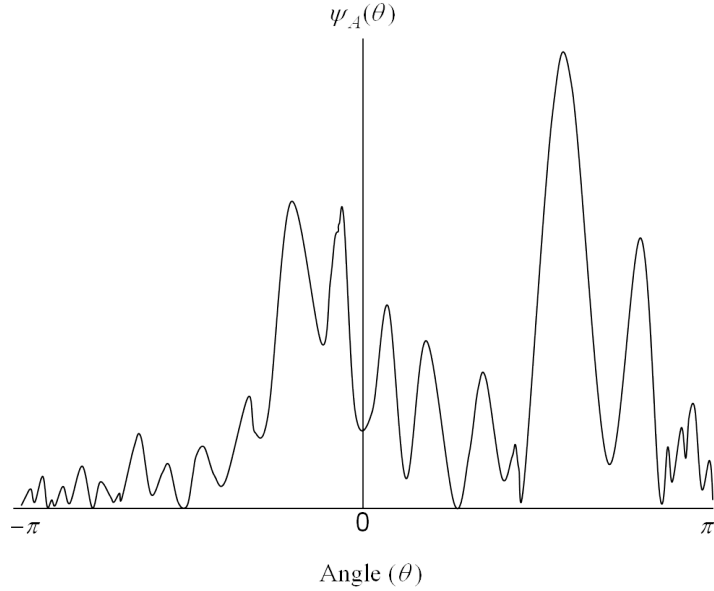


Figure 2.5: The Angular power spectrum is the average power as a function of angle θ .

make the a PDF of the envelope of signals to be a Rayleigh distribution, as shown in Eq. (2.3).

LOS- Under this condition, signals propagating as direct wave will not encounters any physical interference along the link path. In the LOS path, the envelope of received signal is no longer Rayleigh function, but a Nakagami-Rice distribution. Nakagami-Rice distribution is often defined in terms of Rice factor K , which is the ratio of the direct wave power of the channel to the power in the scattered component. The PDF of Nakagami-Rice distribution can be given by

$$f(x) = \frac{2x(K+1)}{\Omega} e^{(-K - \frac{(K+1)x^2}{\Omega})} I_0 \left(2x \sqrt{\frac{K(K+1)}{\Omega}} \right) \quad (2.10)$$

where Ω is the mean received power as defined in Eq. (2.3) and I_0 is the zero-order modified Bessel function of the first kind defined as

$$I_0(x) = \frac{1}{2\pi} \int_0^{2\pi} e^{-x \cos \theta} d\theta. \quad (2.11)$$

In fact, the NLOS path indicates a propagation environment where the power of direct wave component is zero, therefore it can be involved as a special case of

2. MULTIPATH IN WIRELESS COMMUNICATIONS & DIVERSITY TECHNIQUES IN MIMO SYSTEMS

LOS path. The statistics of NLOS signal can be obtained from the function of LOS path with the condition that $I_0(x) = 1$.

2.1.3 The Treatment of Multipath Phenomenon

It seems that the fading effect caused by multipath is completely an enemy for the transmission of wireless radio wave. However it is the case if a fading radio signal is received through only one channel, then the signal which experiences a deep fading could be lost and at the receiver side there is nothing that can be done. Creating multiple channels or branches that have different versions of the same signal provides the possibility of obtaining the transmitted signal even under different levels of fading and interferences. The concept of multipath forms the motivation of diversity techniques.

The diversity theory is an effective way to combat fading and channel interference. It refers to a method for improving the reliability of a message signal by using two or more propagation channels with different characteristics. Based on the fact that individual channels experience different levels of fading and interference, multiple versions of the same signal may be transmitted and/or received and combined in the receiver. Alternatively, a redundant forward error correction code may be added when different parts of the message are transmitted over different channels. Therefore the diversity techniques actually exploit the multipath propagation rather than suffer from it, and result in a diversity gain which is often measured in decibels.

2.2 Diversity Techniques in MIMO Systems

2.2.1 Classification of Diversity Schemes

Diversity schemes can generally be identified as follows:

Time diversity- Multiple versions of the same signal are transmitted at different time instants. Alternatively, a redundant forward error correction code is added and the message is spread in time by means of bit-interleaving before it is transmitted. Thus, error bursts are avoided, which simplifies the error correction.

2.2 Diversity Techniques in MIMO Systems

Frequency diversity- The signal is transmitted using several frequency channels or spread over a wide spectrum that is affected by frequency-selective fading. Middle-late 20th century microwave radio relay lines often used several regular wide-band radio channels, and one protection channel for automatic use by any faded channel. Later examples include OFDM modulation in combination with sub-carrier interleaving and forward error correction. There is also spread spectrum, for example frequency hopping or Direct Spread Code Division Multiple Access (DS-CDMA).

Space diversity- The signal is transmitted over several different propagation paths. In the case of wired transmission, this can be achieved by transmitting via multiple wires. In the case of wireless transmission, it can be achieved by antenna diversity using multiple transmitter antennas (transmit diversity) and/or multiple receiving antennas (reception diversity). In the latter case, a diversity combining technique is applied before further signal processing takes place. If the antennas are far apart, for example at different cellular base station sites or Wireless Local Area Networks (WLAN) access points, this is called macro-diversity or site diversity. If the antennas are at a distance in the order of one wavelength, this is called micro-diversity. A special case is phased antenna arrays, which also can be used for beam-forming, MIMO and Spacetime coding.

Polarization diversity- Multiple versions of a signal are transmitted and received via antennas with different polarizations. A diversity combining technique is applied on the receiver side.

Multiuser diversity- Multiuser diversity is obtained by opportunistic user scheduling at either the transmitter or the receiver. Opportunistic user scheduling is as follows: the transmitter selects the best user among candidate receivers according to the qualities of each channel between the transmitter and each receiver. In Frequency Division Duplex (FDD) systems, a receiver must feedback the channel quality information to the transmitter with the limited level of resolution.

Cooperative diversity- Achieves antenna diversity gain by using the cooperation of distributed antennas belonging to each node.

From the preceding introduction it is clear that the utilization of time/frequency diversity incurs an expense of time in the case of time diversity and bandwidth in the case of frequency diversity to introduce redundancy. Space diversity is an

2. MULTIPATH IN WIRELESS COMMUNICATIONS & DIVERSITY TECHNIQUES IN MIMO SYSTEMS

attractive alternative that does not sacrifice those. In the meantime it provides array gain from AAs. Because of these features, space diversity is used in MIMO systems against multipath fading.

In addition to realize diversity effect, transmitting scheme and combining technique are required in either transmitter or receiver side. The techniques in receiver side have been thoroughly researched in previous studies, and researches of transmitting techniques of diversity are still attractive, especially as AA is applied in today's wireless communication system. In the dissertation, we focus on space diversity and elaborate on the transmit techniques and combining techniques in the case of space diversity.

2.2.2 Diversity Reception

The diversity gain is obtained by the sum of multiple versions of the same signal. Within combining them from various approaches are three common techniques: Selection Combining, Equal Gain Combining (EGC) and MRC.

Selection Combining- This scheme selects the antenna branch with the best SNR. The scheme is often used in the case of two received antennas because of the simplicity of the configuration.

Equal Gain Combining- All the received signals are summed coherently in this scheme. The phase is adjusted for each receive signal so that signals from each branch are co-phased and vectors add in-phase. Therefore the EGC enables better performance than selection diversity, and is almost as good as MRC, but less complex in terms of signal processing.

Maximal Ratio Combining- The received signals are weighted with respect to their SNR and then summed. In this scheme, the channel state information (CSI) is required for the determination of weights so it performs the best SNR performance with the highest complexity. The resulting SNR yields $\sum_{k=1}^N \text{SNR}_k$ where SNR_k is SNR of the received signal k .

From the viewpoint of obtaining best SNR performance, MRC scheme is considered the most optimal.

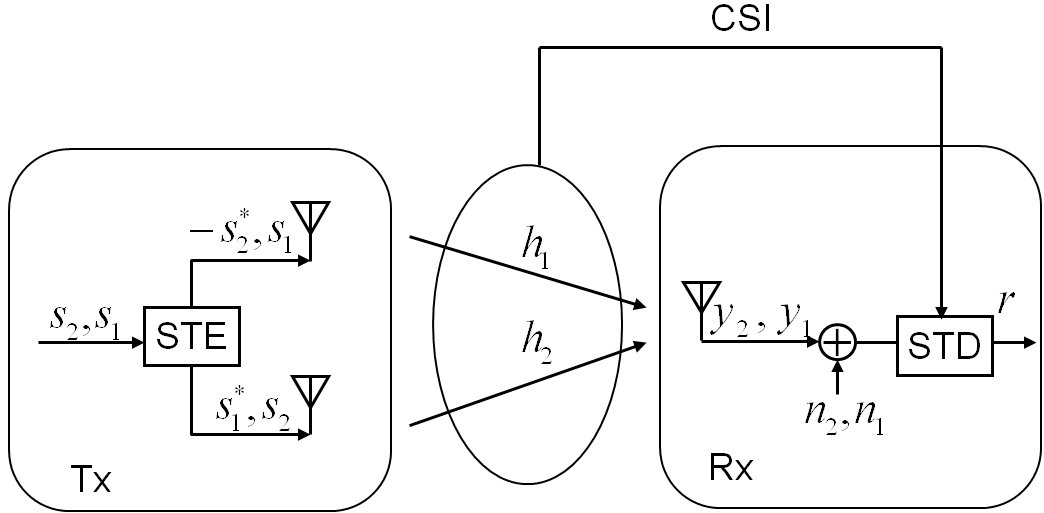


Figure 2.6: The 2×1 Alamouti's Space-time block coding transmission scheme.

2.2.3 Space-Time Transmit Diversity

The MRC scheme enables diversity gain with the best SNR performance when CSI is available at the receiver. It is reasonable that if the requirement of CSI at the transmit side is satisfied perfectly, a transmit diversity technique in which signals are pre-weighted before being transmitted should work as well as that at the receiver. However that requirement is much more difficult than the case at the receiver because of the requisite of feedback or reciprocity for channel estimation. To enjoy the transmit diversity gain without knowing CSI, a simple and effective method is proposed by Alamouti in 1998 [31], in which the data stream is encoded in blocks and distributed among spaced antennas and across time called STBC scheme.

The 2×1 Alamouti STBC transmission scheme is presented in Fig. 2.6, where (*) denotes complex conjugate. Propagated through the wireless environment the received signals can be expressed as

$$\begin{bmatrix} y_1 \\ y_2 \end{bmatrix} = \frac{1}{\sqrt{2}} \begin{bmatrix} s_1 & s_2 \\ -s_2^* & s_1^* \end{bmatrix} \begin{bmatrix} h_1 \\ h_2 \end{bmatrix} + \begin{bmatrix} n_1 \\ n_2 \end{bmatrix} \quad (2.12)$$

2. MULTIPATH IN WIRELESS COMMUNICATIONS & DIVERSITY TECHNIQUES IN MIMO SYSTEMS

or in an alternative way as

$$\begin{bmatrix} y_1 \\ y_2^* \end{bmatrix} = \frac{1}{\sqrt{2}} \begin{bmatrix} h_1 & h_2 \\ h_2^* & -h_1^* \end{bmatrix} \begin{bmatrix} s_1 \\ s_2 \end{bmatrix} + \begin{bmatrix} n_1 \\ n_2^* \end{bmatrix} \quad (2.13)$$

where r_1 and r_2 are the received signals and n_1 and n_2 are complex random variables representing noise and interference. With CSI available at the receiver, the combined signal r under weight H_e^H can be obtained by

$$r = H_e^H y = \frac{1}{\sqrt{2}} (|h_1|^2 + |h_2|^2) s + H_e^H n \quad (2.14)$$

As we can see, by taking two time-slots to transmit two symbols in such an encoded way, it in fact exploits the orthogonality of codes into the spatial domain. The Alamouti STBC concept has a significant impact on not only diversity theory but also the wireless communications industry, however it is limited to no more than two transmit antennas. From then on many other space-time codes like Quasi-OSTBC are developed for more than 2 transmit antennas. Although there are several forms of QOSTBC such as those in [32-35], Alamouti's STBC is proved to be the only one that achieve full-diversity and full-rate. Here one QOSTBC coding scheme from [33] which allows four transmit antennas with full-rate effect is introduced, given by

$$S = \begin{bmatrix} s_1 & s_2 & s_3 & s_4 \\ -s_2^* & s_1^* & -s_4^* & s_3^* \\ -s_3^* & -s_4^* & s_1^* & s_2^* \\ s_4 & -s_3 & -s_2 & s_1 \end{bmatrix} \quad (2.15)$$

MIMO exploits AAs at both sides of the link. When the signal is transmitted from an antenna at the transmitter to another one at the receiver, the transmission scheme is generally called Single-Input Single-Output (SISO). Similarly, there are SIMO and MISO transmission schemes which correspond to Single-Input Multi-Output and Multi-Input Single-Output system, respectively. Since SISO scheme does not allow any space diversity, at least SIMO or MISO is needed for acquiring the diversity gain. Further, in the case of SIMO scheme reception diversity techniques are required for the combination of signals and in the case of MISO scheme transmit diversity techniques are necessary.

2.3 Spatial Multiplexing in MIMO Systems

Taking advantages of the multipath reflections of the signals and adequate diversity techniques, each antenna-radio chain in a MIMO system is a linear combination of the multiple transmitted data streams. The data streams are separated at the receiver using MIMO algorithms that rely on estimates of all channels between each transmitter and each receiver. Therefore we say MIMO employs multiple, spatially separated antennas to take advantages of multiple environment and transfer more data, rather than to bear fading only. In addition to multiplying throughput, range is increased because of an antenna diversity advantage, since each receive antenna has a measurement of each transmitted data stream. With MIMO, the maximum data rate per channel grows linearly with the number of different data streams that are transmitted in the same channel.

In addition to the above, there are also other techniques are used in a MIMO system to improve system performance. Spatial multiplexing is one of these for the purpose of improvement of system capacity and data rate. Unlike the diversity technique in which a single stream is transmitted, the spatial multiplexing technique is a transmission technique that transmits multiple streams from each of the multiple transmit antennas. In spatial multiplexing, a high rate signal is split into multiple lower rate streams and each stream is transmitted from a different transmit antenna in the same frequency channel. If these signals arrive at the receiver antenna array with sufficiently different spatial signatures, the receiver can separate these streams into (almost) parallel channels. Therefore, the space dimension is reused, or multiplexed, more than one time.

If the transmitter is equipped with N_t antennas and the receiver has N_r antennas, the maximum spatial multiplexing order (the number of streams) is,

$$N_s = \min(N_t, N_r) \tag{2.16}$$

if a linear receiver is used. This means that N_s streams can be transmitted in parallel, ideally leading to an N_s increase of the spectral efficiency (the number of bits per second and per Hz that can be transmitted over the wireless channel). The practical multiplexing gain can be limited by spatial correlation, which means that some of the parallel streams may have very weak channel gains.

2. MULTIPATH IN WIRELESS COMMUNICATIONS & DIVERSITY TECHNIQUES IN MIMO SYSTEMS

Chapter 3

Propagation Modeling in the Mixture of NLOS & LOS Environment for Outdoor MIMO System

Taking advantage of diversity technique, multiple channels can be most used for transferring wireless signals synchronously so as to achieve high data rate and increase system capacity. The knowledge of characteristics of propagation and correlation consequently becomes the key issue for benefiting from MIMO system. In this chapter, the channel modeling and channel characteristics in outdoor environment with a relatively low co-channel interference are concerned. In previous studies, propagation modeling for outdoor MIMO system has been widely studied, involving the efforts from such as [36-39] which are based on a LOS environment to those of [40-42] which are based on a NLOS environment. These propagation models have been confirmed to be useful both in their supposed situations.

However, there are still many scenarios which are overlooked. They exist in a medium or relatively short range of transmission. For example in a street range transmission, the multiple channels between base station or transmitter and terminals or receivers could be greatly affected by the road status and traffic situations, and leads to an influence on the propagation model within that. This

3. PROPAGATION MODELING IN THE MIXTURE OF NLOS & LOS ENVIRONMENT FOR OUTDOOR MIMO SYSTEM

result should not be ignored, and it is properly can be explained by a different modeling method. The attention to this issue attracts our interest of study, and the development we made contributes to the main content of this chapter.

3.1 Propagation Channel Modeling

3.1.1 Channel Characteristics of NLOS & LOS path

Propagation modeling of MIMO transmission provides an approach for evaluating MIMO system, including of the characteristics of output combined signals. As we have known, wireless signals through a NLOS environment experience a Rayleigh fading and those through a LOS environment experience a Nakagami-Rice fading. We would like to further investigate the channel characteristics in terms of mean power of transmitted signal.

For signals experiencing Rayleigh fading with the envelope of x , an Exponential distribution function can be used to describe the PDF characteristic of signal power, given by

$$f(z) = \frac{1}{z_S} e^{-\frac{z}{z_S}} \quad (3.1)$$

where $z = x^2$ and $z_S = \Omega = 2\sigma^2$, physically meaning scattering wave power in NLOS path.

Once again, the PDF of envelope of signal in LOS path can be rewritten from Eq. (2.10) with the direct-wave signal amplitude x_0 and σ , given by

$$f(x) = \frac{r}{\sigma^2} e^{-\frac{x_0^2+x^2}{2\sigma^2}} I_0\left(\frac{x_0 x}{\sigma^2}\right) \quad (3.2)$$

The mean power of signal in a LOS environment then has a PDF of a non-central χ^2 distribution, given by

$$f(z) = \frac{1}{2\sigma^2} e^{-\frac{z_D+z}{2\sigma^2}} I_0\left(\frac{\sqrt{z_D z}}{\sigma^2}\right) \quad (3.3)$$

where there is $z_D = x_0^2$ and is the direct wave power of signal through the LOS path. Instituting the definition of z_S and Rice factor defined by $K = \frac{z_D}{z_S}$, it can be rewritten as

$$f(z) = \frac{1}{z_S} e^{-\left(K+\frac{z}{z_S}\right)} I_0\left(2\sqrt{\frac{Kz}{z_S}}\right). \quad (3.4)$$

The PDFs of Rayleigh distribution, Nakagami-Rice distribution, Exponential distribution and non-central χ^2 distribution with $\sigma = 1$ and $x_0 = \sqrt{2}$ is shown in Fig. 3.1, respectively.

3.1.2 General Model within a mixed NLOS & LOS Environment

For multiple channels of MIMO system in urban or cell areas, the physical conditions of each sub-channel are likely to be the same due to the relatively short intervals among array antennas compared with transmission distance. However, sub-channels through which signals experience different propagation do exist in some real communication environments. We give a general framework for the kind of MIMO configuration with mixed NLOS-and-LOS channels, involving the conventional model within a NLOS-only or a LOS-only environment as a special case.

Figure 3.2 illustrates the propagation channel model of MIMO system with N_t transmit antennas, N_r receive antennas and an obstacle inside the propagation route. The system is assumed to be surrounded by scatterers. The inside obstacle leads to a shadowing environment for some sub-channels. Therefore in the mixed NLOS and LOS MIMO transmission, multipath waves are always in existence and the number of NLOS paths geometrically depends on the size and location of the obstacle inside.

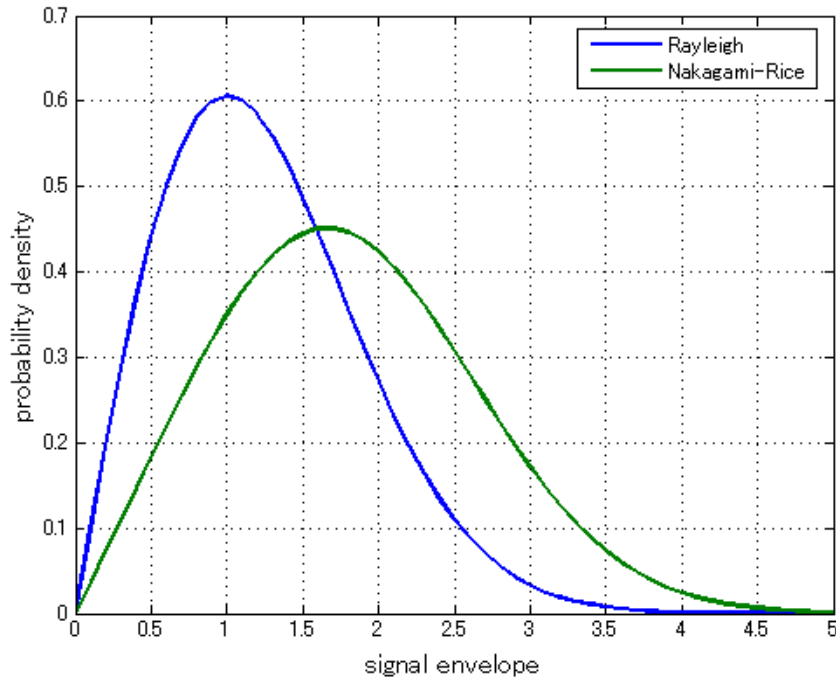
The channel matrix H is given as

$$H = \begin{pmatrix} h_{11} & h_{12} & \dots & h_{1N_t} \\ h_{21} & h_{22} & \dots & h_{2N_t} \\ \vdots & \vdots & \ddots & \vdots \\ h_{N_r1} & h_{N_r2} & \dots & h_{N_rN_t} \end{pmatrix} \equiv \{h_{n_r n_t}\} \quad (3.5)$$

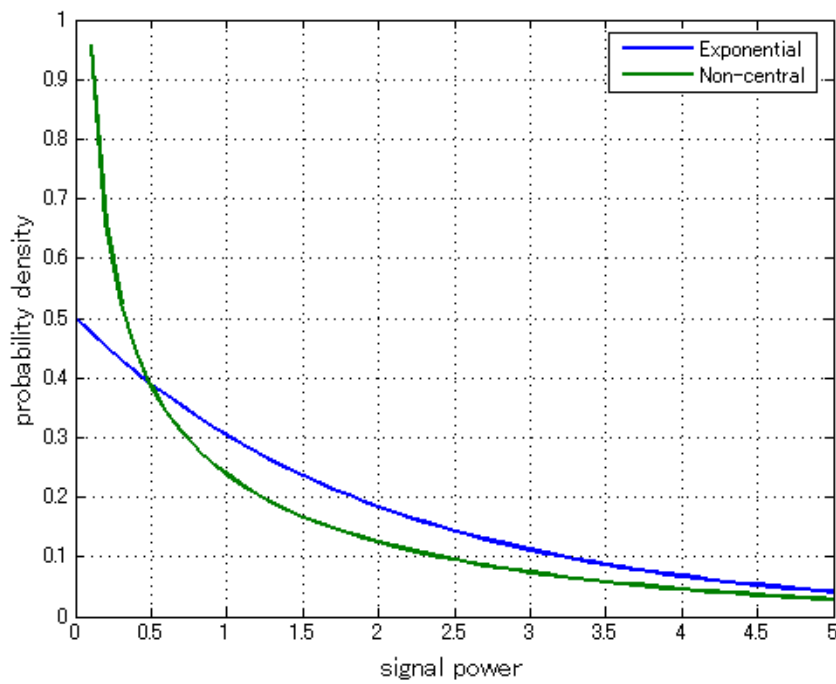
To represent the direct wave and scattering wave components of the channel matrix as H_D and H_S respectively, Eq. (3.5) can be written as

$$H = \sqrt{z_D} H_D + \sqrt{z_S} H_S \quad (3.6a)$$

3. PROPAGATION MODELING IN THE MIXTURE OF NLOS & LOS ENVIRONMENT FOR OUTDOOR MIMO SYSTEM



(a) Rayleigh distribution and Nakagami-Rice distribution



(b) Exponential distribution and non-central χ^2 distribution

Figure 3.1: The PDFs when $\sigma = 1$ and $x_0 = \sqrt{2}$.

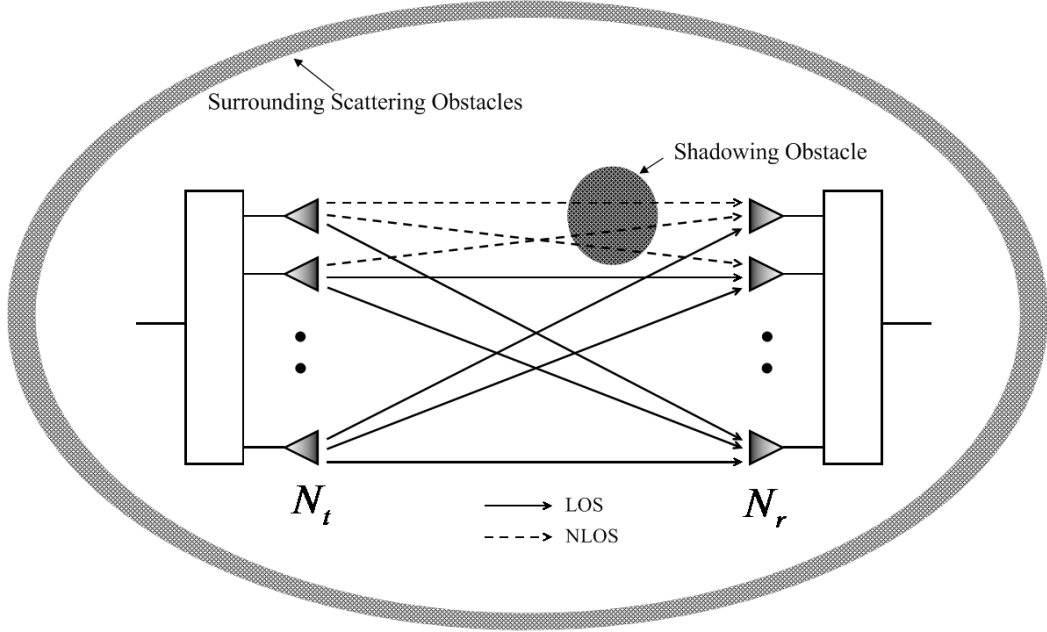


Figure 3.2: MIMO propagation channel in a mixture of NLOS and LOS environment with an obstacle inside.

where

$$H_D \equiv \{ u_{n_r n_t} \} \quad (3.6b)$$

$$H_S \equiv \{ v_{n_r n_t} \} \quad (3.6c)$$

Assuming channels are independent and identically distributed(i.i.d), $u_{n_r n_t}$ and $v_{n_r n_t}$ satisfy that

$$u_{n_r n_t} = \begin{cases} 1 & \text{for } LOS \\ 0 & \text{for } NLOS \end{cases} \quad (3.6d)$$

$$\langle v_{n_r n_t}^* v_{n'_r n'_t} \rangle = \begin{cases} 1 & \text{for } n_t = n'_t \text{ and } n_r = n'_r \text{ (i.i.d)} \\ 0 & \text{for } n_t \neq n'_t \text{ or } n_r \neq n'_r \end{cases} \quad (3.6e)$$

respectively. The notations n_t, n'_t represent transmit antenna numbers while the notations n_r, n'_r represent receive antenna numbers.

3. PROPAGATION MODELING IN THE MIXTURE OF NLOS & LOS ENVIRONMENT FOR OUTDOOR MIMO SYSTEM

3.1.3 SNR Analysis under MRC-like Effect

It is already known that MRC is the optimal combining technique in terms of maximizing the SNR at the combined output. To enjoy the benefits of MIMO transmission besides MRC effect, known as MIMO-MRC system, Alamouti's STBC method (see [31]) provides a simple and attractive scheme to realize full-rate and full-diversity transmission in complex signal space. Although it is proved that this coding method doesn't exist for systems with more than two transmit antennas, the full-diversity property can still be obtained to achieve the MRC-like effect by other designs such as non-full-rate STBC schemes (see [35]). From this viewpoint, it is very promising and also reasonable to investigate MIMO propagation performance under the assumption of MRC-like effect for single-stream transmission.

Most of these methods are derived from Alamouti's orthogonal-STBC method. In such a system with $N_t > 2$, the SNR of output signal, γ , is proved to be proportional to the *Frobenius* norm of channel matrix H , given as

$$\gamma = \| H \|_F^2 \gamma_{ref} \quad (3.7)$$

where

$$\| H \|_F^2 \equiv \sum_{n_t=1}^{N_t} \sum_{n_r=1}^{N_r} |h_{n_r n_t}|^2 \quad (3.8)$$

and γ_{ref} is the SNR normalized by the root of N_t , which is resulted from disability of coding gain in STBC scheme, given as

$$\gamma_{ref} = \frac{1}{N_t} \gamma_0 \quad (3.9)$$

where γ_0 is the system SNR when $N_t = N_r = 1$.

Representing the number of NLOS and LOS paths as N_{NLOS} and N_{LOS} respectively, there is

$$N_{\text{NLOS}} + N_{\text{LOS}} = N_t N_r \quad (3.10)$$

where $N_t N_r$ is the total independent channels. Similarly, representing the SNR of signals in a NLOS path and a LOS path as γ_{NLOS} and γ_{LOS} respectively, we have

$$\gamma = \sum_{i=1}^{N_{\text{NLOS}}} \gamma_{\text{NLOS}}^{(i)} + \sum_{j=1}^{N_{\text{LOS}}} \gamma_{\text{LOS}}^{(j)} \quad (3.11)$$

according to the MRC theory.

3.2 Evaluation of SNR Performance

We investigate the PDF of output SNR for the proposed model.

3.2.1 Derivation of Functions for SNR Performance Evaluation

According to the *Frobenius* norm equation of Eq. (3.7), the PDF of SNR of a single channel is proportional to the mean power of transmitted signals. Thus, with knowing the PDFs of power of signals in a NLOS or LOS environment beforehand, the PDF of SNR of each sub-channel is obtained and then the sum of them according to the MRC theory.

Consequently, for a LOS sub-channel in which signal amplitude follows Nakagami-Rice distribution, the PDF of SNR can be considered as a non-central χ^2 distribution according to Eq. (3.3) or (3.4), given by

$$f_{\text{LOS}}(\gamma) = \frac{K}{\gamma_D} \exp \left\{ -K \left(1 + \frac{\gamma}{\gamma_D} \right) \right\} I_0 \left(2K \sqrt{\frac{\gamma}{\gamma_D}} \right) \quad (3.12)$$

where γ_D is the SNR of direct wave signal and $I_0(\cdot)$ is the modified Bessel function of the first kind with order zero. The PDF of SNR for a NLOS sub-channel is given as an Exponential distribution according to Eq. (3.1), written as

$$f_{\text{NLOS}}(\gamma) = \frac{1}{\gamma_S} \exp \left(-\frac{\gamma}{\gamma_S} \right) \quad (3.13)$$

where γ_S is the average SNR of multipath scattering wave signal. Using the definition of Rice factor K , Eq. (3.13) can be rewritten as

$$f_{\text{NLOS}}(\gamma) = \frac{K}{\gamma_D} \exp \left(-\frac{K\gamma}{\gamma_D} \right) \quad (3.14)$$

This expression including the factor K seems curious in conventional NLOS environment, but in this case, it seems reasonable because the direct signal level can be estimated from other LOS paths.

3. PROPAGATION MODELING IN THE MIXTURE OF NLOS & LOS ENVIRONMENT FOR OUTDOOR MIMO SYSTEM

To obtain the combined output γ in Eq. (3.7), a convenient processing is frequently used, known as moment-generating function calculation. The moment-generating functions for $f_{\text{LOS}}(\gamma)$ and $f_{\text{NLOS}}(\gamma)$ can be obtained through Laplace transforms $\mathcal{L}[\cdot]$, and the results are given as

$$F_{\text{LOS}}(s) \equiv \mathcal{L}[f_{\text{LOS}}(\gamma)] = \left(\frac{K}{K + \gamma_D s} \right) \exp \left(-\frac{K \gamma_D s}{K + \gamma_D s} \right) \quad (3.15)$$

and

$$F_{\text{NLOS}}(s) \equiv \mathcal{L}[f_{\text{NLOS}}(\gamma)] = \frac{K}{K + \gamma_D s} \quad (3.16)$$

respectively. Then the function $F_{\text{MRC}}(s)$ for the desired γ in MIMO-MRC system should be given by

$$F_{\text{MRC}}(s, N_{\text{NLOS}}, N_{\text{LOS}}) = \{F_{\text{NLOS}}(s)\}^{N_{\text{NLOS}}} \{F_{\text{LOS}}(s)\}^{N_{\text{LOS}}} \quad (3.17)$$

Substituting (3.15) and (3.16) into (3.17), we have

$$F_{\text{MRC}}(s, N_{\text{LOS}}, N_{\text{NLOS}}) = \exp \left(-\frac{K N_{\text{LOS}} \gamma_D s}{K + \gamma_D s} \right) \left(\frac{K}{K + \gamma_D s} \right)^{(N_{\text{LOS}} + N_{\text{NLOS}})} \quad (3.18)$$

Then the PDF of SNR for the combined signal can be given by the inverse Laplace transformation $\mathcal{L}^{-1}[\cdot]$ as

$$f_{\text{MRC}}(\gamma, N_{\text{LOS}}, N_{\text{NLOS}}) = \mathcal{L}^{-1}[F_{\text{MRC}}(s, N_{\text{LOS}}, N_{\text{NLOS}})] \quad (3.19)$$

The derivation of (3.19) is probably too complex. With the implementation of modern package like Mathematica software, the final result can be readily approximated to be

$$\begin{aligned} f_{\text{MRC}}(\gamma, N_{\text{LOS}}, N_{\text{NLOS}}) &= \frac{K}{\Gamma(N_{\text{LOS}} + N_{\text{NLOS}}) \gamma_D} \left(\frac{K \gamma}{\gamma_D} \right)^{N_{\text{LOS}} + N_{\text{NLOS}}} \\ &\times \exp \left\{ -K \left(N_{\text{LOS}} + \frac{\gamma}{\gamma_D} \right) \right\} \\ &\times {}_0F_1 \left(N_{\text{LOS}} + N_{\text{NLOS}} ; \frac{K^2 N_{\text{LOS}} \gamma}{\gamma_D} \right) \end{aligned} \quad (3.20)$$

where ${}_0F_1(\cdot)$ denotes a Hypergeometric function and $\Gamma(\cdot)$ denotes a Gamma function. Given the relation of

$${}_0F_1(a; x) = \Gamma(a) \frac{I_{a-1}(2\sqrt{x})}{x^{(a-1)/2}} \quad (3.21)$$

where $I_{a-1}(\cdot)$ is the modified Bessel function of the first kind with order $a - 1$, Eq. (3.20) can be also rewritten as

$$\begin{aligned}
 f_{\text{MRC}}(\gamma, N_{\text{LOS}}, N_{\text{NLOS}}) &= \left(\frac{K}{\gamma_D}\right) \left(\frac{\gamma}{N_{\text{LOS}}\gamma_D}\right)^{(N_{\text{LOS}}+N_{\text{NLOS}}-1)/2} \\
 &\times \exp\left\{-K\left(N_{\text{LOS}} + \frac{\gamma}{\gamma_D}\right)\right\} \\
 &\times I_{N_{\text{LOS}}+N_{\text{NLOS}}-1}\left(2K\sqrt{\frac{N_{\text{LOS}}\gamma}{\gamma_D}}\right). \quad (3.22)
 \end{aligned}$$

Equation (3.22) provides a general function for evaluating the statistic characteristics of SNR performance, which corresponds to a NLOS or LOS and even a mixed NLOS-and-LOS environment. For the cases of $N_{\text{LOS}} = 0$ or $N_{\text{NLOS}} = 0$, it reduces to the PDF of combined output SNR for customary MIMO transmission in a Rayleigh-fading or Nakagami-rice-fading environment, respectively.

3.2.2 Cases of 2×2 MIMO System

Modeling in the mixture of NLOS and LOS environments for MIMO propagation may appear as different cases. For example in 2×2 MIMO system with one sub-channel in shadowing, there are 4 cases according as which one of all sub-channels is shadowed. However after combined by MRC, the output SNRs of those cases will perform the same. Also through the derivations in the previous subsection, it can be found out that SNR characteristic in Eq. (3.22) are only concerned with numbers of NLOS sub-channels and LOS sub-channels because the combined output does not distinguish the signal components. Therefore these 4 cases are considered as the same kind of channel model structure. From the standpoint of model setup, we divide all possible cases into 5 kinds. We mark them from case 0 to case 4 according to the number of LOS sub-channels, as presented in Fig. 3.3. Notice that case 0 and case 4 actually represents a conventional NLOS environment and LOS environment, respectively.

For each case of the 2×2 MIMO configuration with $N_{\text{NLOS}} + N_{\text{LOS}} = 4$, the PDF of combined SNR can be calculated by Eq. (3.22). And we compare the simulations and theoretical values for each case by cumulative distribution functions (CDF), as shown in Fig. 3.4. For simulation method, we consider

3. PROPAGATION MODELING IN THE MIXTURE OF NLOS & LOS ENVIRONMENT FOR OUTDOOR MIMO SYSTEM

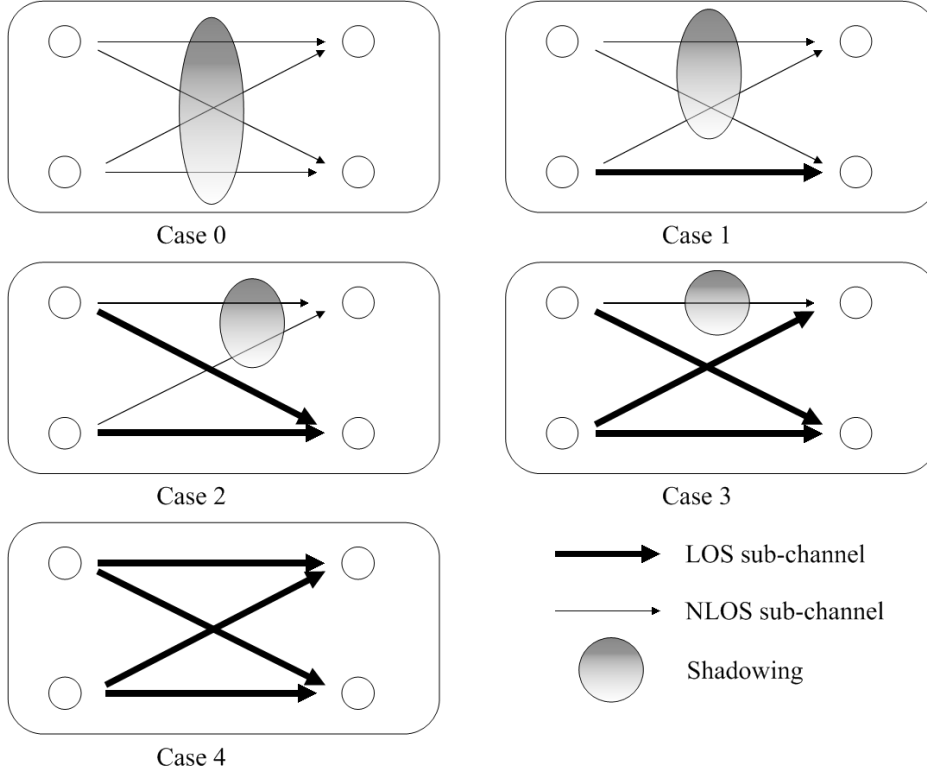


Figure 3.3: Transmission cases based on the proposed model according to the number of LOS paths in 2×2 MIMO configuration.

each LOS sub-channel by Nakagami-Rice distributed signals and each NLOS sub-channel by Rayleigh distributed signals. And the scattering wave components in LOS sub-channels are set equal to those of NLOS sub-channels. For simulation conditions, the value of Rice factor K is set equal to 9 dB and γ_D is set equal to 10. The theoretical values are calculated by Eq. (3.22) under the same transmission conditions. As the result has shown, for a sufficiently precise estimation by 10^{-5} the simulation results are completely in agreement with the theoretical results.

3.3 Application of the Model to ITS-IVC

The study on ITS is more and more active in recent years (see [43-46]). Application of wireless technology to ITS enables information communication so as to let

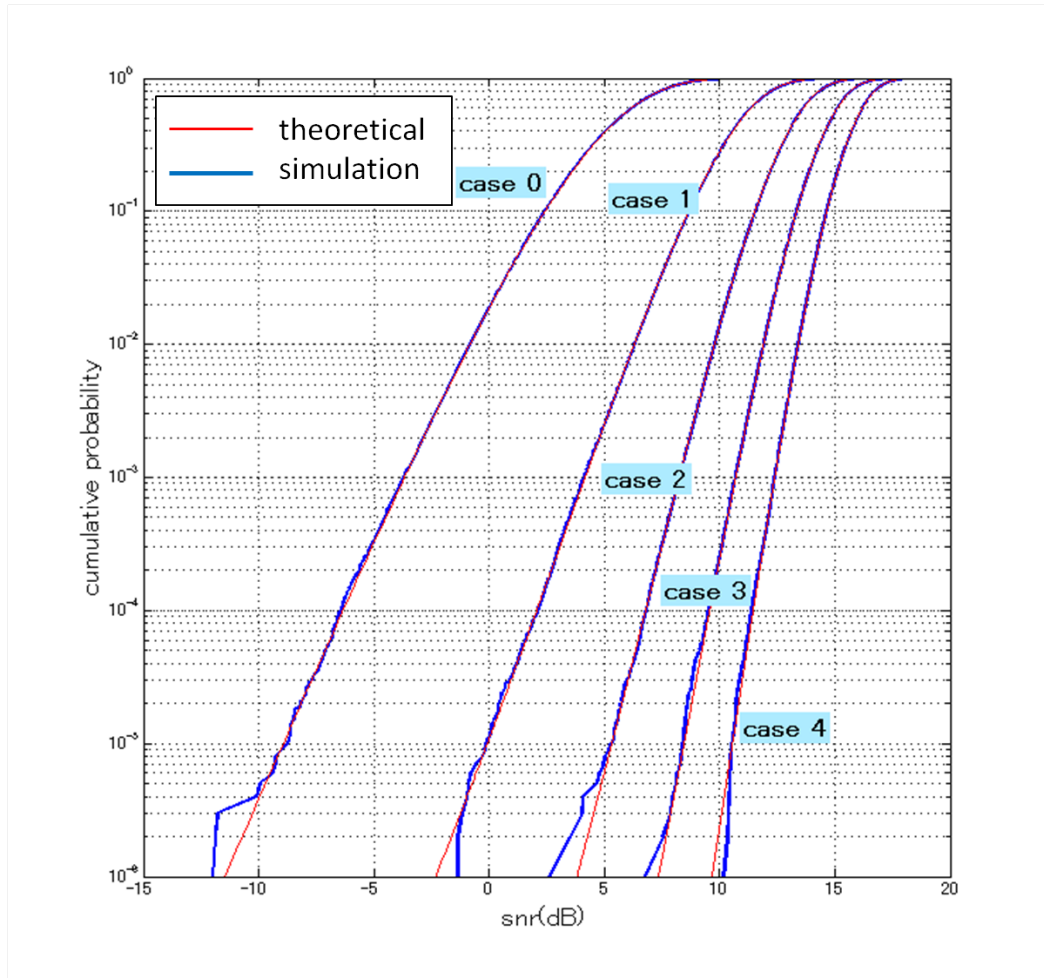


Figure 3.4: The CDFs of output SNR of simulative and theoretical values for 5 cases of 2×2 MIMO propagation model, with $K = 9$ dB and $\gamma_D = 10$.

3. PROPAGATION MODELING IN THE MIXTURE OF NLOS & LOS ENVIRONMENT FOR OUTDOOR MIMO SYSTEM

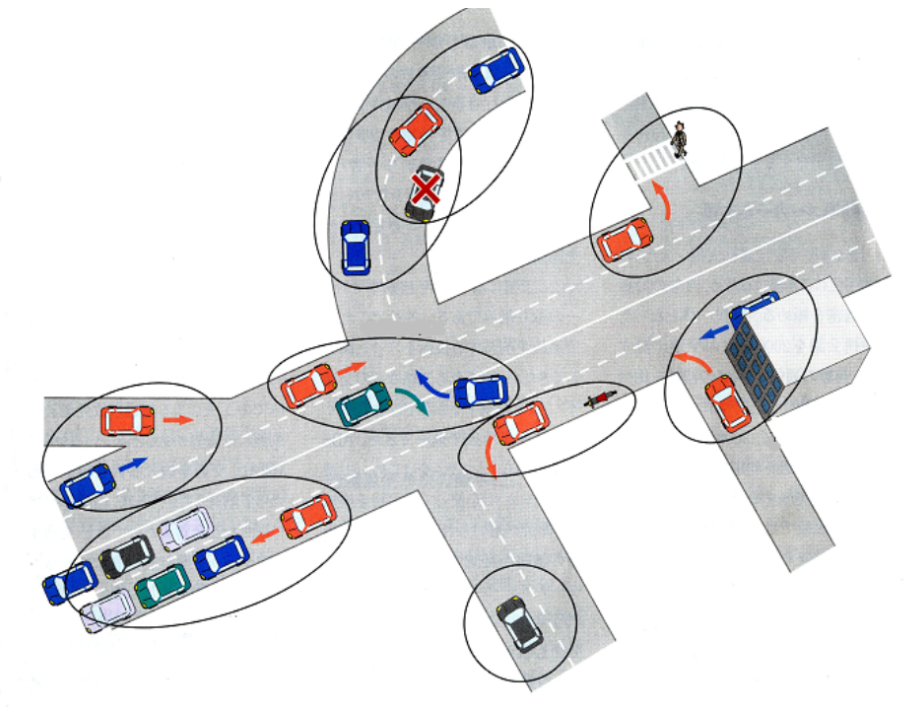


Figure 3.5: A scenario of dangerous situations in traffic systems.

drivers avoid accidents and users enjoy smart terminals. A sketch of situations that may cause traffic accidents is shown in Fig. 3.5. Because of the request of high reliability of transmission in ITS, the adoption of MIMO technique seems promising. However, conventional modeling based on Rayleigh fading channel or Nakagami-Rice fading channel is deficient and inconvenience for the multipath channel environment in the environment of ITS is more complex and variable. On the other hand, there are some features of ITS-IVC appealing to us, large intervals of transmit antennas or receive antennas, and similar physical environment for each sub-channel for instance. Applying the new developed model to MIMO propagation for the mixture of NLOS and LOS sub-channels in ITS-IVC therefore seems fairly suitable and effective.

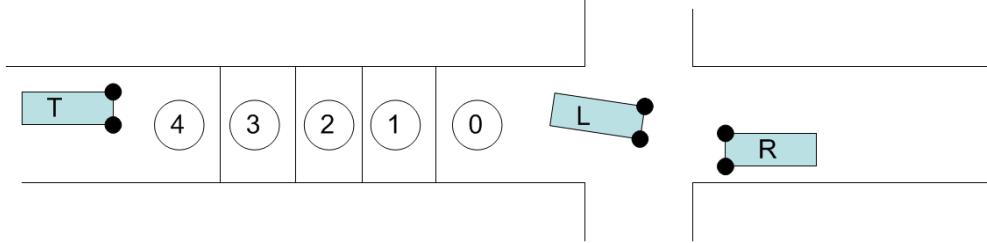


Figure 3.6: Applying MIMO to a right-turn collision scenario.

3.3.1 Proposal of MIMO-ITS Model in A Right-turn Scenario

In one of these situations shown in Fig. 3.5, a right-turn collision scenario nearby the intersection is concerned as shown in Fig. 3.6. In the situation vehicle R and a large vehicle L is about to make a right turn (driving in the left lane in Japan), while another vehicle T is going straight towards the intersection, behind the large vehicle L. The sight of driver in vehicle T may be obstructed by the shadowing of vehicle L so that IVC technology is highly anticipated to realize collision avoidance warning system.

For the purpose of model setup, two-antenna-setting is adopted in the physical layer considering the simplicity and efficiency, and then 2×2 MIMO configuration is constructed. Vehicle T is the transmitter and vehicle R is the receiver in the situation. The shadowing by vehicle L produces a mixture environment according to the physical conditions. As a result, some of the direct paths (LOS paths) among array elements may be completely broken due to vehicle movement, and attenuate into NLOS paths. The propagation conditions in such a situation are divided into 5 possible cases according to the number of LOS paths as shown in the figure. As what we have derived, the PDF of SNR for each case can be calculated quantitatively, through incorporating parameter values into Eq. (3.22).

3.3.2 A Field Experiment

A field experiment is conducted by Toyota Central R&D Labs in a related research [47]. The experimental conditions shown in Fig. 3.7. In the experiment,

3. PROPAGATION MODELING IN THE MIXTURE OF NLOS & LOS ENVIRONMENT FOR OUTDOOR MIMO SYSTEM

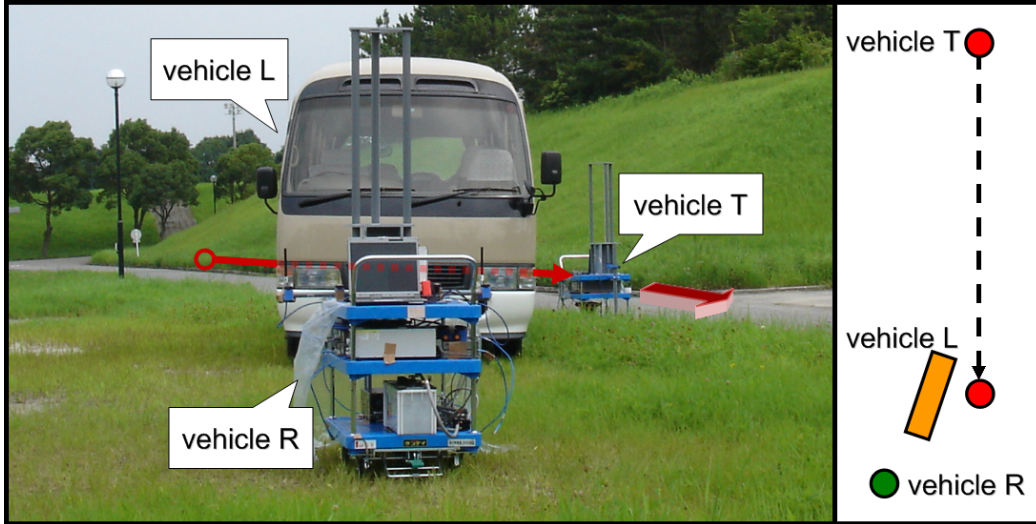


Figure 3.7: A field experiment for using MIMO in ITS-IVC in a shadowing environment.

the obstacle was an actual micro-bus, namely vehicle L in the figure. The transmitter and receiver which were fixed in steels represented vehicle T and vehicle R, respectively. Each of them was equipped with two antenna elements. The interval between antennas in front of vehicles was 1 m. The antenna height was set 0.8 m. The transmission power of each antenna is 10 dBm. Transmission frequency was set at 5 GHz band and carrier signal was unmodulated. A schematic plan view depicted by information, such as sizes of vehicle L and antenna interval, is shown in Fig. 3.8.

From that we can geometrically indicate that all sub-channels should have been shadowed in the range of distance 8.79 to 25.4 m, namely case 0. The range of distance 25.4 to 30.4 m should be case 1. And then between distance 30.4 and 55 m was case 2. Fig. 3.8 also illustrates that if the distance of vehicle T from the intersection had been long enough, for example more than 70 m, case 3 between the distance of 55 to 67 m and case 4 over the distance 67 m, would appear. The range of distance 8.79 m to intersection seems to be case 4. However, in such a short transmission distance it is difficult to ignore channel interferences for modeling. In addition, the capability of our model is to evaluate transmission performance of MIMO system in mixed propagation environment in a comparative

3.3 Application of the Model to ITS-IVC

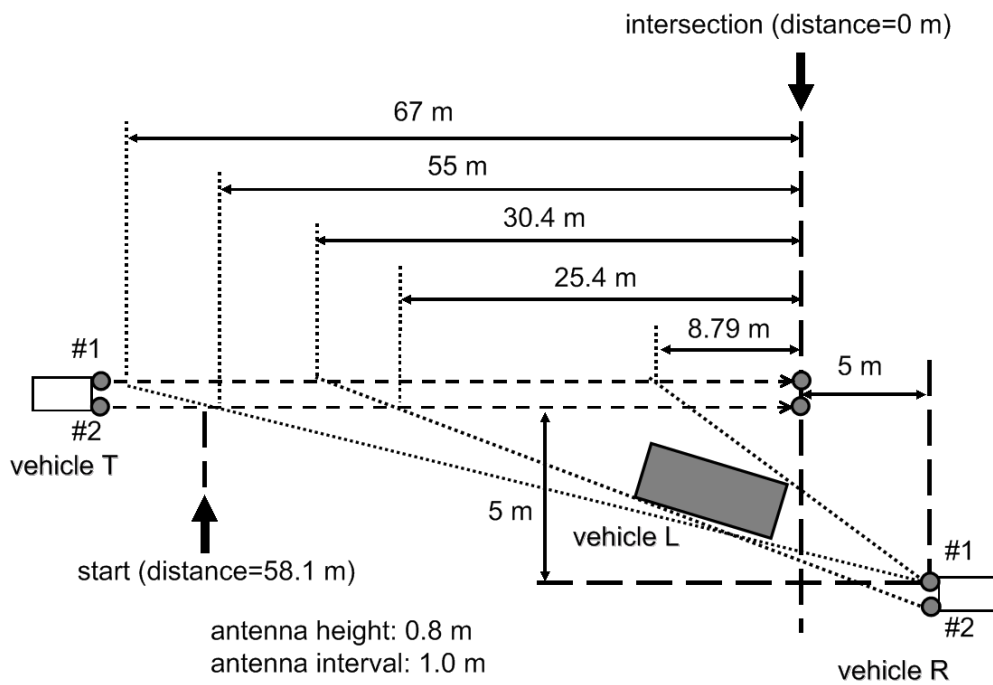


Figure 3.8: The schematic plan view of the field experiment.

3. PROPAGATION MODELING IN THE MIXTURE OF NLOS & LOS ENVIRONMENT FOR OUTDOOR MIMO SYSTEM

distance, especially when applying to ITS-IVC. Because of all above, case 0, case 1 and case 2 will be used for modeling for the field experiment. The experiment is very similar to the application example discussed in the previous subsection. Although our obtained data in this experiment are amplitude-only variations for each sub-channel, we can use these data for MRC estimation because the MRC works power-sum of each sub-channel power.

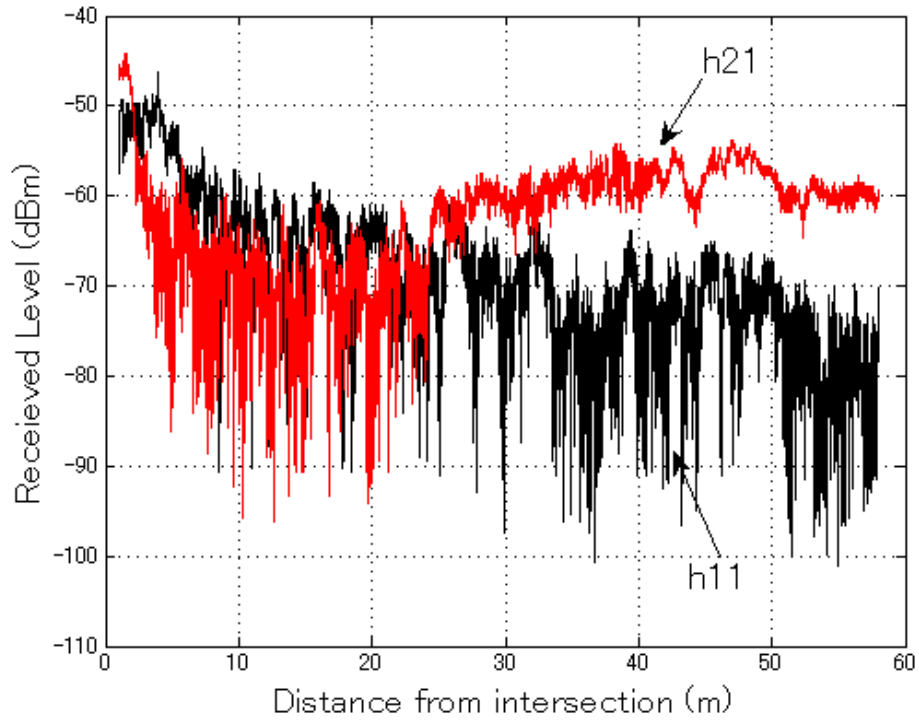
The received signal power of each antenna at vehicle R was measured whenever vehicle T moved 5 mm in that experiment. The power level of Rx#1 and Rx#2 from transmit antenna Tx#1 and transmit antenna Tx#2 were recorded and the results are shown in Fig. 3.9, with respect to the distance of vehicle T from the intersection.

3.3.3 Analysis & Calculations

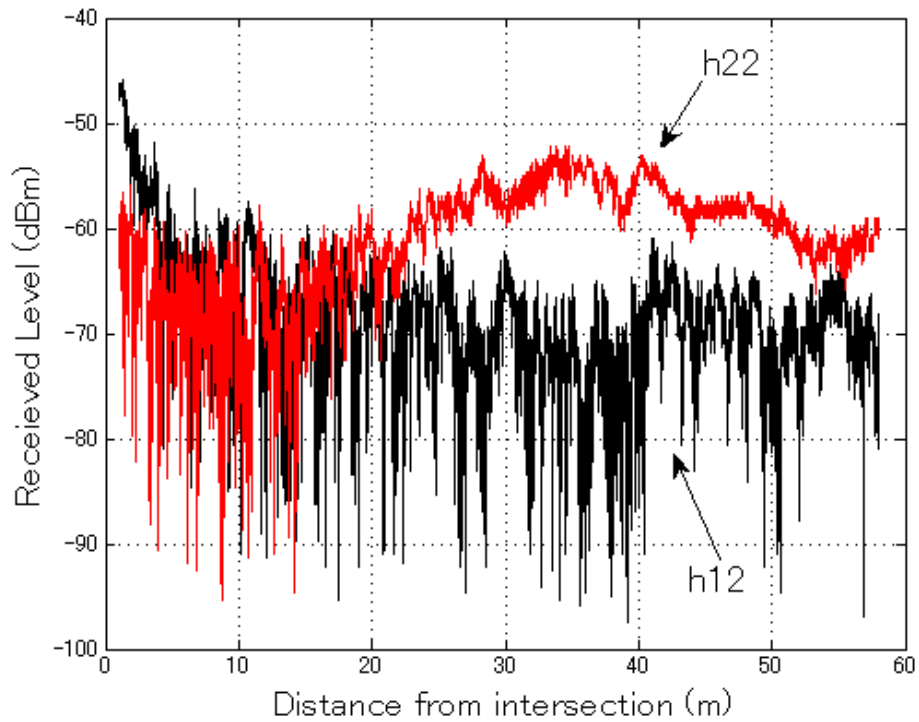
In order to highlight the average value of received power as a function of distance, smoothing operation by means of moving average method is imposed. The number of data of each subset when exploiting this method is 501. Because received signal power was measured whenever vehicle T moved 5 mm in the field experiment, the distance window size is 2.5 m. The results are shown in Fig. 3.10. Obviously, large differences can be observed between the values of the receive antenna Rx#1 and the receive antenna Rx#2, when the distance of vehicle T from the intersection was in the range of distance about 30 to 50 m. On the other hand, received power of 4 sub-channels were almost in the same level for the range of 10 to 20 m. According to the schematic analysis of Fig. 3.8 and with the consideration of weakness of edge diffraction effect in actual propagation environment, fitting these two areas as case 2 and case 0 is valid. And the area between them is considered to be a transition region.

In addition, performance evaluation for IVC system in which transmission range varies because of driving movement should take the path loss effect into account. For this purpose, a general model is developed by considering Rice factor K and received level of LOS path as functions of distance variable x . The

3.3 Application of the Model to ITS-IVC



(a) received level from Tx#1



(b) received level from Tx#2

Figure 3.9: Received signal power with respect to distance from intersection.

3. PROPAGATION MODELING IN THE MIXTURE OF NLOS & LOS ENVIRONMENT FOR OUTDOOR MIMO SYSTEM

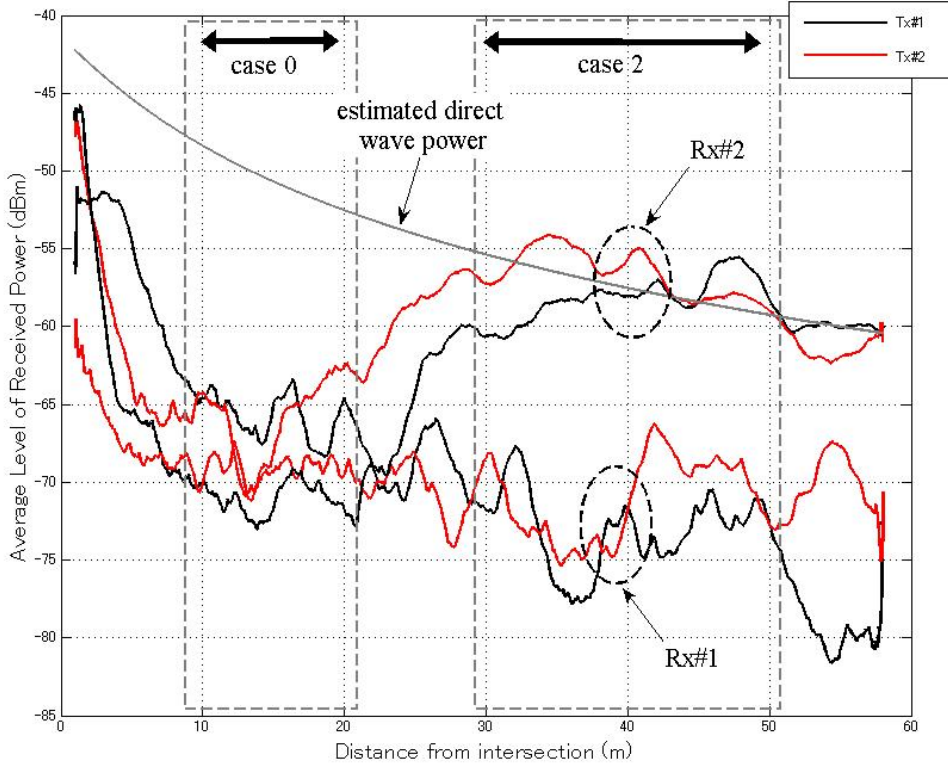


Figure 3.10: Moving average values of received level.

average PDF of received power z then can be given by

$$f_{\text{overall}}(z) = \frac{1}{x_{\text{max}} - x_{\text{min}}} \times \int_{x_{\text{min}}}^{x_{\text{max}}} f_{\text{MRC}} \{z; K(x), \gamma_D(x), N_{\text{LOS}}(x), N_{\text{NLOS}}(x)\} dx \quad (3.23)$$

Hereafter, in order to discuss model from PDF point of view, we treat the combined received power level variations z rather than SNR γ because physical values obtained in the experiment is the power variation as shown in Fig. 3.9.

In order to exploit our proposed model, we estimated the direct wave power for the whole area, as shown in Fig. 3.10. The basic principle of achieving direct wave power curve is to use free space propagation model, i.e. the Friis Equation (2.1). The path loss rate was set 2. However, because we have supposed that the

3.3 Application of the Model to ITS-IVC

transmission of signals received by Rx#2 in the range of case 2 is in LOS path, and because transmission power and the antenna gains of transmitter and receiver are considered constant during vehicle moving, we can utilize the measurement result of case 2 to be a baseline, and consequently we can inversely estimate the direct wave power in other areas. In the analysis, we take the point at which distance from intersection is 45 m as a reference. The average received power of sub-channel h_{21} and h_{22} at that point is z_{ref} . Also note that the transmission distance of Friis Equation is $d_T(x) = \sqrt{(x+5)^2 + 5^2}$ because variable x is the distance from intersection. Then the estimated direct wave power is obtained by $z_D = [d_T(x)/d_T(45)]^{-2} \times z_{\text{ref}}$. In the fitting, the value of K in decibel is roughly estimated by the difference between the estimated direct wave power value and the received power value of NLOS sub-channels in Fig. 3.10. As results, we employ it as 13 dB for case 2 and 15 dB for case 0.

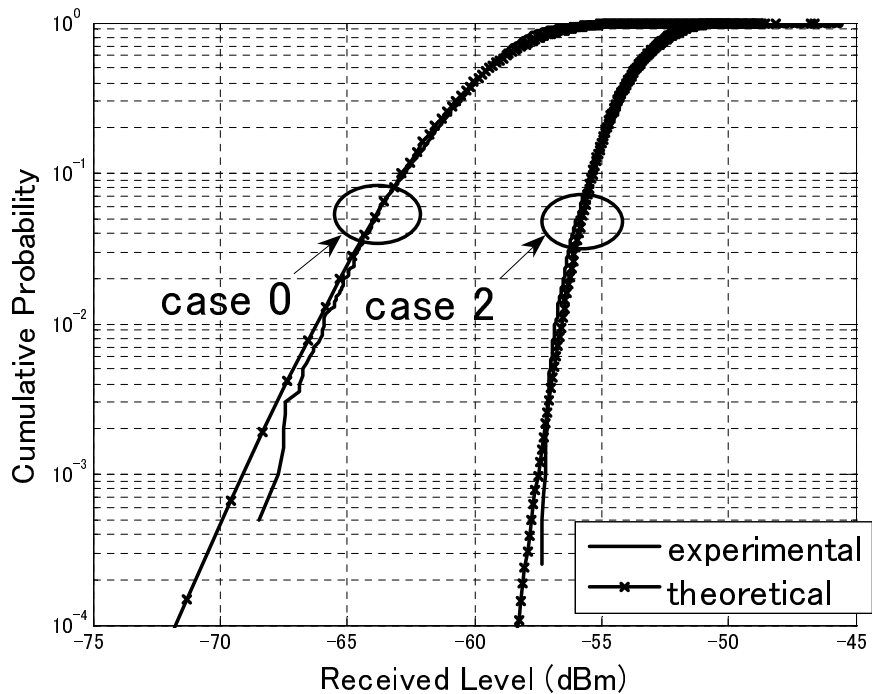
CDFs for case 0 and case 2 applying our model Eq. (3.23) are depicted in Fig. 3.11 (a), as well as the CDFs of combined signal power derived from experimental data. For comparison, the cumulative distribution curves are plotted by logarithmic scales and normalized at CDF=50% point. We can see that the comparison result shows fairly good coincidences for the cumulative probabilities of more than 10^{-3} , which confirms the effectiveness for evaluation using the proposed model.

In addition, if we assume the transition region between case 2 and case 0 as case 1, an overall evaluation result throughout the range of 10 to 50 m is achieved, as shown in Fig. 3.11 (b). By normalized at the value of CDF at 50%, the overall CDF curve based on theoretical model coincides with the experimental result as indicated. The good agreement result identifies the effectiveness of the proposed model.

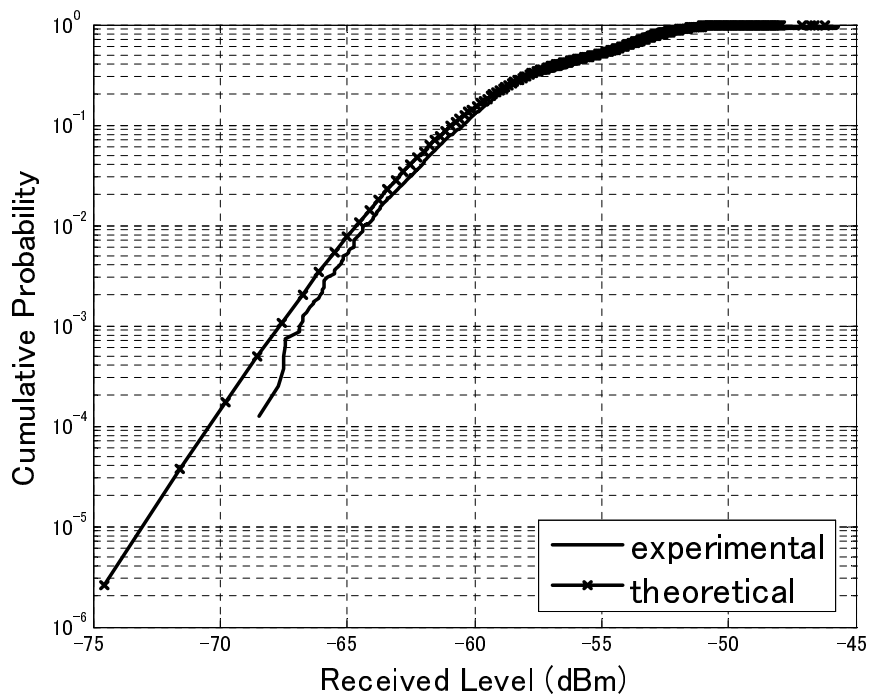
3.3.4 Evaluation of MIMO Merit

The proposed model Eq. (3.23) enables to evaluate propagation performance in the mixture of LOS and NLOS environments, even for SISO transmission and SIMO transmission. Therefore we would like to make an evaluation for each of them under the same conditions and identify the merit of applying MIMO

3. PROPAGATION MODELING IN THE MIXTURE OF NLOS & LOS ENVIRONMENT FOR OUTDOOR MIMO SYSTEM



(a) case 0 and case 2



(b) over-all

Figure 3.11: The CDFs of received power in MRC of the theoretical values and experimental values.

3.3 Application of the Model to ITS-IVC

technique in ITS-IVC application in this situation, based on the developed model and general function.

For comparison, the received levels are enhanced by 3 dB for SISO and SIMO transmission so as to be equal for total transmission power. We consider SISO configuration in this situation by two ways: using Tx#1, Rx#1 as the worst way and Tx#2, Rx#2 as the best way, according to the physical conditions. Similarly for SIMO configuration, using Tx#1 only as transmitter and Tx#2 only as transmitter will be considered respectively.

The comparison result is shown in Fig. 3.12. From the result we can see that SISO transmission in the best way and SIMO transmissions give nearly the same performance as MIMO method for the region of cumulative probability of above about 0.5. But when the received power degrades, MIMO transmission offers a superior performance compared with SISO and SIMO transmissions. We can expect that MIMO technique shows its apparent advantage when applied to ITS-IVC system.

3. PROPAGATION MODELING IN THE MIXTURE OF NLOS & LOS ENVIRONMENT FOR OUTDOOR MIMO SYSTEM

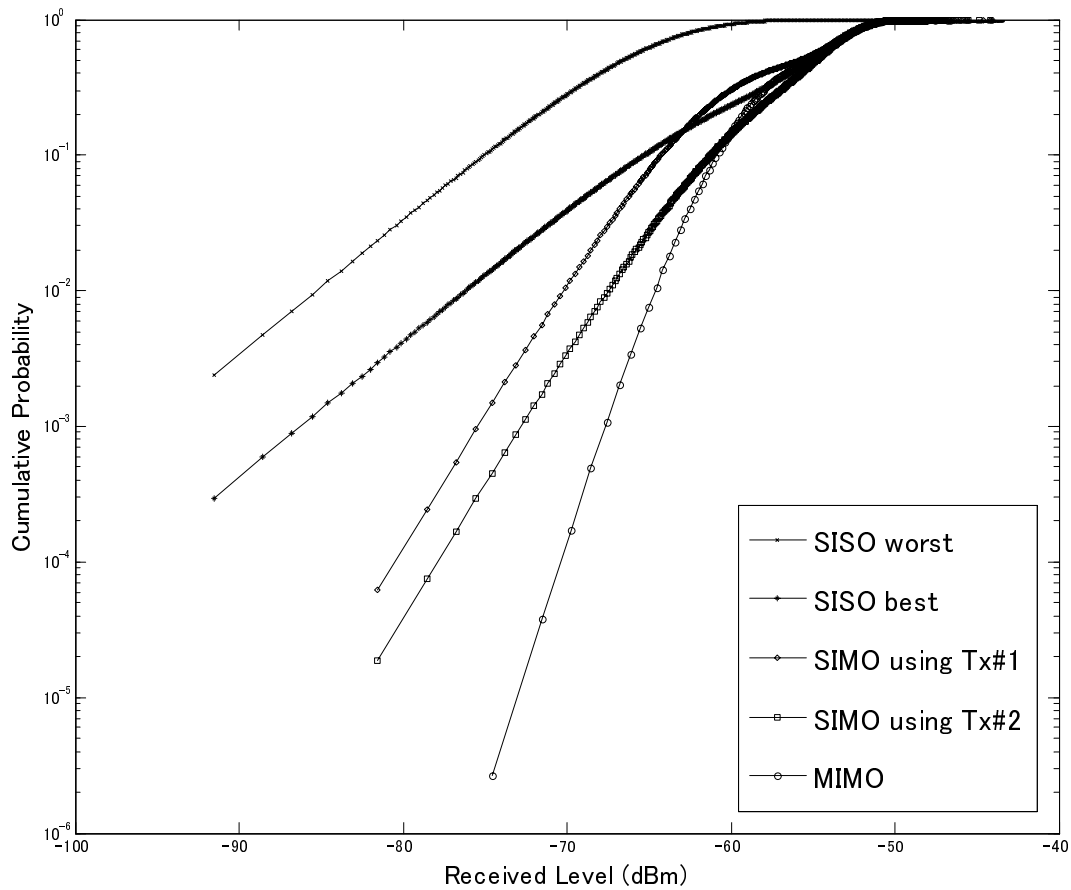


Figure 3.12: Evaluations of received power through distance from intersection of 10 to 50 m in the right-turn situation of ITS-IVC for SISO worst transmission, SISO best transmission, SIMO transmission using Tx#1 as transmitter, SIMO transmission using Tx#2 as transmitter and proposed MIMO transmission.

Chapter 4

Spatial Correlation Modeling & Characterization with Three-dimensional APS of $\cos^n \theta$ for Indoor MIMO Terminal

In the previous chapter, we demonstrated the importance of channel modeling for the evaluation of MIMO system and a proposal which enables the consideration of the coexistence of NLOS and LOS paths. The proposed model is practical for modeling outdoor MIMO propagation in some certain situations and evaluating the system output performance. The effectiveness and validity is well proved by an application to ITS-IVC with a low interruption among the elements of antennas at the same side. However, it is not the case for some other wireless propagation scenarios, especially the indoor MIMO environment where the multipath-richness takes a significant influence of channel interference. Multipath-richness refers to an environment which is surrounded by many scatterings or tall buildings resulting in waves coming from many different spatial directions. Indoor propagation environment is a typical multipath-rich situation. In such kind of environments, multiple channels between different antennas are often strongly correlated and therefore the expected multi-antenna gains may not always be obtainable. This is called spatial correlation as it can be interpreted as a correlation between a signal's spatial direction.

4. SPATIAL CORRELATION MODELING & CHARACTERIZATION WITH THREE-DIMENSIONAL APS OF $\text{COS}^N \theta$ FOR INDOOR MIMO TERMINAL

When it is difficult to directly use a geometrical approach, i.e. NLOS/LOS path identification, for channel modeling and characterization for indoor MIMO propagation, the analytical approach probably works for describing system performance with the characterization of correlation. Consequently evaluation of spatial correlation at the link-end of MIMO transmission is highly desired. However, correlation performance is not easy to calculate directly. One difficulty comes from modeling of the angular power distribution (APD) profile for a variety of scenarios in multipath environment. Besides, the impact of antennas with different patterns and polarizations increases the difficulty of identifying the effects of antennas. As employing MIMO and AA technology in next-generation communication system ranging from indoor to outdoor environment, the expectation of applicable models and functions for evaluating spatial correlation performance remains high.

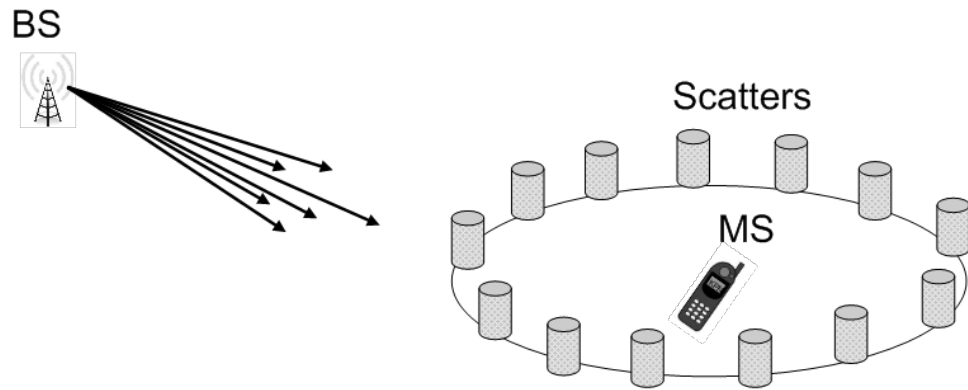
In the chapter, a method that can approximate spatial correlation in three-dimensional multipath fading environment is proposed. The model achieves a closed-form solution in terms of a Hypergeometric function and doesn't deprive the practical applicability. The validity of the proposed method is well confirmed by numerical results and measurements in a reverberation chamber experiment.

4.1 Spatial Correlation Modeling

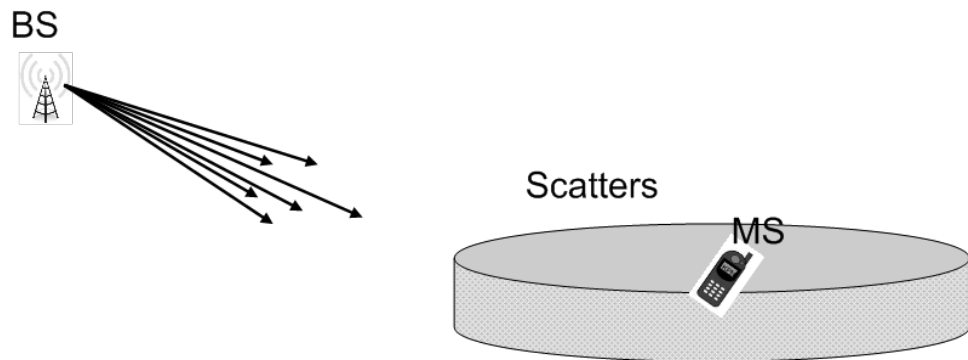
4.1.1 Previous 2D Spatial Correlation Models

Since employing techniques such as MIMO and array techniques in next-generation systems, evaluation of the spatial correlation of signals has attracted a great deal of attention. In order to model the APD, a number of previous studies, e.g. [30, 48], have assumed the power azimuth spectrum (PAS or azimuth APD) as a uniform distribution (also known as the Jakes model) and a Gaussian function, and measurement campaigns, such as that described in [49, 50], revealed that that using a Laplacian function as a PAS provides a good approximation for a number of real propagation environments. The physical environments for these models are shown in Fig. 4.1.

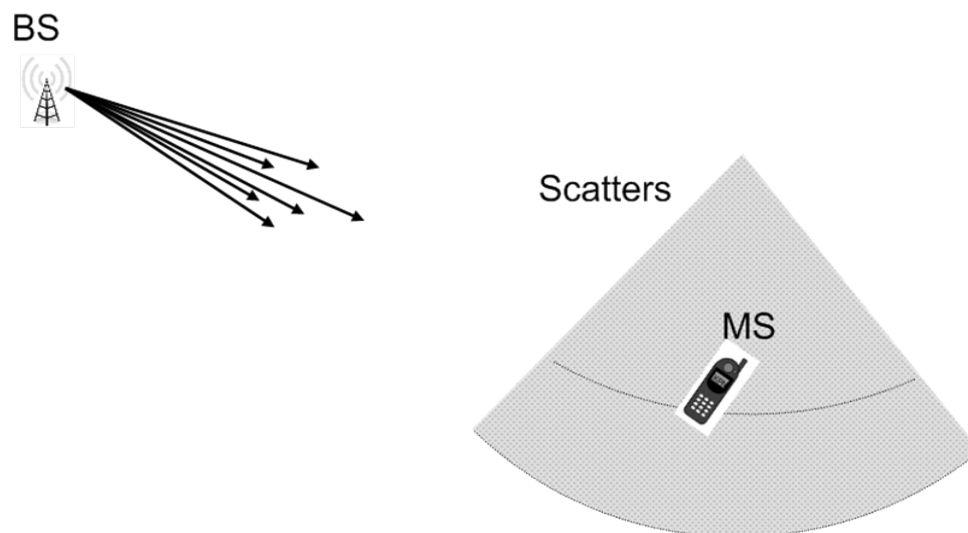
4.1 Spatial Correlation Modeling



(a) Uniform-distributed scatterings model



(b) Gaussian-distributed scatterings model



(c) Laplace-distributed scatterings model

Figure 4.1: Widely used two-dimensional multipath propagation models.

4. SPATIAL CORRELATION MODELING & CHARACTERIZATION WITH THREE-DIMENSIONAL APS OF $\text{COS}^N \theta$ FOR INDOOR MIMO TERMINAL

As for a relatively large range of transmission, it is a good approximation for assuming waves are coming horizontally, i.e. two-dimensionally and these models are proved to be useful for most outdoor areas. The requirements of spatial correlation analysis of waves with a three-dimensional AOA are claimed by studies and measurements such as [22, 23], which reported that there is an elevation spread for several environments, ranging from indoor to outdoor environments, and the multipath richness in these environments leads to a significant error due to the azimuth-only assumption.

4.1.2 3D Spatial Correlation Modeling

In a recent study [51], the azimuth and elevation of the AOA are taken into account and are assumed to be independent and uniformly distributed on the sphere. This study provided some useful expressions, but these expressions are not likely to characterize the propagation environment in general. In [52] the author derived a generalized Doppler Power Spectrum for arbitrary 3D scattering environments, but the resultant form is highly complex. A recent study attempted to develop a practical generalized method [53], where the authors initially consider the angular power spectrum (APS) as the n -th power of a cosine function with respect to the elevation of the AOA.

Generally, an incident wave in Cartesian coordinates for 3D spatial correlation modeling can be shown as Fig. 4.2. The incident wave vector $\boldsymbol{\alpha}$ in a 3D multipath fading environment as follows:

$$\boldsymbol{\alpha} = \mathbf{i} \cos \phi \cos \theta + \mathbf{j} \sin \phi \cos \theta + \mathbf{k} \sin \theta \quad (4.1)$$

where $\{\mathbf{i}, \mathbf{j}, \mathbf{k}\}$ are the corresponding unit vectors in Cartesian coordinates and $\{\phi, \theta\}$ are the azimuth and elevation of the AoA in spherical coordinates, respectively. The APS at the reception point is represented as $\Omega(\phi, \theta)$, which is given by

$$\Omega(\phi, \theta) = G(\phi, \theta)\Omega_p(\phi, \theta) \quad (4.2)$$

where $G(\phi, \theta)$ denotes the antenna angular power gain, and $\Omega_p(\phi, \theta)$ denotes the APD of the multipath environment. Considering the effects of the received powers

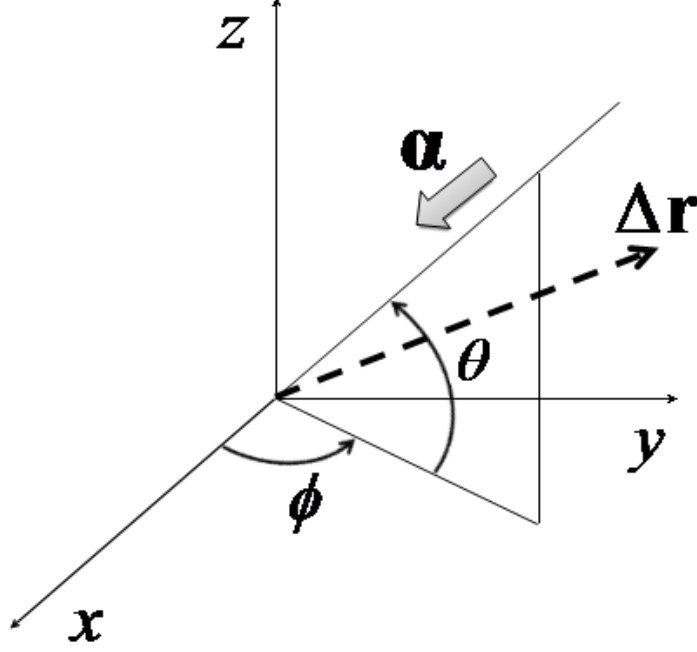


Figure 4.2: An incident wave α with moving vector $\Delta \mathbf{r}$.

of the vertically and horizontally polarized radio waves, respectively, Eq. (4.2) can be rewritten as

$$\Omega(\phi, \theta) = G_\theta(\phi, \theta)\Omega_{p,\theta}(\phi, \theta) + G_\phi(\phi, \theta)\Omega_{p,\phi}(\phi, \theta) \quad (4.3)$$

Given moving vector $\Delta \mathbf{r}$, representing the moving direction of the reception point, the spatial fading correlation of the incoming wave α is calculated by [30]

$$\rho_\alpha(\Delta \mathbf{r}) = \frac{1}{P_R} \int_{-\frac{\pi}{2}}^{\frac{\pi}{2}} \int_0^{2\pi} \Omega(\phi, \theta) \exp(jk\Delta \mathbf{r} \cdot \alpha) \cos \theta d\phi d\theta \quad (4.4)$$

where k is the wave number defined by $k = 2\pi/\lambda$ with λ being the signal wavelength and P_R is the average received power under the multipath condition, given by

$$P_R = \int_{-\frac{\pi}{2}}^{\frac{\pi}{2}} \int_0^{2\pi} \Omega(\phi, \theta) \cos \theta d\phi d\theta \quad (4.5)$$

4. SPATIAL CORRELATION MODELING & CHARACTERIZATION WITH THREE-DIMENSIONAL APS OF $\text{COS}^N \theta$ FOR INDOOR MIMO TERMINAL

4.1.3 Spatial Correlation Approximation

Equation (4.4) provides a theoretical method for the characterization of spatial correlation in a spherical field. If considering the moving vector in three-dimensional Cartesian coordinates, we have

$$\Delta \mathbf{r} = \mathbf{i}\Delta x + \mathbf{j}\Delta y + \mathbf{k}\Delta z \quad (4.6)$$

where $\{\Delta x, \Delta y, \Delta z\}$ are the corresponding projections of $\Delta \mathbf{r}$ in Cartesian coordinates, and spatial correlation can be approximated by

$$\rho_a(\Delta \mathbf{r}) \approx \rho_{a,x}(\Delta x)\rho_{a,y}(\Delta y)\rho_{a,z}(\Delta z) \quad (4.7)$$

where $\{\rho_{a,x}(\Delta x), \rho_{a,y}(\Delta y), \rho_{a,z}(\Delta z)\}$ denote the corresponding functions of the spatial correlation characteristics in Cartesian coordinates, given by

$$\rho_{a,x}(\Delta x) = \frac{1}{P_R} \int_{-\frac{\pi}{2}}^{\frac{\pi}{2}} \int_0^{2\pi} \Omega(\phi, \theta) \exp(jk\Delta x \cos \phi \cos \theta) \cos \theta d\phi d\theta \quad (4.8)$$

$$\rho_{a,y}(\Delta y) = \frac{1}{P_R} \int_{-\frac{\pi}{2}}^{\frac{\pi}{2}} \int_0^{2\pi} \Omega(\phi, \theta) \exp(jk\Delta y \sin \phi \cos \theta) \cos \theta d\phi d\theta \quad (4.9)$$

$$\rho_{a,z}(\Delta z) = \frac{1}{P_R} \int_{-\frac{\pi}{2}}^{\frac{\pi}{2}} \int_0^{2\pi} \Omega(\phi, \theta) \exp(jk\Delta z \sin \theta) \cos \theta d\phi d\theta \quad (4.10)$$

respectively.

4.2 Characterization of Spatial Correlation Performance

4.2.1 In the Case of APS with $\text{cos}^n \theta$

We focus on the analysis of APS for the case in which

$$\Omega(\phi, \theta) = \text{cos}^n \theta, n \geq 0 \quad (4.11)$$

which is a combination of antenna effects and propagation properties of the environment. For example, in a reverberation chamber and some other multipath-rich indoor environments, where the incoming waves are three-dimensionally uniform,

4.2 Characterization of Spatial Correlation Performance

the cross polarization power ratio (XPR) is 0 dB, so we have approximately $\Omega_{p,\theta}(\phi, \theta) = \Omega_{p,\phi}(\phi, \theta) = \text{const}$. Furthermore, for the case in which vertically polarized radio waves are received by a dipole antenna, we have $G_\theta(\phi, \theta) \approx \cos^2 \theta$ and $G_\phi(\phi, \theta) = 0$. Then, we can approximate the combined characteristic of APS using $\Omega(\phi, \theta) = \cos^2 \theta$ under the assumption that $\Omega_{p,\theta}(\phi, \theta) = \Omega_{p,\phi}(\phi, \theta) = 1$, for simplicity. For other cases of vertical polarization with a strong directivity, the APS can be represented by $\cos^n \theta$ with $n \gg 2$.

On the other hand, for the case in which the antenna directivity is weak, while the vertical angular power spectrum of incoming waves is sharp, as in outdoor mobile propagation environments for instance, the APDs, $\Omega_{p,\theta}(\phi, \theta)$ and $\Omega_{p,\phi}(\phi, \theta)$, perform as $\cos^n \theta$ with $n \gg 2$, and it follows that we can nevertheless obtain $\Omega(\phi, \theta) \propto \cos^n \theta$.

4.2.2 Derivation of Functions for Spatial Correlation Characterization

The analysis of spatial correlation in the 3D APS using $\Omega(\phi, \theta) = \cos^n \theta$, can represent many existing propagation situations. The primary purpose of the present study is to generalize the spatial correlation function and derive closed-form solutions from that, and is realized by applying the Mellin-transform (MT) method proposed in [54] to solve antenna problems.

For spatial correlation of the x coordinate, using the following expression:

$$J_0(x) = \frac{1}{2\pi} \int_0^{2\pi} \exp(jx \cos \phi) d\phi \quad (4.12)$$

where $J_0(\cdot)$ is the zeroth-order Bessel function of the first kind, $\rho_{a,x}(\Delta x)$ and $\rho_{a,z}(\Delta z)$ can be given by

$$\rho_{a,x}(\Delta x) = \frac{4\pi}{P_R} \int_0^{\frac{\pi}{2}} \cos^{n+1} \theta J_0(k\Delta x \cos \theta) d\theta \quad (4.13)$$

$$\rho_{a,z}(\Delta z) = \frac{4\pi}{P_R} \int_0^{\frac{\pi}{2}} \cos^{n+1} \theta \cos(k\Delta z \sin \theta) d\theta, \quad (4.14)$$

respectively.

Here, we provide a step-by-step application of the MT-method to the derivation of Eq. (4.13). The derivation of Eq. (4.14) is shown in the Appendix.

4. SPATIAL CORRELATION MODELING & CHARACTERIZATION WITH THREE-DIMENSIONAL APS OF $\text{COS}^N \theta$ FOR INDOOR MIMO TERMINAL

Let the integral component in (4.13) be denoted as $f_x(u)$, where $u = k\Delta x$. Thus, we have

$$f_x(u) = \int_0^{\frac{\pi}{2}} \cos^{n+1} \theta J_0(u \cos \theta) d\theta \quad (4.15)$$

In order to apply the MT-method as shown in [54], we define $g_x(u)$ and $h_x(v)$, respectively, as

$$g_x(u) = J_0(u) \quad (4.16)$$

$$h_x(v) = \begin{cases} (1-v^2)^{-1/2} v^\tau, & \text{for } 0 < v < 1 \\ 0, & \text{for } v > 1 \end{cases} \quad (4.17)$$

Thus, we can rewrite $f_x(u)$ as

$$f_x(u) = \int_0^1 J_0(uv) (1-v^2)^{-1/2} v^\tau dv \quad (4.18)$$

where $v = \cos \theta$ and $\tau = n + 1, n > 0$. Representing the MT of $f(x)$ as $\tilde{f}(s)$, the integral above converges when s is valued within a certain scale of the complex plane, which is referred to as the strip of initial definition (SID). By MT-method, the MT of $f_x(u)$ can be given by

$$\begin{aligned} \tilde{f}_x(s) &\equiv \tilde{g}_x(s) \tilde{h}_x(1-s) \\ &= \left[\frac{1}{2} \left(\frac{1}{2}\right)^{-s} \frac{\Gamma(\frac{s}{2})}{\Gamma(1-\frac{s}{2})} \right] \left[\frac{\sqrt{\pi}}{2} \frac{\Gamma(\frac{1}{2} + \frac{\tau}{2} - \frac{s}{2})}{\Gamma(1 + \frac{\tau}{2} - \frac{s}{2})} \right] \end{aligned} \quad (4.19)$$

where $\Gamma(\cdot)$ is the Gamma function, and the overlap of the SID of $\tilde{g}_x(s)$ and $\tilde{h}_x(1-s)$ is $0\text{Re}\{s\} < 1$. Then, by the inversion of MT, we have

$$\begin{aligned} f_x(u) &= \frac{\sqrt{\pi}}{4} \frac{1}{2\pi i} \int_{c-i\infty}^{c+i\infty} \frac{\Gamma(\frac{s}{2}) \Gamma(\frac{1}{2} + \frac{\tau}{2} - \frac{s}{2})}{\Gamma(1-\frac{s}{2}) \Gamma(1 + \frac{\tau}{2} - \frac{s}{2})} \left(\frac{u}{2}\right)^{-s} ds \end{aligned} \quad (4.20)$$

in which the poles on the left-hand side are contributed by $\Gamma(\frac{s}{2})$ and located at $s = 0, -2, -4, \dots$. Furthermore, according to the residue theorem, upon

4.2 Characterization of Spatial Correlation Performance

approaching the contour at the left-hand side, we obtain the following

$$\begin{aligned}
f_x(u) &= \sum_{m=0}^{\infty} \text{Res} \left\{ \tilde{f}_x(s) u^{-s}; s = -2m \right\} \\
&= \frac{\sqrt{\pi}}{4} \sum_{m=0}^{\infty} \text{Res} \left\{ \frac{\Gamma(\frac{s}{2}) \Gamma(\frac{1}{2} + \frac{\tau}{2} - \frac{s}{2})}{\Gamma(1 - \frac{s}{2}) \Gamma(1 + \frac{\tau}{2} - \frac{s}{2})} \left(\frac{u}{2}\right)^{-s}; s = -2m \right\} \\
&= \frac{\sqrt{\pi}}{4} \sum_{m=0}^{\infty} \frac{\Gamma(\frac{1}{2} + \frac{\tau}{2} + \frac{2m}{2})}{\Gamma(1 + \frac{2m}{2}) \Gamma(1 + \frac{\tau}{2} + \frac{2m}{2})} \\
&\quad \times \text{Res} \left\{ \Gamma(\frac{s}{2}) \left(\frac{u}{2}\right)^{-s}; s = -2m \right\} \\
&= \frac{\sqrt{\pi}}{2} \frac{\Gamma(\frac{1}{2} + \frac{\tau}{2})}{\Gamma(1) \Gamma(1 + \frac{\tau}{2})} \sum_{m=0}^{\infty} \frac{(\frac{1}{2} + \frac{\tau}{2})_m}{(1)_m (1 + \frac{\tau}{2})_m} \frac{(-u^2/4)^m}{m!}
\end{aligned} \tag{4.21}$$

where $(s)_m$ is the Pochhammer symbol given by

$$(s)_m = \frac{\Gamma(s+m)}{\Gamma(s)}, m = 0, 1, 2, \dots \tag{4.22}$$

According to the definition of the Hypergeometric function, the series in Eq. (4.21) is further identified as

$$f_x(u) = \frac{\sqrt{\pi}}{2} \frac{\Gamma(\frac{1}{2} + \frac{\tau}{2})}{\Gamma(1 + \frac{\tau}{2})} {}_1F_2\left(\frac{1}{2} + \frac{\tau}{2}; 1, 1 + \frac{\tau}{2}; -\frac{u^2}{4}\right) \tag{4.23}$$

The average received power P_R can be calculated by $4\pi f_x(k\Delta x) |_{\Delta x=0}$ with substitutions of $u = k\Delta x$, $\tau = n + 1$, given as

$$P_R = 2\pi\sqrt{\pi} \frac{\Gamma(\frac{n}{2} + 1)}{\Gamma(\frac{n}{2} + \frac{3}{2})} \tag{4.24}$$

Then, Eq. (4.26) is obtained by

$$\begin{aligned}
\rho_{a,x}(\Delta x) &= \frac{4\pi}{P_R} f_x(k\Delta x) \\
&= {}_1F_2\left(\frac{n+2}{2}; 1, \frac{n+3}{2}; -\frac{k^2\Delta x^2}{4}\right)
\end{aligned} \tag{4.25}$$

Although the notation m in the derivation is defined as a non-negative integer, the Gamma function $\Gamma(\cdot)$ and the residue theory also hold for real numbers.

4. SPATIAL CORRELATION MODELING & CHARACTERIZATION WITH THREE-DIMENSIONAL APS OF $\text{COS}^N \theta$ FOR INDOOR MIMO TERMINAL

Consequently, the results in terms of the Hypergeometric function ${}_pF_q(\cdot)$ are applicable and can conveniently achieve analytic results for the non-negative real values of parameter n .

As shown in the Appendix, the results of Eq. (4.13) and Eq. (4.14) are given in terms of the generalized Hypergeometric function ${}_pF_q(\cdot)$, which are written as

$$\rho_{a,x}(\Delta x) = {}_1F_2\left(\frac{n+2}{2}; 1, \frac{n+3}{2}; -\frac{k^2\Delta x^2}{4}\right) \quad (4.26)$$

$$\rho_{a,z}(\Delta z) = {}_0F_1\left(; \frac{n+3}{2}; -\frac{k^2\Delta z^2}{4}\right) \quad (4.27)$$

respectively. Since $\{\rho_{a,x}(\Delta x), \rho_{a,y}(\Delta y)\}$ satisfy the symmetrical characteristics in the azimuth plane, $\rho_{a,y}(\Delta y)$ is obtained by replacing (Δx) with (Δy) in Eq. (4.26).

4.2.3 Calculations of Existing Formulas by the New Expressions

The generalized Hypergeometric function can already be well handled by modern packages, such as Mathematica or Matlab. Therefore, these results are also very useful and practicable. Given certain values of n , some previous analyses on spatial correlation easily turn out to be special cases of the proposed formula. For example, for the case in which $n = 0$, which represents a spherically uniform pattern, as given in [30], Eqs. (4.26) and (4.27) reduce to

$$\rho_{a,x,n=0}(\Delta x) = {}_1F_2\left(1; 1, \frac{3}{2}; -\frac{k^2\Delta x^2}{4}\right) = \text{sinc}(k\Delta x) \quad (4.28)$$

$$\rho_{a,z,n=0}(\Delta z) = {}_0F_1\left(; \frac{3}{2}; -\frac{k^2\Delta z^2}{4}\right) = \text{sinc}(k\Delta z), \quad (4.29)$$

respectively. For $n = 2$, which is appropriately the case of a half-wave dipole, these expressions reduce to the following expressions, which are also shown in

4.3 An Example of Two-element MIMO Terminal

[55]:

$$\begin{aligned}\rho_{a,x,n=2}(\Delta x) &= {}_1F_2\left(2; 1, \frac{5}{2}; -\frac{k^2\Delta x^2}{4}\right) \\ &= \frac{3}{2} \left\{ \frac{\sin(k\Delta x)}{k\Delta x} \left[1 - \frac{1}{(k\Delta x)^2} \right] + \frac{\cos(k\Delta x)}{(k\Delta x)^2} \right\}\end{aligned}\quad (4.30)$$

$$\begin{aligned}\rho_{a,z,n=2}(\Delta z) &= {}_0F_1\left(; \frac{5}{2}; -\frac{k^2\Delta z^2}{4}\right) \\ &= \frac{3}{(k\Delta z)^2} \left[\frac{\sin(k\Delta z)}{k\Delta z} - \cos(k\Delta z) \right],\end{aligned}\quad (4.31)$$

respectively. For $n \rightarrow \infty$, which signifies the case for a 2D plane, the above reduce to the classical Jakes model in [30], which are given as

$$\rho_{a,x,n \rightarrow \infty}(\Delta x) = \rho_{2D}(\Delta x) = J_0(k\Delta x) \quad (4.32)$$

$$\rho_{a,z,n \rightarrow \infty}(\Delta z) = 1, \quad (4.33)$$

respectively.

4.3 An Example of Two-element MIMO Terminal

4.3.1 Matching of Angular Power Spectrum

For the examination of a case having higher value of n , a dipole array of two elements with vertical interval distance $d = \lambda$ is considered, as shown in Fig. 4.3. The radiation patterns in the case of $n = 0, 2, 8$ and the pattern corresponding to the dipole AA given in Fig. 4.3 are described in Fig. 4.4. For simplicity, we assume that $\Omega_{p,\theta}(\phi, \theta) = \Omega_{p,\phi}(\phi, \theta) = 1$ and $G_\phi(\phi, \theta) = 0$. As shown in this figure, the lobe of the pattern in the case of $G_\theta(\phi, \theta) \approx \cos^{23} \theta$, and thus $\Omega(\phi, \theta) \approx \cos^{23} \theta$, is found to be suitable by normalizing the half-power beamwidth to approach the main lobe of the radiation pattern of AA.

4.3.2 Numerical Results

We calculate the correlation coefficient ρ_p by $\rho_p = |\rho_a|^2$ with respect to antenna spatial distance. For spatial correlation along the x direction, the characteristics

4. SPATIAL CORRELATION MODELING & CHARACTERIZATION WITH THREE-DIMENSIONAL APS OF $\text{COS}^N \theta$ FOR INDOOR MIMO TERMINAL

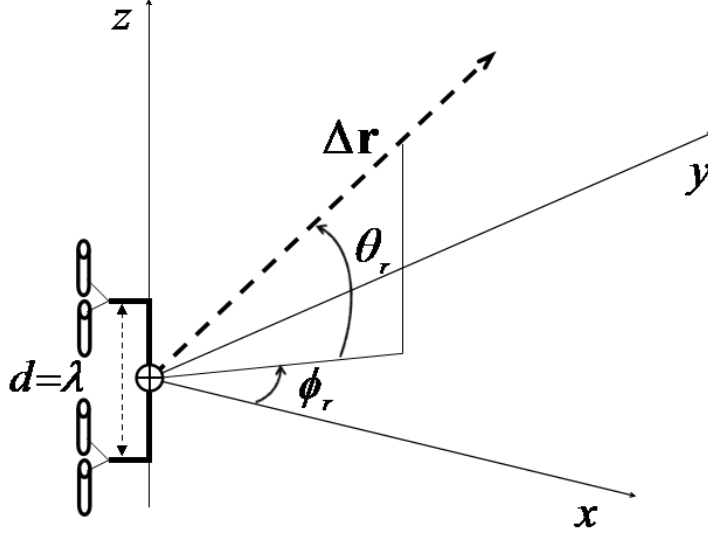


Figure 4.3: A dipole array of two elements with vertical interval distance $d = \lambda$ and moving vector $\Delta \mathbf{r}$ with angular of $\{\phi_r, \theta_r\}$.

of the patterns for the cases in which $n = 0, 2, 8$ and ∞ are calculated with aid of Eq. (4.26), as shown in Fig. 4.5. The figure shows that the spatial correlation characteristics change slightly and approach that of the Jakes model for $n = 8$. This agrees with the previous conclusion that, for many cases of the multipath environment in the 2D plane, the Jakes model is a reasonable approximation for the analysis of spatial correlation performance.

Spatial correlation evaluations along the z axis, which are calculated using Eq. (4.27), are also shown in Fig. 4.6. As we can see, the performance changes gradually as n increases, and the side lobes are restrained. The results illustrate that the correlation performance in the z direction is visibly influenced by the APS with elevation spread. The correlation coefficient will reach 1 as n approaches infinity.

Finally, for the AA given in Figs. 4.3 and 4.4, we approximate the spatial correlation characteristics when the moving direction of the reception point $\Delta \mathbf{r}$ is $\phi_r = 30^\circ$ and $\theta_r = 45^\circ, 60^\circ$ and 90° , respectively. We compare the approximated results given by Eq. (4.7) together with Eqs. (4.26) and (4.27) to the theoretical values obtained from Eq. (4.4), as shown in Fig. 4.7. The side lobe patterns in

4.3 An Example of Two-element MIMO Terminal

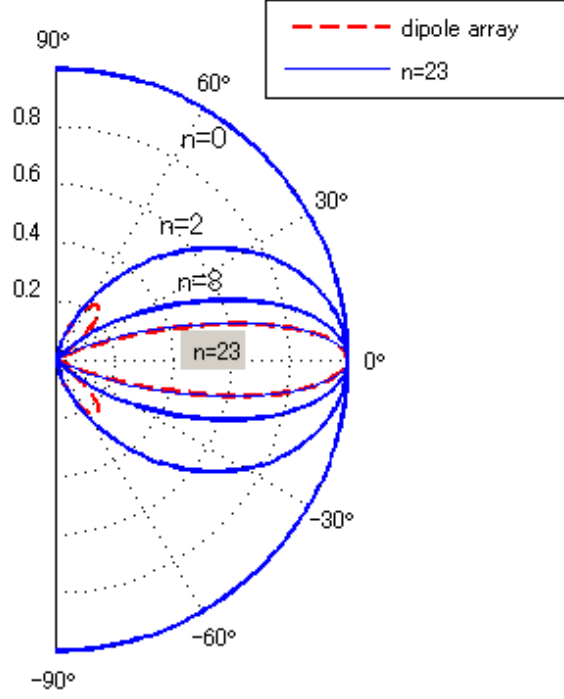


Figure 4.4: The reception patterns in the case of $n = 0, 2, 8$ and the case of $n = 23$ which corresponds to the half-power beamwidth of the dipole array given in Fig. 4.3.

spatial correlation for $\theta_r = 45^\circ$ and 60° disappear in the approximation case. This is because we ignore the side lobes by implementing the corresponding pattern of $\cos^{23} \theta$. Nevertheless, the main lobes of the approximated and theoretical values are shown to be in good agreement. For $\theta_r = 90^\circ$, the approximated and theoretical values coincide well.

4.3.3 Measurements in a Reverberation Chamber

There are some measurement completed in a reverberation chamber in the work of MIMO-OTA in [56], as shown in Fig. 4.8. For the measurement, a vector network analyzer (VNA) is used. Data of 1601 measurement points were obtained in each

4. SPATIAL CORRELATION MODELING & CHARACTERIZATION WITH THREE-DIMENSIONAL APS OF $\text{COS}^N \theta$ FOR INDOOR MIMO TERMINAL

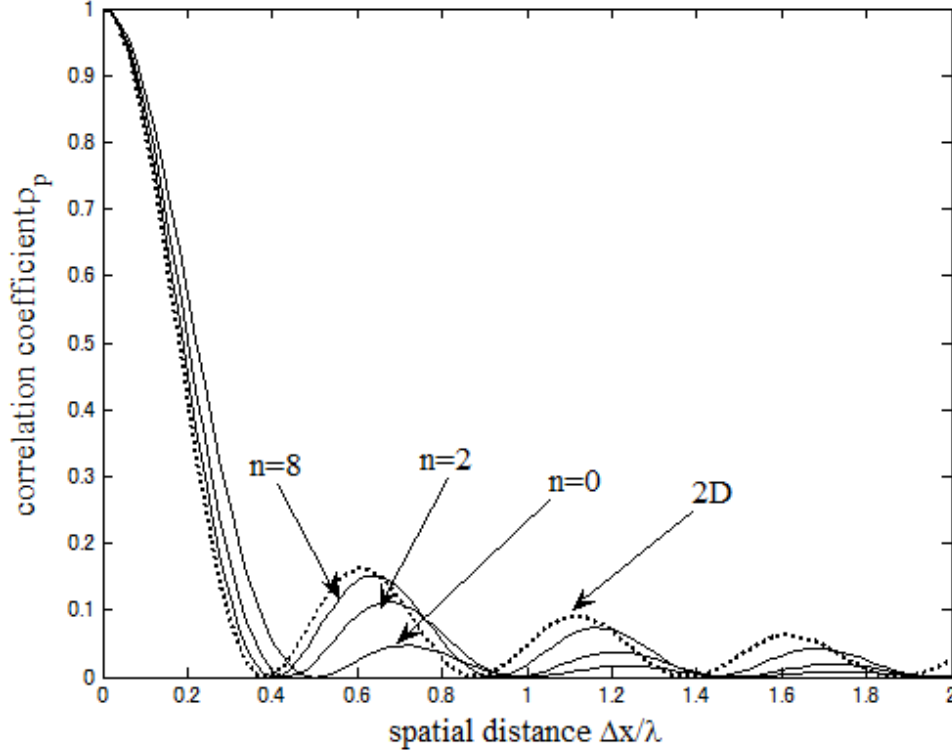


Figure 4.5: Spatial correlation calculations along x axis for the cases in which $n = 0, 2, 8$ and ∞ with aid of Eq. (4.26).

200MHz bandwidth with 125 kHz interval. Standard dipole antennas which have V (vertical) polarization for transmitting antennas, and V and H (horizontal) for receiving antennas are used. To increase the number of data points and to analyze spatial correlation, 41 points are used with a total length ± 1.5 wavelength across each of the points at an interval of $1/20$ wavelength, respectively.

The spatial correlation results are compared with the approximation values of $n = 2.75$ applying the *cos*-function and Eqs. (4.26) and (4.27), as shown in Fig. 4.9. As indicated, although there is a tiny difference between the measurement values and approximation values, spatial correlation performance can be averagely approximated by our proposal and newly-developed solutions very well.

4.3 An Example of Two-element MIMO Terminal

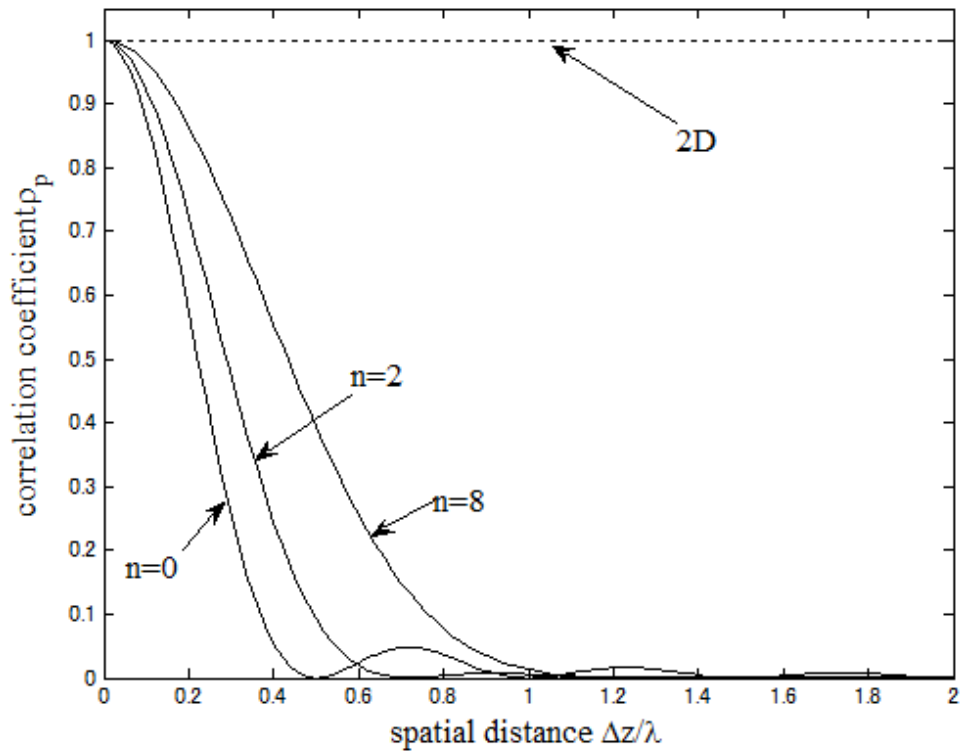


Figure 4.6: Spatial correlation calculations along z axis for the cases in which $n = 0, 2, 8$ and ∞ with aid of Eq. (4.27).

4. SPATIAL CORRELATION MODELING & CHARACTERIZATION WITH THREE-DIMENSIONAL APS OF $\text{COS}^N \theta$ FOR INDOOR MIMO TERMINAL

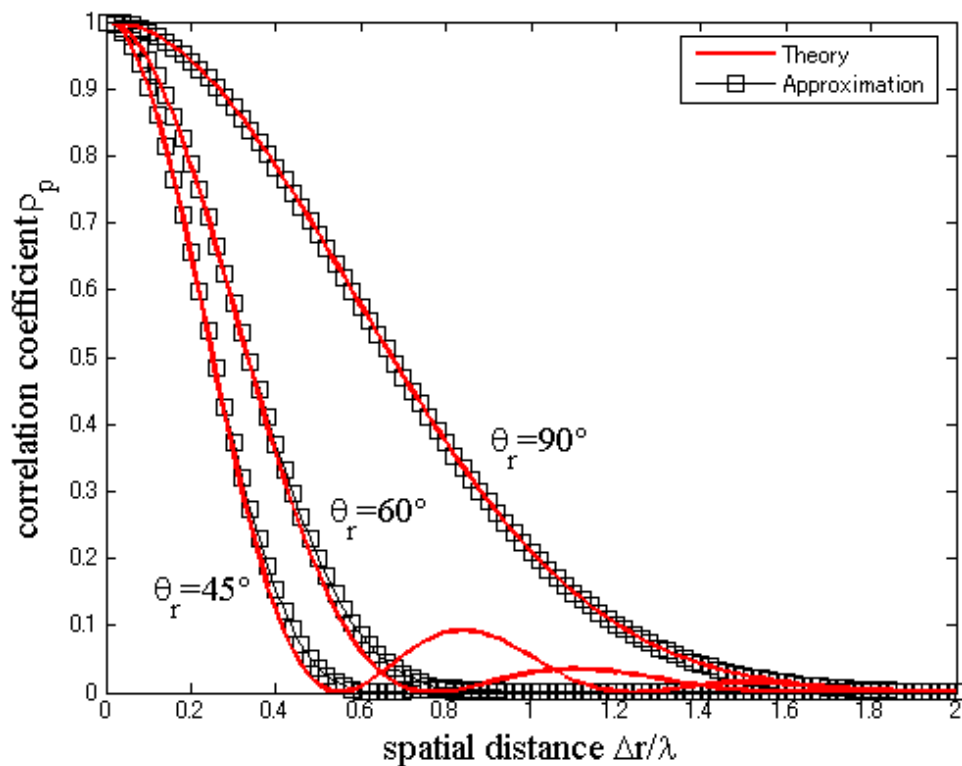


Figure 4.7: Spatial correlation calculations of theoretical value and approximated value for the case in which $n = 23$ and $\phi_r = 30^\circ$, $\theta_r = 45^\circ$, 60° and 90° , respectively.

4.3 An Example of Two-element MIMO Terminal



Figure 4.8: Outside view of the chamber.

4. SPATIAL CORRELATION MODELING & CHARACTERIZATION WITH THREE-DIMENSIONAL APS OF $\text{COS}^N \theta$ FOR INDOOR MIMO TERMINAL

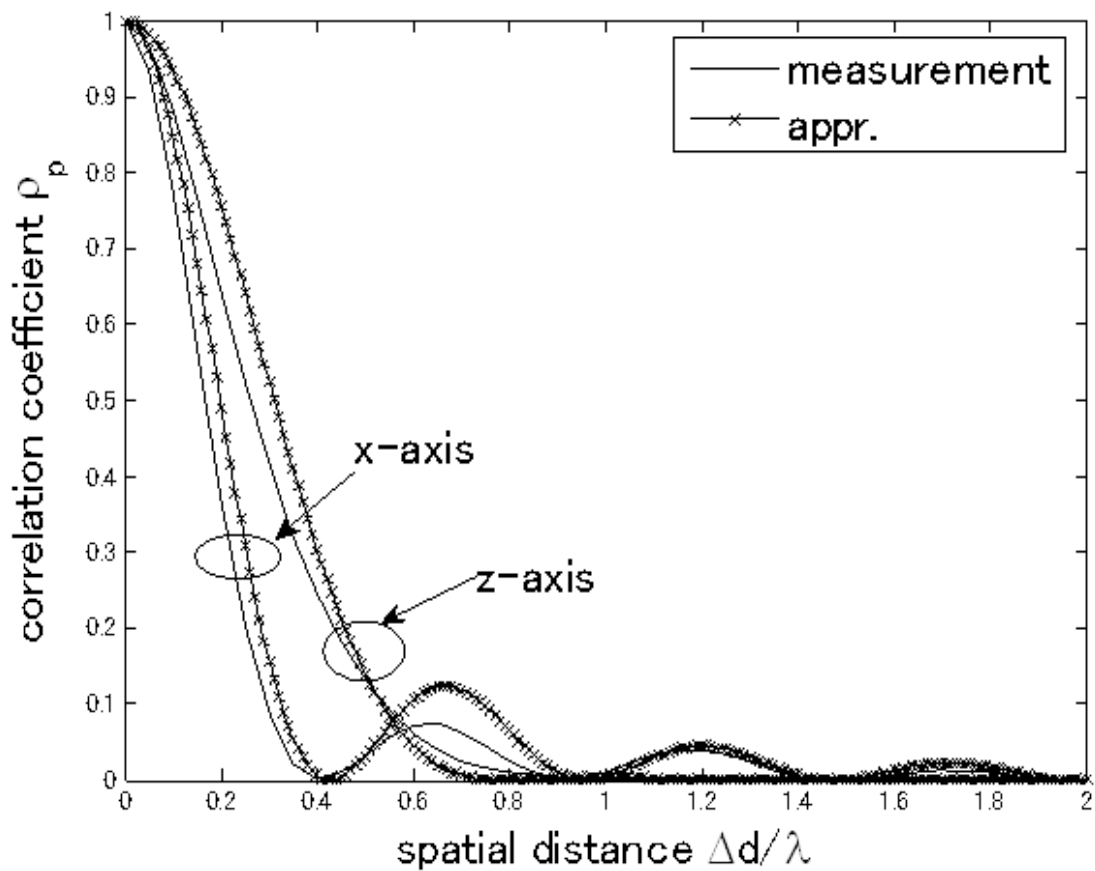


Figure 4.9: Performance comparison of spatial correlation of x and z axis in a reverberation chamber with the approximation values of $n = 2.75$ applying Eqs. (4.26) and (4.27).

Chapter 5

Conclusions & Future Work

5.1 Conclusions

MIMO channel modeling and evaluating in multipath environment is discussed in the dissertation. In the meantime for the characterization of MIMO system, we bring several newly-developed general functions. These functions not only enable a comprehensive method for modeling MIMO system but also satisfy the practicability for certain realistic environments. Noting that most of the derived results contain a factor in terms of a Hypergeometric function, these functions can be readily handled in today's modern packages and to some extent reveal the insight of mechanism of MIMO communications.

Firstly, beginning with channel modeling of MIMO in the mixed NLOS and LOS environment, the achieved function under the assumption of i.i.d. multi-channels with MRC-like effects enables an analytical approach for the calculation of SNR performance in such kind of scenario. Secondly, a field experiment conducted in a related research was introduced for the validation of effectiveness of the proposed model. The experiment conducted the same right-turn collision scenario with that in our simulation. Comparisons are made case by case at first and over all range of driving at last to show the practicality of our theoretical function. Lastly, we also discussed the advantages of MIMO comparing to SISO and SIMO when applied to ITS-IVC in the right-turn collision scenario. The proposed approach would be useful to analyze the MIMO channels in complex propagation environment such as that in ITS-IVC. The advantage of MIMO in

5. CONCLUSIONS & FUTURE WORK

IVC is also understandable and such application is pretty reasonable. The proposal has a merit for researchers who take a great interest in an outdoor MIMO radio communication with a relatively short communication distance.

Secondly, the efforts we have done on evaluation of spatial correlation which is a primary characteristic for analytically/correlation-based MIMO modeling reach a preferable neat generalization in Cartesian coordinates. The proposed generalization for evaluating spatial correlation with a three-dimensional APS in the case of $\cos^n \theta$ is further derived to be the products of simple expressions in terms of Hypergeometric functions. As the APS $\cos^n \theta$ is a combination of antenna effects and physical environments, it can integrate various situations of multipath richness without too complicated channel modeling. Some previous results such as Jakes Model are turned out to be special cases of our proposal. In the following example of two elements array antenna, we compared the spatial correlation performance of theoretical values with that obtained by our proposal. Although side lobes are ignored by our proposal due to the corresponding pattern of $\cos^{23} \theta$, main lobes of the theoretical values and approximated values are shown to be in pretty good agreement for each direction of the MIMO terminal in motion.

5.2 Future Work

Although the proposed general functions are useful for many certain situations, there are always conditions and assumptions associated. These conditions and assumptions on the one hand assure the effectiveness and practicability of models with acceptable errors or variations; they on the other hand limit the range of application for other scenarios. The overlooked scenarios in the dissertation which are still notable for further study are highlighted as follows:

Correlated MIMO channel modeling in high mobility situation- In the proposed general method of channel modeling in a mixture environment, it is reasonable to assume an i.i.d channel matrix because the transmission range is relatively short and the antenna elements are separated from each other by the vehicle body in an occasion of ITS-IVC. However the method may not be applicable to other areas when significant correlation occurs. In addition, the functions are good under MRC-like effect, in our case which could rest assured by

a proved OSTBC scheme. However OSTBC scheme is sensitive to the temporal channel variation. A high mobility of vehicle, which is unlike the right-turn occasion in our dissertation, may break the MRC-like effect and degrade the performance of approximation using our proposal. For future applications to ITS, MIMO channel modeling considering the above may be very expected.

Arbitrary pattern of 3D APS- Our general functions are derived under the assumption that radio waves spread uniformly in azimuth direction and directionally in elevation direction. As introduced in Chapter 4, most multipath-rich situations such as typical indoor offices can be supposed to approximate the limitation. But that is still significant and preferable if an arbitrary general model with low computation is developed.

5. CONCLUSIONS & FUTURE WORK

Appendix

Derivation of $\rho_{a,z}(\Delta z)$

With similar procedures, $\rho_{a,z}(\Delta z)$ is hopefully to be rewritten as

$$\begin{aligned}\rho_{a,z}(\Delta z) &= \frac{4\pi}{P_R} f_z(u) \\ &= \frac{4\pi}{P_R} \int_0^1 (1 - \sin^2 \theta)^{\frac{n}{2}} \cos(k\Delta z \sin \theta) d(\sin \theta) \\ &= \frac{4\pi}{P_R} \int_0^\infty g_z(uv) h_z(v) dv\end{aligned}\tag{1}$$

where $g_z(u)$ and $h_z(v)$ are respectively given by

$$g_z(u) = \cos u\tag{2}$$

$$h_z(v) = \begin{cases} (1 - v^2)^{-\frac{\tau}{2}}, & \text{for } 0 < v < 1 \\ 0, & \text{for } v > 1 \end{cases}\tag{3}$$

with the substitutions of $u = k\Delta z$, $v = \sin \theta$ and $\tau = n, n > 0$. Then, the corresponding MTs can be given as

$$\tilde{g}_z(s) = \Gamma(s) \cos \frac{\pi s}{2}\tag{4}$$

$$\tilde{h}_z(s) = \frac{1}{2} \frac{\Gamma(1 + \frac{\tau}{2}) \Gamma(\frac{s}{2})}{\Gamma(1 + \frac{\tau}{2} + \frac{s}{2})}\tag{5}$$

Therefore the product $\tilde{f}_z(s)$ is given as

$$\begin{aligned}\tilde{f}_z(s) &= \tilde{g}_z(s) \tilde{h}_z(1 - s) \\ &= \frac{1}{2} \cos \frac{\pi s}{2} \left[\frac{\Gamma(s) \Gamma(1 + \frac{\tau}{2}) \Gamma(\frac{1}{2} - \frac{s}{2})}{\Gamma(\frac{3}{2} + \frac{\tau}{2} - \frac{s}{2})} \right]\end{aligned}\tag{6}$$

. APPENDIX

holding for $0 < \text{Re}\{s\} < 1$. Note from properties of the Gamma function that

$$\Gamma(s + \frac{1}{2})\Gamma(\frac{1}{2} - s) = \frac{\pi}{\cos(\pi s)} \quad (7)$$

$$\Gamma(2s) = \frac{1}{2\sqrt{\pi}} 2^{2s}\Gamma(s)\Gamma(s + \frac{1}{2}) \quad (8)$$

$\tilde{f}_z(s)$ can be derived as

$$\tilde{f}_z(s) = \frac{\sqrt{\pi}\Gamma(1 + \frac{\tau}{2})}{4} \frac{2^s\Gamma(\frac{s}{2})}{\Gamma(\frac{3}{2} + \frac{\tau}{2} - \frac{s}{2})} \quad (9)$$

There are simple poles located at $s = -2m$ for $\tilde{f}_z(s)$. We hence deduce that

$$\begin{aligned} f_z(u) &= \sum_{m=0}^{\infty} \text{Res} \left\{ \tilde{f}_z(s) u^{-s}; s = -2m \right\} \\ &= \frac{\sqrt{\pi}\Gamma(1 + \frac{\tau}{2})}{4} \sum_{m=0}^{\infty} \frac{1}{\Gamma(\frac{3}{2} + \frac{\tau}{2} + m)} \\ &\quad \times \text{Res} \left\{ \Gamma(\frac{s}{2}) \left(\frac{u}{2}\right)^{-s}; s = -2m \right\} \\ &= \frac{\sqrt{\pi}}{2} \frac{\Gamma(1 + \frac{\tau}{2})}{\Gamma(\frac{3}{2} + \frac{\tau}{2})} {}_0F_1\left(; \frac{3}{2} + \frac{\tau}{2}; -\frac{u^2}{4}\right) \end{aligned} \quad (10)$$

Then because of (4.24) and (1) and substituting $u = k\Delta z, \tau = n$ into (10), $\rho_{a,z}(\Delta z)$ is obtained by

$$\begin{aligned} \rho_{a,z}(\Delta z) &= \frac{4\pi}{P_R} f_z(k\Delta z) \\ &= {}_0F_1\left(; \frac{3}{2} + \frac{n}{2}; -\frac{k^2\Delta z^2}{4}\right) \end{aligned} \quad (11)$$

References

- [1] A. Kaye and D. George, “Transmission of multiplexed pam signals over multiple channel and diversity systems,” *IEEE Transactions on Communication Technology*, vol. 18, no. 5, pp. 520–526, Oct. 1970.
- [2] L. Brandenburg and A. Wyner, “Capacity of the gaussian channel with memory: The multivariate case,” *Bell Syst. Tech. J.*, vol. 53, no. 5, pp. 745–778, 1974.
- [3] W. Van Etten, “An optimum linear receiver for multiple channel digital transmission systems,” *IEEE Transactions on Communications*, vol. 23, no. 8, pp. 828–834, 1975.
- [4] —, “Maximum likelihood receiver for multiple channel transmission systems,” *IEEE Transactions on Communications*, vol. 24, no. 2, pp. 276–283, 1976.
- [5] J. Salz, “Digital transmission over cross-coupled linear channels,” *AT&T Technical Journal*, vol. 64, pp. 1147–1159, 1985.
- [6] G. Foschini, “Layered space-time architecture for wireless communication in a fading environment when using multi-element antennas,” *Bell labs technical journal*, vol. 1, no. 2, pp. 41–59, 1996.
- [7] X. Cheng, C. Wang, H. Wang, X. Gao, X. You, D. Yuan, B. Ai, Q. Huo, L. Song, and B. Jiao, “Cooperative mimo channel modeling and multi-link spatial correlation properties,” *IEEE Journal on Selected Areas in Communications*, vol. 30, no. 2, pp. 388–396, Feb. 2012.
- [8] J. Poutanen, F. Tufvesson, K. Haneda, V. Kolmonen, and P. Vainikainen, “Multi-link mimo channel modeling using geometry-based approach,” *IEEE Transactions on Antennas and Propagation*, vol. 60, no. 2, pp. 587–596, Feb. 2012.

REFERENCES

- [9] R. Schoenen and C. Teijeiro, “A correlation-based mimo performance model for the system level analysis on mac layer,” in *IEEE International Conference on Communication Systems*, Nov. 2010, pp. 122 –126.
- [10] Z. Luo, X. Chen, and T. Jin, “Simplified simulator for correlation-based mimo radio channel model,” in *Global Mobile Congress*, Oct. 2009, pp. 1 –5.
- [11] Y. Jing, Z. Wen, H. Kong, S. Duffy, and M. Rumney, “Two-stage over the air (ota) test method for mimo device performance evaluation,” in *IEEE International Symposium on Antennas and Propagation*, Jul. 2011, pp. 71 –74.
- [12] A. Kosako, M. Shinozawa, and Y. Karasawa, “Simplified configuration of fading emulator system for mimo-ota testing,” in *2nd International Conference on Wireless Communication, Vehicular Technology, Information Theory and Aerospace Electronic Systems Technology*, Mar. 2011, pp. 1 –5.
- [13] A. Marin-Soler and D. Sanchez-Hernandez, “New mimo ota figures of merit,” in *6th European Conference on Antennas and Propagation*, Mar. 2012, pp. 2123 –2126.
- [14] W. Kotterman, A. Heuberger, and R. Thoma, “On the accuracy of synthesised wave-fields in mimo-ota set-ups,” in *Proceedings of the 5th European Conference on Antennas and Propagation*, Apr. 2011, pp. 2560 –2564.
- [15] Y. Feng, W. Schroeder, and T. Kaiser, “Straightforward mimo ota characterization and statistical metrics for lte devices,” in *6th European Conference on Antennas and Propagation*, Mar. 2012, pp. 2294 –2298.
- [16] C. Orlenius, C. Patane, A. Skarbratt, J. Asberg, and M. Franzen, “Analysis of mimo ota measurements for lte terminals performed in reverberation chamber,” in *6th European Conference on Antennas and Propagation*, Mar. 2012, pp. 1934 –1938.
- [17] Y. Yang, G. Xu, and H. Ling, “An experimental investigation of wideband mimo channel characteristics based on outdoor non-los measurements at 1.8 ghz,” *IEEE Transactions on Antennas and Propagation*, vol. 54, no. 11, pp. 3274 –3284, Nov. 2006.
- [18] L. Tsai and D. Shiu, “Channel modeling and capacity evaluation for relay-aided mimo systems in los environments,” in *International Symposium on Communications and Information Technologies*, Oct. 2007, pp. 796 –801.

REFERENCES

- [19] I. Sarris and A. Nix, “Design and performance assessment of high-capacity mimo architectures in the presence of a line-of-sight component,” *IEEE Transactions on Vehicular Technology*, vol. 56, no. 4, pp. 2194–2202, Jul. 2007.
- [20] S. Wyne, A. Molisch, P. Almers, G. Eriksson, J. Karedal, and F. Tufvesson, “Outdoor-to-indoor office mimo measurements and analysis at 5.2 ghz,” *IEEE Transactions on Vehicular Technology*, vol. 57, no. 3, pp. 1374–1386, May 2008.
- [21] X. Gao, J. Zhang, G. Liu, D. Xu, P. Zhang, Y. Lu, and W. Dong, “Large-scale characteristics of 5.25 ghz based on wideband mimo channel measurements,” *IEEE Antennas and Wireless Propagation Letters*, vol. 6, pp. 263–266, Dec. 2007.
- [22] A. Kuchar, J. Rossi, and E. Bonek, “Directional macro-cell channel characterization from urban measurements,” *IEEE Transactions on Antennas and Propagation*, vol. 48, no. 2, pp. 137–146, 2000.
- [23] K. Kalliola, K. Sulonen, H. Laitinen, O. Kivekas, J. Krogerus, and P. Vainikainen, “Angular power distribution and mean effective gain of mobile antenna in different propagation environments,” *IEEE Transactions on Vehicular Technology*, vol. 51, no. 5, pp. 823–838, 2002.
- [24] S. Obayashi, T. Ohishi, and Y. Karasawa, “Effect of vertical angle spread of propagation channel on mimo ota measurement method,” in *Asia-Pacific Microwave Conference Proceedings*, Dec. 2010, pp. 1934–1937.
- [25] Y. Wang, K. Ito, and Y. Karasawa, “Propagation channel modeling in the mixture of nlos and los environments for mimo-mrc system and its application to its-ivc,” *IEICE Transactions on Communications*, vol. 94, no. 5, pp. 1207–1214, 2011.
- [26] Y. Wang, H. L. Dang, and Y. Karasawa, “Spatial correlation functions in three-dimensional aps with $\cos^n \theta$,” *IEEE Antennas and Wireless Propagation Letters*, vol. 11, pp. 511–514, 2012.
- [27] Y. Okumura, E. Ohmori, T. Kawano, and K. Fukuda, “Field strength and its variability in vhf and uhf land-mobile radio service,” *Rev. Elec. Commun. Lab*, vol. 16, no. 9, pp. 825–73, 1968.
- [28] M. Hata, “Empirical formula for propagation loss in land mobile radio services,” *IEEE Transactions on Vehicular Technology*, vol. 29, no. 3, pp. 317–325, 1980.

REFERENCES

- [29] V. Erceg, L. Greenstein, S. Tjandra, S. Parkoff, A. Gupta, B. Kulic, A. Julius, and R. Bianchi, “An empirically based path loss model for wireless channels in suburban environments,” *IEEE Journal on Selected Areas in Communications*, vol. 17, no. 7, pp. 1205–1211, 1999.
- [30] J. WC Jr, “Microwave mobile communications,” 1974.
- [31] S. Alamouti, “A simple transmit diversity technique for wireless communications,” *IEEE Journal on Selected Areas in Communications*, vol. 16, no. 8, pp. 1451–1458, 1998.
- [32] V. Tarokh, H. Jafarkhani, and A. Calderbank, “Space-time block codes from orthogonal designs,” *IEEE Transactions on Information Theory*, vol. 45, no. 5, pp. 1456–1467, 1999.
- [33] H. Jafarkhani, “A quasi-orthogonal space-time block code,” *IEEE Transactions on Communications*, vol. 49, no. 1, pp. 1–4, 2001.
- [34] C. Yuen, Y. Guan, and T. Tjhung, “Quasi-orthogonal stbc with minimum decoding complexity,” *IEEE Transactions on Wireless Communications*, vol. 4, no. 5, pp. 2089–2094, 2005.
- [35] W. Su and X. Xia, “Signal constellations for quasi-orthogonal space-time block codes with full diversity,” *IEEE Transactions on Information Theory*, vol. 50, no. 10, pp. 2331–2347, 2004.
- [36] M. Cabrera, J. Vidal, and M. Payaro, “2ghz mimo channel model from experimental outdoor data analysis in umts,” in *IEEE 58th Vehicular Technology Conference*, vol. 2, Oct. 2003, pp. 1172 – 1176 Vol.2.
- [37] I. Sarris and A. Nix, “Performance investigation of a line-of-sight optimised 2×2 mimo system,” in *3rd International Symposium on Wireless Communication Systems*, Sept. 2006, pp. 608 –611.
- [38] —, “A line-of-sight optimised mimo architecture for outdoor environments,” in *IEEE 64th Vehicular Technology Conference*, Sept. 2006, pp. 1 –5.
- [39] X. Cheng, C. Wang, D. Laurenson, H. Chen, and A. Vasilakos, “A generic geometrical-based mimo mobile-to-mobile channel model,” in *Wireless Communications and Mobile Computing Conference*, Aug. 2008, pp. 1000 –1005.

REFERENCES

- [40] D. Smith and T. Abhayapala, “Generalised space-time modelling of rayleigh mimo channels,” in *Proceedings in 6th Australian Communications Theory Workshop*, Feb. 2005, pp. 145 –150.
- [41] W. Kim, H. Lee, J. Park, M. Kim, and H. Chung, “Modeling of eigenvalues for mimo channel capacity based on outdoor measurements,” in *IEEE 69th Vehicular Technology Conference*, Apr. 2009, pp. 1 –5.
- [42] A. Gaya and D. Panda, “Modeling, calculating and capacity enhancement of a rayleigh fading mimo channel,” in *IEEE Applied Electromagnetics Conference*, Dec. 2011, pp. 1 –3.
- [43] M. Sun, W. Feng, T. Lai, K. Yamada, H. Okada, and K. Fujimura, “Gps-based message broadcast for adaptive inter-vehicle communications,” in *IEEE 52nd Vehicular Technology Conference*, vol. 6, 2000, pp. 2685 –2692 vol.6.
- [44] A. Shah and J. Lee, “Intelligent transportation systems in transitional and developing countries,” *IEEE Aerospace and Electronic Systems Magazine*, vol. 22, no. 8, pp. 27 –33, Aug. 2007.
- [45] M. Natvig and H. Westerheim, “National multimodal travel information - a strategy based on stakeholder involvement and intelligent transportation system architecture,” *IET Intelligent Transport Systems*, vol. 1, no. 2, pp. 102 –109, Jun. 2007.
- [46] J. Zhang, F. Wang, K. Wang, W. Lin, X. Xu, and C. Chen, “Data-driven intelligent transportation systems: A survey,” *IEEE Transactions on Intelligent Transportation Systems*, vol. 12, no. 4, pp. 1624 –1639, Dec. 2011.
- [47] K. Ito, N. Suzuki, and Y. Karasawa, “Performance evaluation of mimo-stbc for inter-vehicle communications in a shadowing environment generated by a large vehicle,” in *IEEE 66th Vehicular Technology Conference*, 2007, pp. 758–762.
- [48] M. Feeney and J. Parsons, “Cross-correlation between 900 mhz signals received on vertically separated antennas in small-cell mobile radio systems,” in *IEE Proceedings I-Communications, Speech and Vision*, vol. 138, no. 2, 1991, pp. 81–86.
- [49] K. Pedersen, P. Mogensen, and B. Fleury, “A stochastic model of the temporal and azimuthal dispersion seen at the base station in outdoor propagation environments,” *IEEE Transactions on Vehicular Technology*, vol. 49, no. 2, pp. 437–447, 2000.

REFERENCES

- [50] A. Poon and M. Ho, “Indoor multiple-antenna channel characterization from 2 to 8 ghz,” in *IEEE International Conference on Communications*, vol. 5, 2003, pp. 3519–3523.
- [51] S. Yong and J. Thompson, “Three-dimensional spatial fading correlation models for compact mimo receivers,” *IEEE Transactions on Wireless Communications*, vol. 4, no. 6, pp. 2856 – 2869, Nov. 2005.
- [52] J. Ho, “Generalized doppler power spectrum for 3d non-isotropic scattering environments,” in *IEEE Global Telecommunications Conference*, vol. 3, Nov. 2005, p. 4 pp.
- [53] H. Dang and Y. Karasawa, “Spatial correlation characteristics in three-dimensional multipath channels,” in *IEICE Technical Report*, vol. 109, no. 1, Apr. 2009, pp. 31 – 36.
- [54] G. Fikioris, “Integral evaluation using the mellin transform and generalized hypergeometric functions: Tutorial and applications to antenna problems,” *IEEE Transactions on Antennas and Propagation*, vol. 54, no. 12, pp. 3895 –3907, Dec. 2006.
- [55] P. Doncker *et al.*, “Spatial correlation functions for fields in three-dimensional rayleigh channels,” *Progress In Electromagnetics Research*, vol. 40, pp. 55–69, 2003.
- [56] F. Tamrin, I. Oshima, and Y. Karasawa, “A reverberation chamber to realize multipath-rich environment [iv]– frequency dependence of propagation characteristics in the chamber,” in *IEICE Technical Report*, ser. AP2012-113, vol. 112, no. 285, Nov. 2012, pp. 115–120.

Journal Publications

- [1] Y. Wang, K. Ito and Y. Karasawa, "Propagation Channel Modeling in the Mixture of NLOS and LOS Environments for MIMO-MRC System and Its Application to ITS-IVC," IEICE Trans. Communications, Vol.E94-B, NO.5, pp.1204-1214, 2011.5.
- [2] Y. Wang, H. L. Dang and Y. Karasawa, "Spatial Correlation Functions in Three-Dimensional APS With $\cos^n \theta$ ", IEEE Antennas and Wireless Propagation Letters, vol.11, pp.511-514, May. 2012.

International Conferences

- [1] Y. Wang, K. Ito and Y. Karasawa, "ITS-IVC Propagation Channel Model applying MIMO technology," Triangle Symposium on Advanced ICT (TriSAI), 2009.
- [2] Y. Wang and Y. Karasawa, "A Generalized Formula for Spatial Correlation in Three-dimensional Fading Environment," International Symposium on Antennas and Propagation (ISAP2011), Oct. 2011.

Domestic Conferences

- [1] 王軼, 伊藤健二, 唐沢好男, "ITS-IVC Propagation Channel Model for MIMO-STBC Transmissin at an Intersection where a Large Vehicle Shadows the Oncomming Car,"信学ソ大, B-1-196, 2009.09.
- [2] Y. Wang and Y. Karasawa, "A Generalized Formula for Spatial Correlation in Three-dimensional Fading Environment," 電子情報通信学会技術研究報告. A・P, アンテナ・伝播 111(128), 19-24, 2011-07-06.

Propagation Channel Modeling in the Mixture of NLOS and LOS Environments for MIMO-MRC System and Its Application to ITS-IVC

Yi WANG^{†a)}, Student Member, Kenji ITO^{††}, Member, and Yoshio KARASAWA[†], Fellow

SUMMARY This paper presents a Multiple-Input Multiple-Output (MIMO) propagation model for independent and identically distributed (i.i.d.) channels in the mixture of none-Line-of-Sight (NLOS) and Line-of-Sight (LOS) environments. The derived model enables to evaluate the system statistical characteristics of Signal-to-Noise-Ratio (SNR) for MIMO transmission based on Maximal Ratio Combining (MRC). An application example applying the model in 2×2 configuration to ITS Inter-Vehicle Communication (IVC) system is introduced. We clarify the effectiveness of the proposed model by comparisons of both computer simulations and measurement results of a field experiment. We also use the model to show the better performance of SNR when applying MIMO to IVC system than SISO and SIMO.

key words: propagation model, MIMO-MRC system, mixture of NLOS and LOS environments, ITS, Inter-Vehicle Communication (IVC), Signal-to-Noise-Ratio (SNR)

1. Introduction

A wide variety of efforts have proved that using Multiple-Input Multiple-Output (MIMO) technology achieves high data rate and reliability improvements for wireless communications in multipath environment [1]–[3]. Therefore MIMO propagation channel modeling for performance evaluation of transmission attracts persistent attention in recent years, for example a model in none-Line-of-Sight (NLOS) environment proposed in the reference [4], and a study of MIMO modeling in Line-of-Sight (LOS) environment [5]. However, so far most of these models or analysis considered MIMO systems in a pure NLOS or LOS environment. Propagation in NLOS environment was modeled by Rayleigh fading, and in LOS environment, Nakagami-Rice fading or Nakagami-m fading was widely used. The mixed environment with LOS and NLOS among array antenna elements, on the other hand, is likely to occur in some cases, but rarely considered for channel modeling. This kind of scenario can be found in the presence of obstacle, when there are large intervals between antenna elements and the propagation range between transmitter and receiver is comparatively small.

In addition, it is also well known that Maximal Ra-

tio Combining (MRC) is the optimal combining technique in terms of maximizing the Signal-to-Noise-Ratio (SNR) at the combiner output. To enjoy the benefits of MIMO transmission besides MRC effect, known as MIMO-MRC system, Alamouti's space-time block coding (STBC) method [6] provides a simple and attractive scheme to realize full-rate and full-diversity transmission in complex signal space. Although it is proved that this coding method doesn't exist for systems with more than two transmit antennas, the full-diversity property can still be achieved by other designs such as non-full-rate STBC schemes [7]. From this viewpoint, it is very promising to investigate MIMO propagation performance under the assumption of MRC for single-stream transmission.

In this paper, first, we develop a model of MIMO system performed in the mixture of NLOS and LOS environments for evaluation of SNR under MRC assumption. As an example, we demonstrate the effectiveness of our proposed model with an application to Inter-Vehicle Communication for Intelligent Transport systems (ITS-IVC) where a large vehicle at an intersection shadows the on-coming car. The model is presented in Sect. 2. The application in detail and performance results of simulations and comparisons are given in Sect. 3. And in Sect. 4 we achieve the conclusion.

2. Proposed System Model in STBC

2.1 System Model

For a MIMO system with N_t transmit antennas and N_r receive antennas, we assume that the propagation environment is surrounded by scatterers and partly shadowed by an obstacle located across parts of the direct links among array elements, as shown in Fig. 1. Therefore multipath waves are always in existence and propagation characteristics depend on the mixed LOS and NLOS environment.

The channel matrix H is given as

$$H = \begin{pmatrix} h_{11} & h_{12} & \dots & h_{1N_t} \\ h_{21} & h_{22} & \dots & h_{2N_t} \\ \vdots & \vdots & \ddots & \vdots \\ h_{N_r,1} & h_{N_r,2} & \dots & h_{N_r,N_t} \end{pmatrix} \equiv \{h_{n_r,n_t}\} \quad (1)$$

To represent direct wave power components and scattering wave power components of the channel matrix as

Manuscript received August 23, 2010.

Manuscript revised December 16, 2010.

[†]The authors are with Advanced Wireless Communication Research Center (AWCC), The University of Electro-Communications, Chofu-shi, 182-8585 Japan.

^{††}The author is with the Toyota Central R&D Labs., Inc., Aichi-ken, 480-1192 Japan.

a) E-mail: eason@radio3.ee.uec.ac.jp

DOI: 10.1587/transcom.E94.B.1207

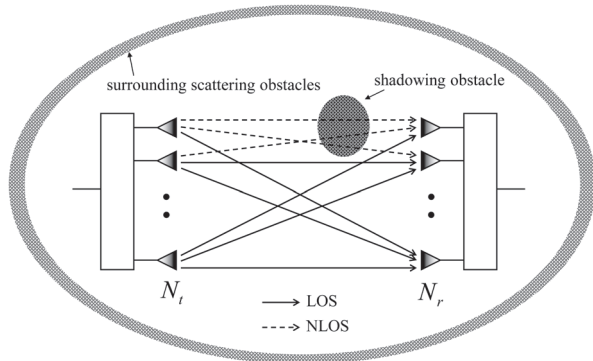


Fig. 1 MIMO propagation model in a mixture of NLOS and LOS channels.

H_D , H_S , respectively, with independent and identically distributed (i.i.d.) channels assumption, (1) can be rewritten as

$$H = \sqrt{z_D} H_D + \sqrt{z_S} H_S \quad (2a)$$

where

$$H_D \equiv \{u_{n,n'}\} \quad (2b)$$

$$H_S \equiv \{v_{n,n'}\} \quad (2c)$$

and

$$u_{n,n'} = \begin{cases} 1 & \text{for LOS} \\ 0 & \text{for NLOS} \end{cases} \quad (2d)$$

$$\langle v_{n,n'}^*, v_{n',n''} \rangle = \begin{cases} 1 & \text{for } n_t = n'_t \text{ and } n_r = n'_r \text{ (i.i.d.)} \\ 0 & \text{for } n_t \neq n'_t \text{ or } n_r \neq n'_r \end{cases} \quad (2e)$$

The notations n_t and n'_t represent transmit antenna numbers while the notations n_r and n'_r represent receive antenna numbers.

The Rice factor K is defined by the ratio of direct wave power z_D and averaged scattering wave power z_S , given by

$$K \equiv \frac{z_D}{z_S} \quad (3)$$

Up to now, we have described a system model for MIMO communication in such an environment, which is a mixture of NLOS and LOS sub-channels and sub-channels are uncorrelated. The next we would like to investigate the characteristics of output SNR. We use MRC method for evaluation because of obtaining good SNR performance.

2.2 SNR in STBC

As presented, the previous efforts on STBC have enabled full diversity transmission even in the case of $N_t > 2$. We review the SNR characteristics under the assumption of MRC by the general STBC scheme. For MIMO system, the output SNR, γ , is proved to be proportional to the Frobenius norm of channel matrix H , given by

$$\gamma = \|H\|_F^2 \gamma_{\text{ref}} \quad (4)$$

where the Frobenius norm is given as

$$\|H\|_F^2 \equiv \sum_{n_r=1}^{N_r} \sum_{n_t=1}^{N_t} |h_{n_r,n_t}|^2 \quad (5)$$

and γ_{ref} is the reference SNR normalized by N_t , which is resulted from total transmit power constraint in STBC scheme, given as

$$\gamma_{\text{ref}} = \frac{1}{N_t} \gamma_0 \quad (6)$$

where γ_0 is the system SNR when $N_t = N_r = 1$ for the path with direct wave component only.

Besides the assumption of i.i.d. channels for the $N_t \times N_r$ MIMO system, the number of LOS sub-channels is represented as N_{LOS} and SNR for i -th sub-channel in LOS environment is $\gamma_{\text{LOS}}^{(i)}$, similarly for NLOS environment, the number is represented as N_{NLOS} , and the SNR is $\gamma_{\text{NLOS}}^{(j)}$, then we have

$$N_{\text{LOS}} + N_{\text{NLOS}} = N_t N_r \quad (7)$$

where $N_t N_r$ is the total number of sub-channels, and

$$\gamma = \sum_{i=1}^{N_{\text{LOS}}} \gamma_{\text{LOS}}^{(i)} + \sum_{j=1}^{N_{\text{NLOS}}} \gamma_{\text{NLOS}}^{(j)} \quad (8)$$

according to MRC theory.

2.3 Probability Density Function

We investigate the transmission performance of output SNR in terms of probability density function (PDF) for the proposed model.

For a LOS sub-channel in which signal amplitude follows Nakagami-Rice distribution, the PDF of SNR is considered as a non-central χ^2 distribution, given by

$$f_{\text{LOS}}(\gamma) = \frac{K}{\gamma_D} \exp\left\{-K\left(1 + \frac{\gamma}{\gamma_D}\right)\right\} I_0\left(2K \sqrt{\frac{\gamma}{\gamma_D}}\right) \quad (9)$$

where γ_D is the SNR of direct wave signal and $I_0(\cdot)$ is the modified Bessel function of the first kind with order zero. The PDF of SNR for a NLOS sub-channel is known as an exponential distribution given by

$$f_{\text{NLOS}}(\gamma) = \frac{1}{\gamma_S} \exp\left(-\frac{\gamma}{\gamma_S}\right) \quad (10)$$

where γ_S is the average SNR of multipath scattering wave signal. Using the definition of K in (3), (10) can be rewritten as

$$f_{\text{NLOS}}(\gamma) = \frac{K}{\gamma_D} \exp\left(-\frac{K\gamma}{\gamma_D}\right) \quad (11)$$

This expression including the factor K seems curious in conventional NLOS environment, but in this case, it seems reasonable because the direct signal level can be estimated from

other LOS paths.

To derive the expression of γ in (4) for the system in mixed LOS and NLOS environment, a transformation of each PDF into moment-generating function is employed. The moment-generating function $F_{\text{LOS}}(s)$ and $F_{\text{NLOS}}(s)$ for $f_{\text{LOS}}(\gamma)$ and $f_{\text{NLOS}}(\gamma)$ can be obtained through Laplace transformation $\mathcal{L}[\cdot]$, and the results are given as

$$\begin{aligned} F_{\text{LOS}}(s) &\equiv \mathcal{L}[f_{\text{LOS}}(s)] \\ &= \left(\frac{K}{K + \gamma_D s} \right) \exp\left(-\frac{K\gamma_D s}{K + \gamma_D s} \right) \end{aligned} \quad (12)$$

$$F_{\text{NLOS}}(s) \equiv \mathcal{L}[f_{\text{NLOS}}(s)] = \frac{K}{K + \gamma_D s} \quad (13)$$

respectively. Because of i.i.d. assumption, the function $F_{\text{MRC}}(s)$ for the desired γ in MIMO system can be obtained by

$$\begin{aligned} F_{\text{MRC}}(s, N_{\text{LOS}}, N_{\text{NLOS}}) \\ = \{F_{\text{LOS}}(s)\}^{N_{\text{LOS}}} \{F_{\text{NLOS}}(s)\}^{N_{\text{NLOS}}} \end{aligned} \quad (14)$$

Substituting (12) and (13) into (14), we have

$$\begin{aligned} F_{\text{MRC}}(s, N_{\text{LOS}}, N_{\text{NLOS}}) \\ = \exp\left(-\frac{KN_{\text{LOS}}\gamma_D s}{K + \gamma_D s} \right) \left(\frac{K}{K + \gamma_D s} \right)^{(N_{\text{LOS}} + N_{\text{NLOS}})} \end{aligned} \quad (15)$$

Then the PDF of the combined signal is given by the inverse Laplace transformation $\mathcal{L}^{-1}[\cdot]$ as

$$\begin{aligned} f_{\text{MRC}}(\gamma, N_{\text{LOS}}, N_{\text{NLOS}}) \\ = \mathcal{L}^{-1}[F_{\text{MRC}}(s, N_{\text{LOS}}, N_{\text{NLOS}})] \end{aligned} \quad (16)$$

The derivation of (16) is very complex and with the implementation of the Mathematica software, the final result can be proved to be

$$\begin{aligned} f_{\text{MRC}}(\gamma, N_{\text{LOS}}, N_{\text{NLOS}}) \\ = \frac{K}{\Gamma(N_{\text{LOS}} + N_{\text{NLOS}})\gamma_D} \left(\frac{K\gamma}{\gamma_D} \right)^{N_{\text{LOS}} + N_{\text{NLOS}}} \\ \times \exp\left\{ -K \left(N_{\text{LOS}} + \frac{\gamma}{\gamma_D} \right) \right\} \\ \times {}_0F_1\left(N_{\text{LOS}} + N_{\text{NLOS}}; \frac{K^2 N_{\text{LOS}} \gamma}{\gamma_D} \right) \end{aligned} \quad (17)$$

Here ${}_0F_1(\cdot)$ denotes a Hypergeometric function and $\Gamma(\cdot)$ denotes a Gamma function. With the relation of

$${}_0F_1(a; x) = \Gamma(a) \frac{I_{a-1}(2\sqrt{x})}{x^{(a-1)/2}} \quad (18)$$

where $I_{a-1}(\cdot)$ is the modified Bessel function of the first kind with order $a-1$, (17) can be also rewritten as

$$\begin{aligned} f_{\text{MRC}}(\gamma, N_{\text{LOS}}, N_{\text{NLOS}}) \\ = \left(\frac{K}{\gamma_D} \right) \left(\frac{\gamma}{N_{\text{LOS}}\gamma_D} \right)^{(N_{\text{LOS}} + N_{\text{NLOS}} - 1)/2} \\ \times \exp\left\{ -K \left(N_{\text{LOS}} + \frac{\gamma}{\gamma_D} \right) \right\} \end{aligned}$$

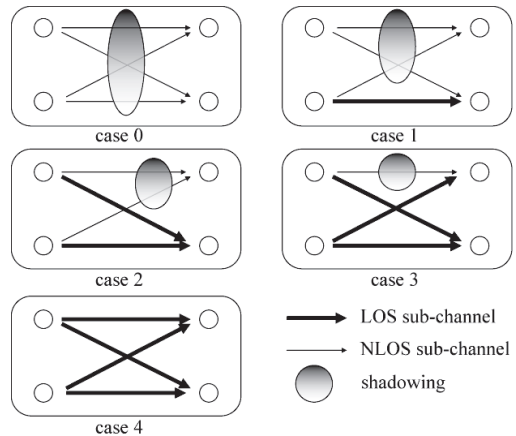


Fig. 2 Transmission cases based on the proposed model according to the number of LOS paths in 2×2 MIMO configuration.

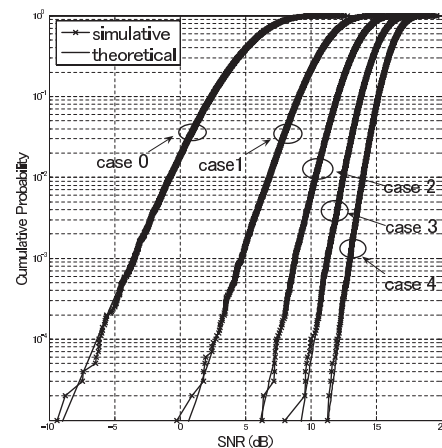


Fig. 3 The CDFs of output SNR of simulative and theoretical values for 5 cases of 2×2 MIMO propagation model, with $K = 10$ dB and $\gamma_D = 10$.

$$\times I_{N_{\text{LOS}} + N_{\text{NLOS}} - 1} \left(2K \sqrt{\frac{N_{\text{LOS}} \gamma}{\gamma_D}} \right) \quad (19)$$

2.4 Cases of 2×2 MIMO

Modeling in the mixture of NLOS and LOS environments for MIMO propagation may appear as different cases. For example in 2×2 MIMO system with one sub-channel in shadowing, there are 4 cases according as which one of all sub-channels is shadowed. However after combined by MRC, the output SNRs of those cases will perform the same. Also through the derivations in the last subsection, it can be found out that SNR characteristics in (19) are only concerned with numbers of NLOS sub-channels and LOS sub-channels. Therefore these 4 cases can be considered as the same kind of channel model structure. From the standpoint of model setup, we divide all possible cases into 5 kinds. We mark them from case 0 to case 4 according to the number of LOS sub-channels, as presented in Fig. 2. Notice that case 0 and case 4 actually represents a conventional NLOS environment and LOS environment, respectively.

For each case in 2×2 MIMO system with $N_{\text{NLOS}} + N_{\text{LOS}} = 4$, the PDF of combined SNR can be calculated by (19). And we compare the simulations and theoretical values for each case by cumulative distribution functions (CDF), as shown in Fig. 3. For simulation method, we consider a LOS sub-channel by Nakagami-Rice distributed signals and a NLOS sub-channel by Rayleigh distributed signals. And the scattering wave components in LOS sub-channels are set equal to those of NLOS sub-channels. For simulation conditions, the value of Rice factor K is set equal to 10 dB and γ_D is set equal to 10. As the result has shown, the theoretical results are completely in agreement with the simulative results.

3. Application to ITS-IVC Propagation Analysis

The adoption of MIMO technique in ITS-IVC system is promising from the viewpoint of highly reliable transmission. In addition, the multipath channel environment in ITS-IVC system is more complex and variable. Single model based on Rayleigh fading channel or Nakagami-Rice fading channel is deficient and inconvenience. Meanwhile, there are some characteristics of ITS-IVC appeal to us, large intervals of transmit antennas or receive antennas, and similar shadowing environment for each sub-channel for instance. Applying the proposed model to MIMO propagation for the mixture of NLOS and LOS sub-channels in ITS-IVC therefore seems very suitable and effective.

3.1 ITS-IVC in Shadowing Environment by a Large Vehicle

In this section, we show the evaluation example of the model in a situation that may cause traffic accidents nearby an intersection, as shown in Fig. 4. In the situation, vehicle R and a large vehicle L is about to make a right turn (driving in the left lane in Japan), while another vehicle T is going straight towards the intersection, behind the large vehicle L. The sight of driver in vehicle T may be obstructed by the shadowing of vehicle L so that IVC technology is highly

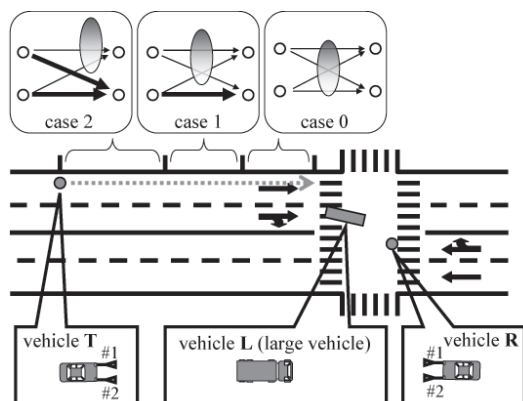


Fig. 4 ITS-IVC situations applying 2×2 MIMO propagation model depending on the shadowing extent.

anticipated to realize collision avoidance warning system.

For the purpose of model setup, two-antenna-setting is adopted in the physical layer considering the simplicity and efficiency, and then 2×2 MIMO configuration is constructed. Vehicle T is the transmitter and vehicle R is the receiver in the situation. The shadowing by vehicle L produces a mixture environment according to the physical conditions. As a result, some of the direct paths (LOS paths) among array elements may be completely broken due to vehicle movement, and attenuate into NLOS paths. The propagation conditions in such a situation are divided into 5 possible cases as shown in Fig. 2, and case 2, case 1 and case 0 according to the number of LOS paths, are shown in Fig. 4 as an example. Accordingly, the PDF of SNR for each case can be calculated quantitatively, through incorporating parameter values into (19).

3.2 Experiment

3.2.1 Experimental Setup

A field experiment conducted by Toyota Central R&D Labs was carried out [8], as the experimental conditions shown in Fig. 5. In the experiment, the obstacle was an actual microbus, namely vehicle L in Fig. 5. The transmitter and receiver which were fixed in steels represented vehicle T and vehicle R, respectively. Each of them was equipped with two antenna elements. The interval between antennas in front of vehicles was 1 m. The antenna height was set 0.8 m. The transmission power of each antenna is 10 dBm. Trans-

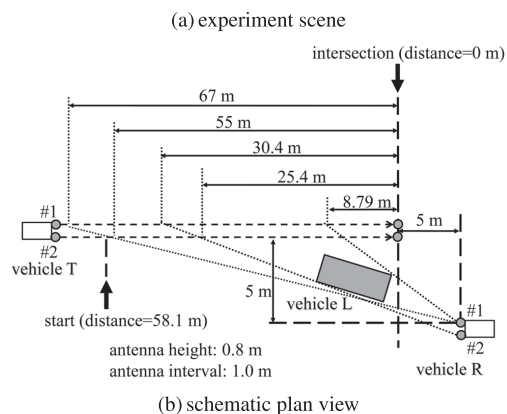
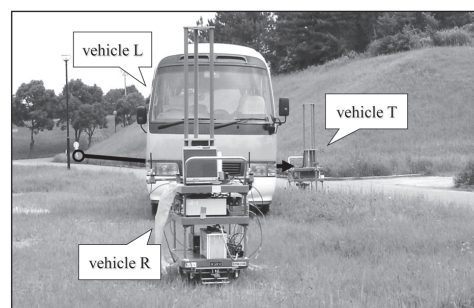


Fig. 5 Experimental conditions.

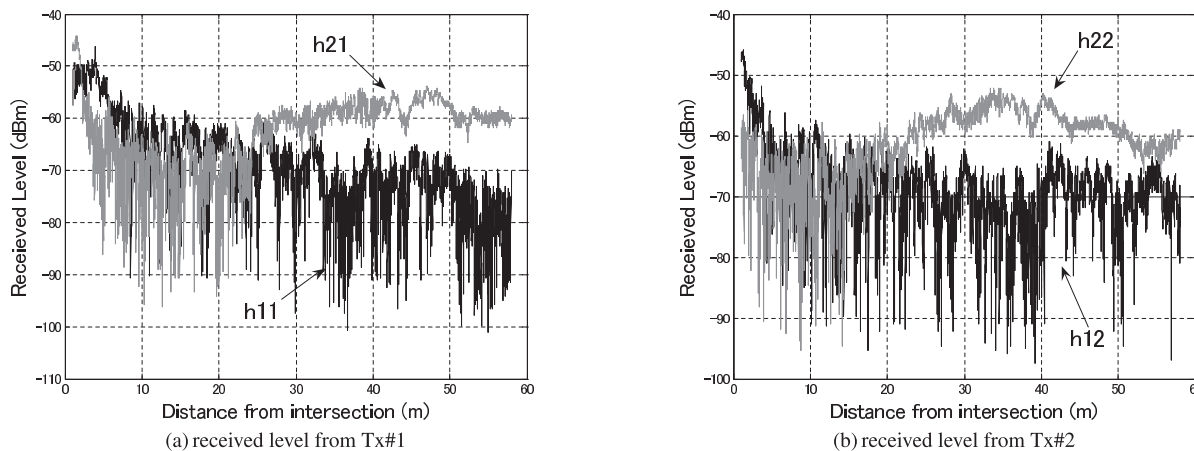


Fig. 6 Received signal power with respect to distance from intersection.

mission frequency was set at 5 GHz band and carrier signal was unmodulated. A schematic plan view depicted by information, such as sizes of vehicle L and antenna interval, is shown in (b) of Fig. 5. From that we can indicate, geometrically, that all sub-channels should have been shadowed in the range of distance 8.79 to 25.4 m, namely case 0. The range of distance 25.4 to 30.4 m should be case 1. And then between distance 30.4 and 55 m was case 2. Figure 5 also illustrates that if the distance of vehicle T from the intersection had been long enough, for example more than 70 m, case 3 between the distance of 55 to 67 m and case 4 over the distance 67 m, would appear. The range of distance 8.79 m to intersection seems to be case 4. However, in such a short transmission distance it is difficult to ignore channel interferences for modeling. In addition, the capability of our model is to evaluate transmission performance of MIMO system in mixed propagation environment in a comparative distance, especially when applying to ITS-IVC. Because of all above, case 0, case 1 and case 2 will be used for modeling. The field experiment is very similar to the application example discussed in this paper. Although our obtained data in this experiment are amplitude-only variations for each sub-channel, we can use these data for MRC estimation because the MRC works power-sum of each sub-channel power.

3.2.2 Experimental Results

The received signal power of each antenna at vehicle R was measured whenever vehicle T moved 5 mm in that experiment. The power level of Rx#1 and Rx#2 from transmit antenna Tx#1 and transmit antenna Tx#2 were recorded and the results are shown in Fig. 6, with respect to the distance of vehicle T from the intersection.

3.3 Modeling

In order to highlight the average value of received power as a function of distance, smoothing operation by means of moving average method is imposed. The number of data of

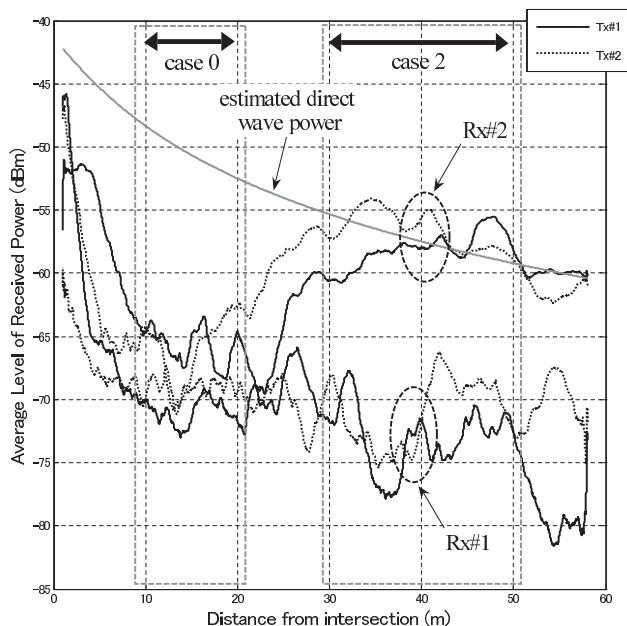


Fig. 7 Moving average values of received level.

each subset when exploiting this method is 501. Because received signal power was measured whenever vehicle T moved 5 mm in the field experiment, the distance window size is 2.5 m. The results are shown in Fig. 7. Obviously, large differences can be observed between the values of the receive antenna Rx#1 and the receive antenna Rx#2, when the distance of vehicle T from the intersection was in the range of distance about 30 to 50 m. On the other hand, received power of 4 sub-channels were almost in the same level for the range of 10 to 20 m. According to the schematic analysis of Fig. 5(b) and with the consideration of weakness of edge diffraction effect in actual propagation environment, fitting these two areas as case 2 and case 0 is valid. And the area between them is considered to be a transition region.

In addition, performance evaluation for IVC system in which transmission range varies because of driving movement should take the path loss effect into account. For this

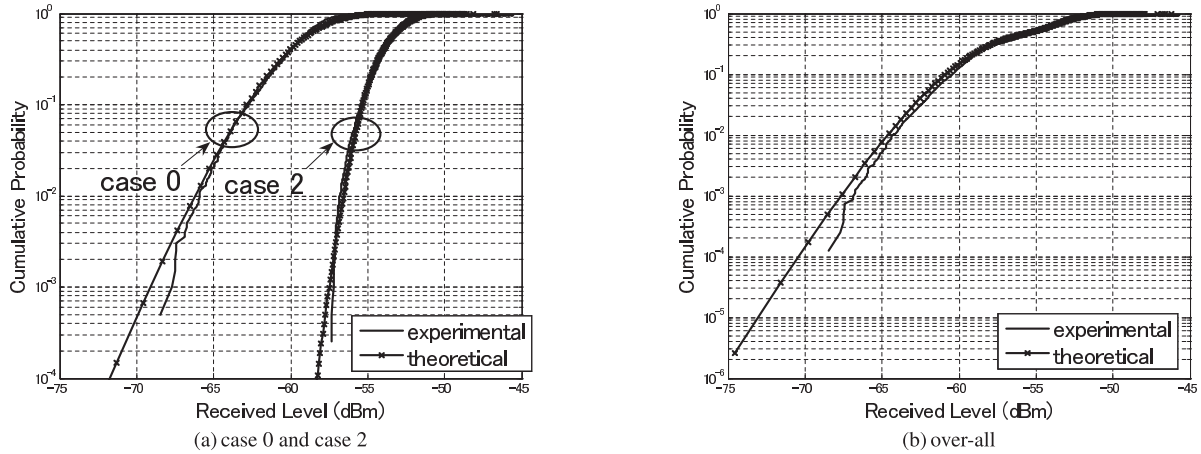


Fig. 8 The CDFs of received power in MRC of the theoretical values and experimental values.

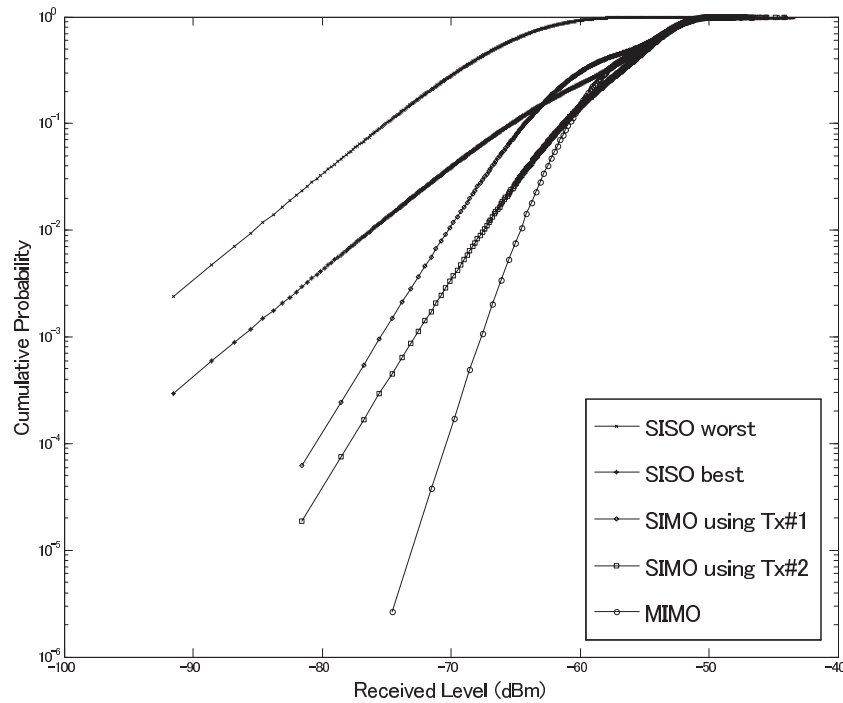


Fig. 9 Evaluations of received power through distance from intersection of 10 to 50 m in the right-turn situation of ITS-IVC for SISO worst transmission, SISO best transmission, SIMO transmission using Tx#1 as transmitter, SIMO transmission using Tx#2 as transmitter and proposed MIMO transmission.

purpose, a general model is achieved through considering Rice factor K and received level of LOS path as functions of distance variable x . The average PDF of received power z then can be given by

$$f_{\text{overall}}(z) = \frac{1}{x_{\text{max}} - x_{\text{min}}} \times \int_{x_{\text{min}}}^{x_{\text{max}}} f_{\text{MRC}}\{z; K(x), \gamma_D(x), N_{\text{LOS}}(x), N_{\text{NLOS}}(x)\} dx \quad (20)$$

Hereafter, in order to discuss model from PDF point of view, we treat the combined received power level variations

z rather than SNR γ because physical values obtained in the experiment is the power variation as shown in Fig. 6.

In order to exploit our proposed model, we estimated the direct wave power for the whole area, as shown in Fig. 7. The basic principle of achieving direct wave power curve is to use free space propagation model, namely Friis Equation. The path loss rate was set 2. However, since we have supposed that the transmission of signals received by Rx#2 in the range of case 2 is in LOS path, and transmission power and the antenna gains of transmitter and receiver are considered constant during vehicle moving, we can utilize the measurement result of case 2 to make a criterion, and based on that we can inversely estimate the direct wave power in

other areas. In our paper, we take the point at which distance from intersection is 45 m as a reference. The average received power of sub-channel h_{21} and h_{22} at that point is z_{ref} . Also note that the transmission distance of Friis Equation is $d_T(x) = \sqrt{(x+5)^2 + 5^2}$ because variable x is the distance from intersection. Then the estimated direct wave power is obtained by $z_D = [d_T(x)/d_T(45)]^{-2} \times z_{\text{ref}}$. In the fitting, the value of K in decibel is roughly estimated by the difference between the estimated direct wave power value and the received power value of NLOS sub-channels in Fig. 7. As results, we employ it as 13 dB for case 2 and 15 dB for case 0. CDFs for case 0 and case 2 applying our model (20) are depicted in Fig. 8(a), as well as the CDFs of combined signal power derived from experimental data. For comparison, the cumulative distribution curves are plotted by logarithmic scales and normalized at CDF=50% point. We can see that the comparison result shows fairly good coincidences for the cumulative probabilities of more than 10^{-3} , which confirms the effectiveness for evaluation using the proposed model.

In addition, if we assume the transition region between case 2 and case 0 as case 1, an overall evaluation result throughout the range of 10 to 50 m is achieved, as shown in Fig. 8(b). By normalized at the value of CDF at 50%, the overall CDF curve based on theoretical model coincides with the experimental result as indicated. The good agreement result identifies the effectiveness of the proposed model.

3.4 Evaluation of MIMO Merit Based on the Proposed Model

The proposed model (20) enables to evaluate propagation performance in the mixture of LOS and NLOS environments, even for SISO transmission and SIMO transmission. Therefore we would like to make an evaluation for each of them under the same conditions and show the merit of applying MIMO technique in ITS-IVC application in this situation, based on our proposed model.

For comparison, the received levels are enhanced by 3 dB for SISO and SIMO transmission so as to be equal for total transmission power. We consider SISO configuration in this situation by two ways: using Tx#1, Rx#1 as the worst way and Tx#2, Rx#2 as the best way, according to the physical conditions. Similarly for SIMO configuration, using Tx#1 only as transmitter and Tx#2 only as transmitter will be considered respectively.

The comparison result is shown in Fig. 9. From the result we can see that SISO transmission in the best way and SIMO transmissions give nearly the same performance as MIMO method for the region of cumulative probability of above about 0.5. But when the received power degrades, MIMO transmission offers a superior performance compared with SISO and SIMO transmissions. We can expect that MIMO technique shows its apparent advantage when applied to ITS-IVC system.

4. Conclusion

In this paper, a propagation channel model for MIMO system in the mixture of NLOS and LOS environment has been presented. Based on MRC diversity, this model provides a computing method that enables to evaluate MIMO transmission characteristics quantitatively. Considering that an attractive application of the proposed MIMO propagation model in ITS-IVC, we have discussed a right-turn collision scenario in the paper deeply and developed a general overall model for evaluation. Compared with the measurement results and simulation results, a good agreement result identifies the effectiveness of the proposed model. At last, we prove the merit of applying MIMO to ITS-IVC compared with SISO and SIMO transmissions based on our proposed model.

At present, since application of the model is too specific, we will try to apply the proposed MIMO propagation model in more general and complex environments, such as macro diversity schemes in cellular mobile systems.

Acknowledgment

We would like to thank researchers in Toyota Central R&D Labs for their field experiment and useful discussion on this topic. This work was partly supported by Grant-in-Aid for Scientific Research (A) (No. 20246066) by JSPS.

References

- [1] G. Foschini and M. Gans, "On limits of wireless communications in a fading environment when using multiple antennas," *Wirel. Pers. Commun.*, vol.6, pp.311–335, March 1998.
- [2] E. Telatar, "Capacity of multi-antenna gaussian channels," *European Trans. Telecommun.*, vol.10, no.6, pp.585–596, Nov. 1999.
- [3] D. Gesbert, M. Shafi, D. Shiu, P.J. Smith, and A. Naguib, "From theory to practice: An overview of MIMO space-time coded wireless systems," *IEEE J. Sel. Areas Commun.*, vol.21, no.3, pp.281–302, April 2003.
- [4] K. Yu, M. Bengtsson, B. Ottersten, D. McNamara, P. Karlsson, and M. Beach, "Modeling of wide-band MIMO radio channels based on NLoS indoor measurements," *IEEE Trans. Veh. Technol.*, vol.53, no.3, pp.655–665, May 2004.
- [5] T. Taniguchi, S. Sha, Y. Karasawa, and M. Tsuruta, "Simple approximation of largest eigenvalue distribution in MIMO channels under Nakagami-Rice fading," *IEICE Trans. Fundamentals*, vol.E90-A, no.9, pp.1862–1870, Sept. 2007.
- [6] S. Alamouti, "A simple transmit diversity technique for wireless communications," *IEEE J. Sel. Areas Commun.*, vol.16, no.8, pp.1451–1458, Oct. 1998.
- [7] V. Tarokh, H. Jafarkhani, and A.R. Calderbank, "Space-time block codes from orthogonal designs," *IEEE Trans. Inf. Theory*, vol.45, pp.1456–1467, July 1999.
- [8] K. Ito, N. Suzuki, and Y. Karasawa, "Performance evaluation of MIMO-STBC for inter-vehicle communications in shadowing environment by large vehicle," *IEEE VTC-Fall*, Sept. 2007.

Spatial Correlation Functions in Three-Dimensional APS With $\cos^n \theta$

Yi Wang, Hung Le Dang, and Yoshio Karasawa, *Fellow, IEEE*

Abstract—This letter describes a generalized formula for spatial correlation of three-dimensional incoming waves with an angular power spectrum of $\cos^n \theta$. Based on the proposed formula, spatial correlation performances at antennas or an antenna array can be approximated by simple computation with closed-form solutions in Cartesian coordinates. The validity of the proposed method is verified numerically.

Index Terms—Angular power spectrum, spatial correlation, three-dimensional.

I. INTRODUCTION

SINCE employing techniques such as multiple-input–multiple-output (MIMO) and antenna array (AA) techniques in next-generation systems, evaluation of the spatial correlation (SC) of signals has attracted a great deal of attention. In order to model the angular power distribution (APD), a number of previous studies, e.g., [1] and [2], assumed the power azimuth spectrum (PAS or azimuth APD) as a uniform distribution (also known as the Jakes model) and a Gaussian function, and measurement campaigns, such as that described in [3] and [4], revealed that using a Laplacian function as a PAS provides a good approximation for a number of real propagation environments. These models are limited to the horizontal two-dimensional (2-D) plane. The requirements of SC analysis of waves with a three-dimensional (3-D) angle of arrival (AoA) are claimed by studies and measurements such as [5] and [6], which reported that there is an elevation spread for several environments, ranging from indoor to outdoor environments, and the multipath richness in these environments leads to a significant error due to the azimuth-only assumption.

In a recent study [7], the azimuth and elevation of the AoA are taken into account and are assumed to be independent and uniformly distributed on the sphere. This study provided some useful expressions, but these expressions are not likely to characterize the propagation environment in general. In [8], the authors derived a generalized Doppler power spectrum for arbitrary 3-D scattering environments, but the resultant form is highly complex. A recent study attempted to develop a practical generalized method [9], where the authors initially consider the angular power spectrum (APS) as the n th power of a cosine function with respect to the elevation of the AoA.

In this letter, we promote this research by achieving a generalized formula. We also derive the SC functions with closed-form expressions by applying the Mellin-transform (MT) method,

Manuscript received January 24, 2012; revised March 26, 2012; accepted April 27, 2012. Date of publication May 04, 2012; date of current version May 22, 2012.

The authors are with the Advanced Wireless Communication Research Center (AWCC), The University of Electro-Communications, Tokyo 182-8585, Japan (e-mail: eason@radio3.ee.ucc.ac.jp).

Digital Object Identifier 10.1109/LAWP.2012.2198042

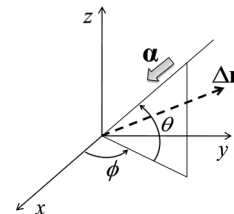


Fig. 1. Incident wave α with moving vector $\Delta \mathbf{r}$.

which is proposed in [10] to solve antenna problems. Based on the proposed method, the resultant closed-form resolution of which can be easily calculated by mathematical tools, some previous results given in [1] and [11] turn out to be special cases of the proposed method in which $n = 0, 2$ and ∞ . This method satisfies the requirement of highly practical applicability, and the validity of this method is verified by numerical results.

II. SPATIAL CORRELATION FORMULATION

A. Three-Dimensional Spatial Correlation

Fig. 1 shows an incident wave vector α in a 3-D multipath fading environment as follows:

$$\alpha = \mathbf{i} \cos \phi \cos \theta + \mathbf{j} \sin \phi \cos \theta + \mathbf{k} \sin \theta \quad (1)$$

where $\{\mathbf{i}, \mathbf{j}, \mathbf{k}\}$ are the corresponding unit vectors in Cartesian coordinates and $\{\phi, \theta\}$ are the azimuth and elevation of the AoA in spherical coordinates, respectively. The APS at the reception point is represented as $\Omega(\phi, \theta)$, which is given by

$$\Omega(\phi, \theta) = G(\phi, \theta) \Omega_p(\phi, \theta) \quad (2)$$

where $G(\phi, \theta)$ denotes the antenna angular power gain, and $\Omega_p(\phi, \theta)$ denotes the APD of the multipath environment. Considering the effects of the received powers of the vertically and horizontally polarized radio waves, respectively, (2) can be rewritten as

$$\Omega(\phi, \theta) = G_\theta(\phi, \theta) \Omega_{p,\theta}(\phi, \theta) + G_\phi(\phi, \theta) \Omega_{p,\phi}(\phi, \theta). \quad (3)$$

Given moving vector $\Delta \mathbf{r}$, representing the moving direction of the reception point, the spatial fading correlation of the incoming wave α is calculated by [1]

$$\rho_\alpha(\Delta \mathbf{r}) = \frac{1}{P_R} \int_{-\frac{\pi}{2}}^{\frac{\pi}{2}} \int_0^{2\pi} \Omega(\phi, \theta) \exp(jk \Delta \mathbf{r} \cdot \alpha) \cos \theta d\phi d\theta \quad (4)$$

where k is the wavenumber defined by $k = 2\pi/\lambda$ with λ being the signal wavelength and P_R is the average received power under the multipath condition, given by

$$P_R = \int_{-\frac{\pi}{2}}^{\frac{\pi}{2}} \int_0^{2\pi} \Omega(\phi, \theta) \cos \theta d\phi d\theta. \quad (5)$$

Equation (4) provides a theoretical method for the calculation of SC in a spherical field. Thus, considering the moving vector in three-dimensional Cartesian coordinates, we have

$$\Delta \mathbf{r} = \mathbf{i}\Delta x + \mathbf{j}\Delta y + \mathbf{k}\Delta z \quad (6)$$

where $\{\Delta x, \Delta y, \Delta z\}$ are the corresponding projections of $\Delta \mathbf{r}$ in Cartesian coordinates, and SC can be approximated by

$$\rho_a(\Delta \mathbf{r}) \approx \rho_{a,x}(\Delta x)\rho_{a,y}(\Delta y)\rho_{a,z}(\Delta z) \quad (7)$$

where $\{\rho_{a,x}(\Delta x), \rho_{a,y}(\Delta y), \rho_{a,z}(\Delta z)\}$ denote the corresponding functions of the SC characteristics in Cartesian coordinates.

B. Case of $\Omega(\phi, \theta) = \cos^n \theta$

In this letter, we focus on the analysis of APS for the case in which

$$\Omega(\phi, \theta) = \cos^n \theta, \quad n \geq 0 \quad (8)$$

which is a combination of antenna effects and propagation properties of the environment. For example, in a reverberation chamber and some other multipath-rich indoor environments, where the incoming waves are three-dimensionally uniform, the cross polarization power ratio (XPR) is 0 dB, so we have approximately $\Omega_{p,\theta}(\phi, \theta) = \Omega_{p,\phi}(\phi, \theta) = \text{const}$. Furthermore, for the case in which vertically polarized radio waves are received by a dipole antenna, we have $G_\theta(\phi, \theta) \approx \cos^2 \theta$ and $G_\phi(\phi, \theta) = 0$. Then, we can approximate the combined characteristic of APS using $\Omega(\phi, \theta) = \cos^2 \theta$ under the assumption that $\Omega_{p,\theta}(\phi, \theta) = \Omega_{p,\phi}(\phi, \theta) = 1$, for simplicity. For other cases of vertical polarization with a strong directivity, the APS can be represented by $\cos^n \theta$ with $n \gg 2$.

On the other hand, for the case in which the antenna directivity is weak while the vertical angular power spectrum of incoming waves is sharp, as in outdoor mobile propagation environments for instance, the APDs $\Omega_{p,\theta}(\phi, \theta)$ and $\Omega_{p,\phi}(\phi, \theta)$ perform as $\cos^n \theta$ with $n \gg 2$, and it follows that we can nevertheless obtain $\Omega(\phi, \theta) \propto \cos^n \theta$.

In this manner, the analysis of SC in the 3-D APS using $\Omega(\phi, \theta) = \cos^n \theta$ can represent many existing propagation situations. The primary purpose of this study is to generalize the SC function and derive closed-form solutions from that.

For SC of the x -coordinate, using the following expression:

$$J_0(x) = \frac{1}{2\pi} \int_0^{2\pi} \exp(jx \cos \phi) d\phi \quad (9)$$

where $J_0(\cdot)$ is the zeroth-order Bessel function of the first kind, $\rho_{a,x}(\Delta x)$ and $\rho_{a,z}(\Delta z)$ can be given by

$$\rho_{a,x}(\Delta x) = \frac{4\pi}{P_R} \int_0^{\frac{\pi}{2}} \cos^{n+1} \theta J_0(k\Delta x \cos \theta) d\theta \quad (10)$$

$$\rho_{a,z}(\Delta z) = \frac{4\pi}{P_R} \int_0^{\frac{\pi}{2}} \cos^{n+1} \theta \cos(k\Delta z \sin \theta) d\theta \quad (11)$$

respectively. Then, by applying the MT method, as shown in the Appendix, the results of (10) and (11) are given in terms of the generalized Hypergeometric function ${}_pF_q(\cdot)$, written as

$$\rho_{a,x}(\Delta x) = {}_1F_2 \left(\frac{n+2}{2}; 1, \frac{n+3}{2}; -\frac{k^2 \Delta x^2}{4} \right) \quad (12)$$

$$\rho_{a,z}(\Delta z) = {}_0F_1 \left(; \frac{n+3}{2}; -\frac{k^2 \Delta z^2}{4} \right). \quad (13)$$

Since $\{\rho_{a,x}(\Delta x), \rho_{a,y}(\Delta y)\}$ satisfy the symmetrical characteristics in the azimuth plane, $\rho_{a,y}(\Delta y)$ is obtained in a straightforward manner from $\rho_{a,x}(\Delta x)$.

The generalized Hypergeometric function can already be well handled by modern packages, such as Mathematica or MATLAB. Therefore, these results are also very useful and practicable. Given certain values of n , some previous analyses on SC easily turn out to be special cases of the proposed formula. For example, for the case in which $n = 0$, which represents a spherically uniform pattern, as given in [1], (12) and (13) reduce to

$$\rho_{a,x,n=0}(\Delta x) = {}_1F_2 \left(1; 1, \frac{3}{2}; -\frac{k^2 \Delta x^2}{4} \right) = \text{sinc}(k\Delta x) \quad (14)$$

$$\rho_{a,z,n=0}(\Delta z) = {}_0F_1 \left(; \frac{3}{2}; -\frac{k^2 \Delta z^2}{4} \right) = \text{sinc}(k\Delta z) \quad (15)$$

respectively. For $n = 2$, which is appropriately the case of a half-wave dipole, these expressions reduce to the following expressions, which are also shown in [11]:

$$\begin{aligned} \rho_{a,x,n=2}(\Delta x) &= {}_1F_2 \left(2; 1, \frac{5}{2}; -\frac{k^2 \Delta x^2}{4} \right) \\ &= \frac{3}{2} \left\{ \frac{\sin(k\Delta x)}{k\Delta x} \left[1 - \frac{1}{(k\Delta x)^2} \right] + \frac{\cos(k\Delta x)}{(k\Delta x)^2} \right\} \end{aligned} \quad (16)$$

$$\begin{aligned} \rho_{a,z,n=2}(\Delta z) &= {}_0F_1 \left(; \frac{5}{2}; -\frac{k^2 \Delta z^2}{4} \right) \\ &= \frac{3}{(k\Delta z)^2} \left[\frac{\sin(k\Delta z)}{k\Delta z} - \cos(k\Delta z) \right] \end{aligned} \quad (17)$$

respectively. For $n \rightarrow \infty$, which signifies the case for a 2-D plane, the above reduce to the classical Jakes model in [1], which are given as

$$\rho_{a,x,n \rightarrow \infty}(\Delta x) = \rho_{2D}(\Delta x) = J_0(k\Delta x) \quad (18)$$

$$\rho_{a,z,n \rightarrow \infty}(\Delta z) = 1 \quad (19)$$

respectively.

Although the examples of n given here are for integer values, the derivation shown in the Appendix reveals that real numbers are also applicable.

III. EXAMPLES AND NUMERICAL RESULTS

A. Reception Pattern

For the examination of a case having higher value of n , a dipole array of two elements with vertical interval distance $d = \lambda$ is considered, as shown in Fig. 2. The radiation patterns in the case of $n = 0, 2, 8$ and the pattern corresponding to the dipole AA given in Fig. 2 are described in Fig. 3. For simplicity, we assume that $\Omega_{p,\theta}(\phi, \theta) = \Omega_{p,\phi}(\phi, \theta) = 1$ and $G_\phi(\phi, \theta) = 0$. As shown in this figure, the lobe of the pattern in the case of $G_\theta(\phi, \theta) \approx \cos^{23} \theta$, and thus $\Omega(\phi, \theta) \approx \cos^{23} \theta$, is found to be suitable by normalizing the half-power beamwidth to approach the main lobe of the radiation pattern of AA.

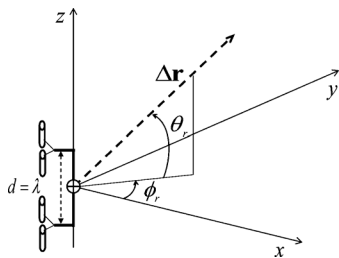


Fig. 2. Dipole array of two elements with vertical interval distance $d = \lambda$ and moving vector $\Delta \mathbf{r}$ with angular of $\{\phi_r, \theta_r\}$.

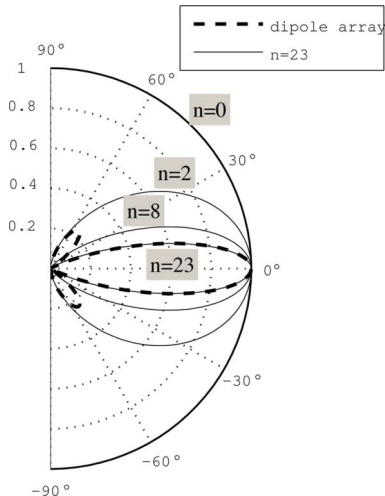


Fig. 3. Reception patterns in the case of $n = 0, 2, 8$ and the case of $n = 23$, which corresponds to the half-power beamwidth of the dipole array given in Fig. 2.

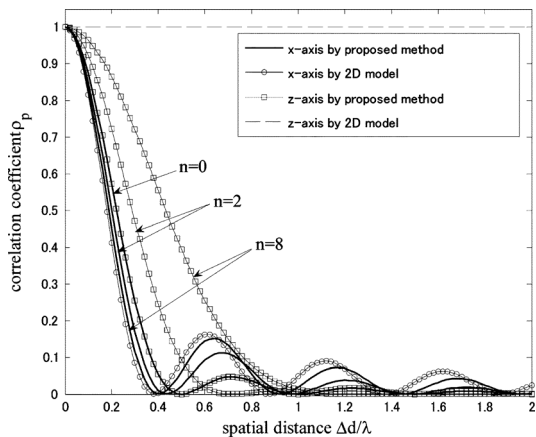


Fig. 4. SC calculations along x -axis and z -axis for the cases in which $n = 0, 2, 8$, and ∞ with aid of (12) and (13), respectively.

B. Calculation Results

We calculate the correlation coefficient ρ_p by $\rho_p = |\rho_a|^2$ with respect to antenna spatial distance. For SC along the x direction, the characteristics of the patterns for the cases in which $n = 0, 2, 8$ and ∞ are calculated with aid of (12), as shown in Fig. 4. The figure shows that the SC characteristics change slightly and approach that of the Jakes model for $n = 8$. This agrees with the previous conclusion that, for many cases of the multipath environment in the 2-D plane, the Jakes model is a reasonable approximation for the analysis of SC performance.

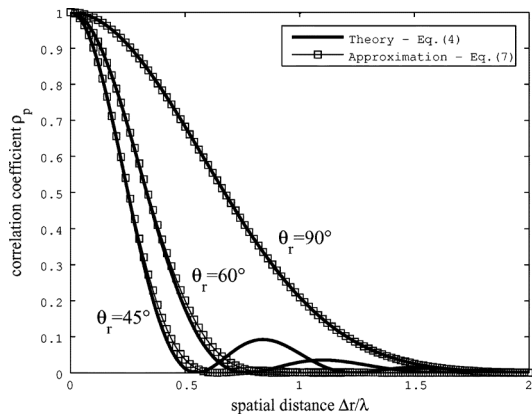


Fig. 5. SC calculations of theoretical value and approximated value for the case in which $n = 23$ and $\phi_r = 30^\circ$, $\theta_r = 45^\circ, 60^\circ$, and 90° , respectively.

Spatial correlation evaluations along the z -axis, which are calculated using (13), are also shown in Fig. 4. As we can see, the performance changes gradually as n increases, and the sidelobes are restrained. The results illustrate that the correlation performance in the z -direction is visibly influenced by the APS with elevation spread. The correlation coefficient will reach 1 as n approaches infinity.

Finally, for the AA given in Figs. 2 and 3, we approximate the SC characteristics when the moving direction of the reception point $\Delta \mathbf{r}$ is $\phi_r = 30^\circ$ and $\theta_r = 45^\circ, 60^\circ$, and 90° , respectively. We compare the approximated results given by (7) together with (12) and (13) to the theoretical values obtained from (4), as shown in Fig. 5. The sidelobe patterns in SC for $\theta_r = 45^\circ$ and 60° disappear in the approximation case. This is because we ignore the sidelobes by implementing the corresponding pattern of $\cos^{23} \theta$. Nevertheless, the main lobes of the approximated and theoretical values are shown to be in good agreement. For $\theta_r = 90^\circ$, the approximated and theoretical values coincide well.

IV. CONCLUSION

A generalized method for the approximation of SC with the reception pattern in the case of $\Omega(\phi, \theta) = \cos^n \theta$ is proposed in this letter. The proposed method using simple closed-form expressions is suitable for evaluating spatial fading correlation of incoming waves with a 3-D environmental spread and is easy to apply through mathematical tools. In addition, other results presented previously in [1] and [11] are shown to be special cases of the proposed formula. The numerical results provided by our formula confirm the accuracy and validity of the proposed method because of the fairly good agreement with the theoretical results.

APPENDIX DERIVATION OF (12)

The resultant forms shown in (12) can be derived by applying the MT method. The reader may refer to [10], in which the author explains the MT method and presents several examples to show how this method works. In order to avoid duplication, we provide a step-by-step application of the MT method to the derivation of (12). The reader is invited to derive (13).

Let the integral component in (10) be denoted as $f_x(u)$, where $u = k\Delta x$. Thus, we have

$$f_x(u) = \int_0^{\frac{\pi}{2}} \cos^{n+1} \theta J_0(u \cos \theta) d\theta. \quad (20)$$

In order to apply the MT method as shown in [10], we define $g_x(u)$ and $h_x(v)$, respectively, as

$$g_x(u) = J_0(u) \quad (21)$$

$$h_x(v) = \begin{cases} (1-v^2)^{-1/2} v^\tau, & \text{for } 0 < v < 1 \\ 0, & \text{for } v > 1. \end{cases} \quad (22)$$

Thus, we can rewrite $f_x(u)$ as

$$f_x(u) = \int_0^1 J_0(uv)(1-v^2)^{-1/2} v^\tau dv \quad (23)$$

where $v = \cos \theta$ and $\tau = n + 1$, $n > 0$. Representing the MT of $f(x)$ as $\tilde{f}(s)$, the integral above converges when s is valued within a certain scale of the complex plane, which is referred to as the strip of initial definition (SID). By MT method, the MT of $f_x(u)$ can be given by

$$\begin{aligned} \tilde{f}_x(s) &\equiv \tilde{g}_x(s)\tilde{h}_x(1-s) \\ &= \left[\frac{1}{2} \left(\frac{1}{2} \right)^{-s} \frac{\Gamma(\frac{s}{2})}{\Gamma(1-\frac{s}{2})} \right] \left[\frac{\sqrt{\pi} \Gamma(\frac{1}{2} + \frac{\tau}{2} - \frac{s}{2})}{2 \Gamma(1 + \frac{\tau}{2} - \frac{s}{2})} \right] \end{aligned} \quad (24)$$

where $\Gamma(\cdot)$ is the Gamma function, and the overlap of the SID of $\tilde{g}_x(s)$ and $\tilde{h}_x(1-s)$ is $0 < \text{Re}\{s\} < 1$. Then, by the inversion of MT, we have

$$f_x(u) = \frac{\sqrt{\pi}}{4} \frac{1}{2\pi i} \int_{c-i\infty}^{c+i\infty} \frac{\Gamma(\frac{s}{2}) \Gamma(\frac{1}{2} + \frac{\tau}{2} - \frac{s}{2})}{\Gamma(1-\frac{s}{2}) \Gamma(1 + \frac{\tau}{2} - \frac{s}{2})} \left(\frac{u}{2}\right)^{-s} ds \quad (25)$$

in which the poles on the left-hand side are contributed by $\Gamma(s/2)$ and located at $s = 0, -2, -4, \dots$. Furthermore, according to the residue theorem, upon approaching the contour at the left-hand side, we obtain the following:

$$\begin{aligned} f_x(u) &= \sum_{m=0}^{\infty} \text{Res}\{\tilde{f}_x(s)u^{-s}; s = -2m\} \\ &= \frac{\sqrt{\pi}}{4} \sum_{m=0}^{\infty} \text{Res}\left\{ \frac{\Gamma(\frac{s}{2})\Gamma(\frac{1}{2} + \frac{\tau}{2} - \frac{s}{2})}{\Gamma(1-\frac{s}{2})\Gamma(1 + \frac{\tau}{2} - \frac{s}{2})} \left(\frac{u}{2}\right)^{-s}; s = -2m \right\} \\ &= \frac{\sqrt{\pi}}{4} \sum_{m=0}^{\infty} \frac{\Gamma(\frac{1}{2} + \frac{\tau}{2} + \frac{2m}{2})}{\Gamma(1 + \frac{2m}{2})\Gamma(1 + \frac{\tau}{2} + \frac{2m}{2})} \\ &\quad \times \text{Res}\left\{ \Gamma\left(\frac{s}{2}\right) \left(\frac{u}{2}\right)^{-s}; s = -2m \right\} \\ &= \frac{\sqrt{\pi}}{2} \frac{\Gamma(\frac{1}{2} + \frac{\tau}{2})}{\Gamma(1)\Gamma(1 + \frac{\tau}{2})} \sum_{m=0}^{\infty} \frac{(\frac{1}{2} + \frac{\tau}{2})_m}{(1)_m (1 + \frac{\tau}{2})_m} \frac{(-u^2/4)^m}{m!} \end{aligned} \quad (26)$$

where $(s)_m$ is the Pochhammer symbol given by

$$(s)_m = \frac{\Gamma(s+m)}{\Gamma(s)}, \quad m = 0, 1, 2, \dots \quad (27)$$

According to the definition of the Hypergeometric function, the series in (26) is further identified as

$$f_x(u) = \frac{\sqrt{\pi} \Gamma(\frac{1}{2} + \frac{\tau}{2})}{2 \Gamma(1 + \frac{\tau}{2})} {}_1F_2\left(\frac{1}{2} + \frac{\tau}{2}; 1, 1 + \frac{\tau}{2}; -\frac{u^2}{4}\right). \quad (28)$$

The average received power P_R can be calculated by $4\pi f_x(k\Delta x) |_{\Delta x=0}$ with substitutions of $u = k\Delta x$, $\tau = n + 1$, given as

$$P_R = 2\pi\sqrt{\pi} \frac{\Gamma(\frac{n}{2} + 1)}{\Gamma(\frac{n}{2} + \frac{3}{2})}. \quad (29)$$

Then, (12) is obtained by

$$\begin{aligned} \rho_{a,x}(\Delta x) &= \frac{4\pi}{P_R} f_x(k\Delta x) \\ &= {}_1F_2\left(\frac{n+2}{2}; 1, \frac{n+3}{2}; -\frac{k^2\Delta x^2}{4}\right). \end{aligned} \quad (30)$$

Although the notation m in the derivation is defined as a nonnegative integer, the Gamma function $\Gamma(\cdot)$ and the residue theory also hold for real numbers. Consequently, the results in terms of the Hypergeometric function ${}_pF_q(\cdot)$ are applicable and can conveniently achieve analytic results for the nonnegative real values of parameter n .

REFERENCES

- [1] W. C. Jakes, *Microwave Mobile Communications*. New York: IEEE Press, 1993.
- [2] M. T. Feeney and J. D. Parsons, "Cross-correlation between 900 MHz signal received on vertically separated antennas in small-cell radio systems," *Inst. Elect. Eng. Proc. I*, vol. 138, no. 2, pp. 81–86, Apr. 1991.
- [3] K. I. Pedersen, P. E. Mogensen, and B. H. Fleury, "A stochastic model of the temporal and azimuthal dispersion seen at the base station in outdoor propagation environments," *IEEE Trans. Veh. Technol.*, vol. 49, no. 2, pp. 437–447, Mar. 2000.
- [4] A. S. Y. Poon and M. Ho, "Indoor multiple-antenna channel characterization from 2 to 8 GHz," in *Proc. IEEE ICC*, May 2003, vol. 5, pp. 3519–3523.
- [5] A. Kuchar, J.-P. Rossi, and E. Bonek, "Directional macro-cell channel characterization from urban measurements," *IEEE Trans. Antennas Propag.*, vol. 48, no. 2, pp. 137–146, Feb. 2000.
- [6] K. Kalliola, K. Sulonen, H. Laitinen, O. Kivekas, J. Krogerus, and P. Vainikainen, "Angular power distribution and mean effective gain of mobile antenna in different propagation environments," *IEEE Trans. Veh. Technol.*, vol. 51, no. 5, pp. 823–838, Sep. 2002.
- [7] S. K. Yong and J. S. Thompson, "Three-dimensional spatial fading correlation models for compact MIMO receivers," *IEEE Trans. Wireless Commun.*, vol. 4, no. 6, pp. 2856–2869, Nov. 2005.
- [8] J. T. Y. Ho, "A generalized Doppler power spectrum for 3D non-isotropic scattering environments," in *Proc. IEEE GLOBECOM*, 2005, vol. 3, pp. 1393–1396.
- [9] H. L. Dang and Y. Karasawa, "Spatial correlation characteristics in three-dimensional multipath channels," *IEICE Tech. Rep.*, Apr. 2009, vol. 109, no. 1, AP2009-6, pp. 31–36.
- [10] G. Fikioris, "Integral evaluation using the Mellin transform and generalized hypergeometric functions: Tutorial and applications to antenna problems," *IEEE Trans. Antennas Propag.*, vol. 54, no. 12, pp. 3895–3907, Dec. 2006.
- [11] D. Doncker, "Spatial correlation functions for fields in three-dimensional Rayleigh channels," *Prog. Electromagn. Res.*, vol. 40, pp. 55–69, 2003.